

AD-A038 624

NATIONAL AVIATION FACILITIES EXPERIMENTAL CENTER ATL--ETC F/G 17/9
TEST AND EVALUATION OF THE RADAR PROCESSING SUBSYSTEMS OF THE A--ETC(U)
MAR 77 M HOLTZ, L WAPELHORST

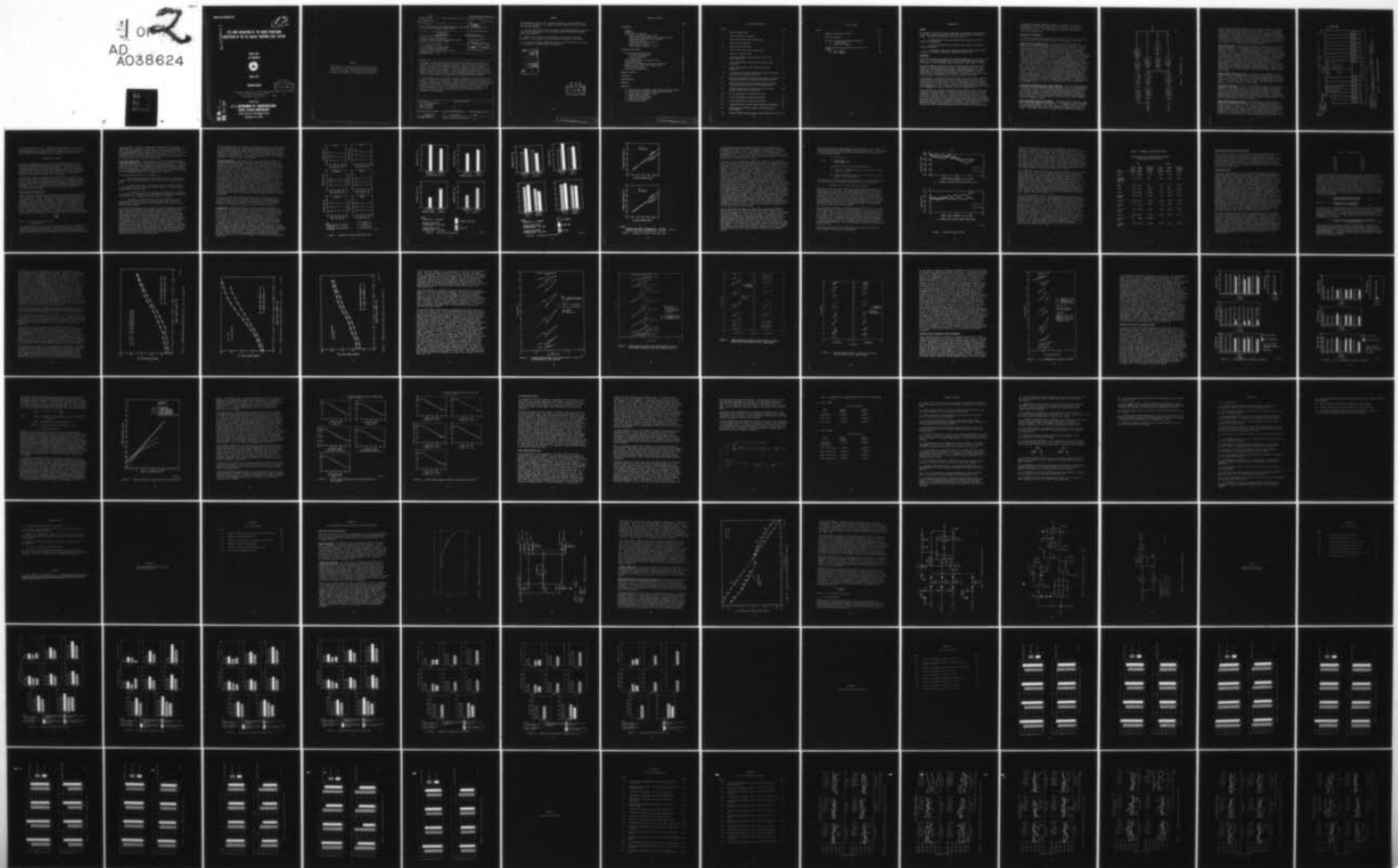
UNCLASSIFIED

FAA-NA-76-22

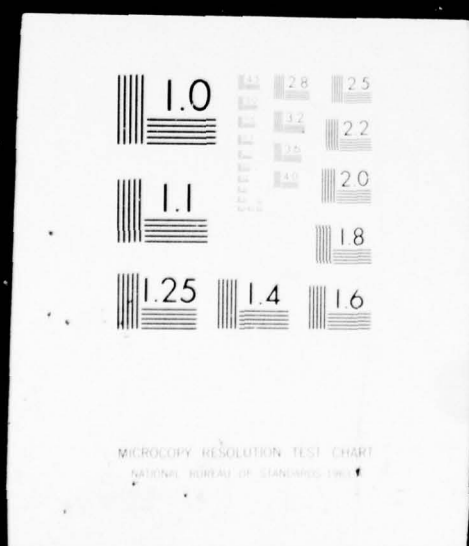
FAA-RD-76-197

NL

2
AD
A038624



1 OF 2
AD
A038624



Report No. FAA-RD-76-197

AD A 038624

**TEST AND EVALUATION OF THE RADAR PROCESSING
SUBSYSTEM OF THE ALL DIGITAL TRACKING LEVEL SYSTEM**

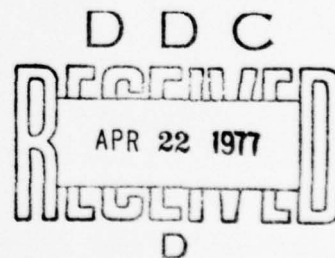
**Martin Holtz
Leo Wapelhorst**



March 1977

INTERIM REPORT

Document is available to the public through the
National Technical Information Service
Springfield, Virginia 22151



**AD No. _____
DDC FILE COPY**

Prepared for
U. S. DEPARTMENT OF TRANSPORTATION
FEDERAL AVIATION ADMINISTRATION
Systems Research & Development Service
Washington, D.C. 20590

NOTICE

This document is disseminated under the sponsorship of the Department of Transportation in the interest of information exchange. The United States Government assumes no liability for its contents or use thereof.

Technical Report Documentation Page

1. Report No. 18 FAA-RD-76-197	2. Government Accession No.	3. Recipient's Catalog No. 14 12 148p
4. Title and Subtitle TEST AND EVALUATION OF THE RADAR PROCESSING SUBSYSTEMS OF THE ALL DIGITAL TRACKING LEVEL SYSTEM		5. Report Date Mar 1977
6. Performing Organization Code		7. Performing Organization Report No. 11 FAA-NA-76-22
8. Author(s) 10 Martin Holtz Leo Wapelhorst	9. Performing Organization Name and Address Federal Aviation Administration National Aviation Facilities Experimental Center Atlantic City, New Jersey 08405	10. Work Unit No. (TRAIS)
11. Sponsoring Agency Name and Address U.S. Department of Transportation Federal Aviation Administration Systems Research and Development Service Washington, D.C. 20590		12. Contract or Grant No. 142-171-000
13. Type of Report and Period Covered Interim March 1975 - February 1976		14. Sponsoring Agency Code
15. Supplementary Notes		
16. Abstract This report contains the results of tests that were conducted to determine the performance of the radar processing subsystem of the All Digital Tracking Level System. The measure of performance was based primarily on target detection sensitivity, false target rates in clutter and clutter-free environments, clutter mapping, and quantizer regulation. The tests consisted of bench tests and tests employing weather clutter samples. Input videos were derived from both an ASP-5 and ASR-7 radar radiating from the National Aviation Facilities Experimental Center (NAFEC) Terminal Facility for Automation and Surveillance Testing (TFAST). It was concluded that the rank-order quantizer delivered by the contractor did not perform to theoretical expectations. However, the model designed and fabricated by NAFEC was successful in achieving expected results. The second-threshold control function regulated false targets in weather clutter environments to a half order of magnitude of a 1×10^{-5} rate. Target detection sensitivity was acceptable, but could be improved by utilizing a hardware detector that does not employ a pre-detector function. Finally, the video select mapping function requires improvement in performance. 00001		
17. Key Words Data Processing Systems Data Transmission Radar Detection Radar Quantizers		18. Distribution Statement
19. Security Classif. (of this report) Unclassified	20. Security Classif. (of this page) Unclassified	21. No. of Pages 149
22. Price		

PREFACE

Acknowledgement is made to the following personnel for their assistance in the test and evaluation of the radar processing subsystem of the All Digital Tracking Level System:

1. Mr. Mark Schoenthal, for his assistance in developing special online data collection programs written for the Automated Radar Terminal System (ARTS) input/output processor.
2. Messrs. Oliver Carlson, Richard Nelson, and David Rice for their assistance in the collection of data required to accomplish this effort.
3. Mr. Michael Saltsman, UNIVAC Corporation, for his assistance in checkout and debugging of the radar processing subsystem.

ACCESSION for	
White Section	<input checked="" type="checkbox"/>
Buff Section	<input type="checkbox"/>
REMARKS	<input type="checkbox"/>
DISTRIBUTION	
DISTRIBUTION/AVAILABILITY NOTES	
AVAIL. and/or SPECIAL	
A	

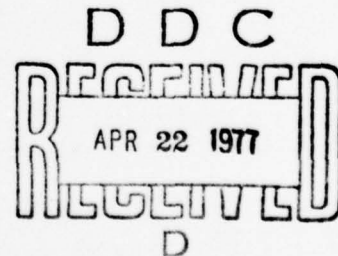


TABLE OF CONTENTS

	Page
INTRODUCTION	1
Purpose	1
Background	1
Description of Equipment	2
Radar Processing Subsystem (RPS)	2
Westinghouse Radiofrequency Test Target Generator	2
Ampex Model FR-950 Video Tape Recorder	2
Rank-Order Quantizer	4
Digital Target Generator Test Set	4
Input/Output Processor	4
Moving Target Indicator Log Video	4
PROCEDURES AND RESULTS	6
Percent Noise Regulation Tests	6
Clutter-Free Environment	7
Clutter Environment	8
Isolated Hits	8
Percent Quantization and Detection Tests	18
Clutter-Free Tests	18
Detection Tests Weather in Clutter Environment	29
Weather Clutter Tests, False Target Rates	31
Hit Distribution Tests	39
Video Select Mapping Tests	40
SUMMARY OF RESULTS	44
CONCLUSIONS	47
RECOMMENDATIONS	49
REFERENCE	49
APPENDIXES	
A - NAFEC Rank-Order Quantizer Design and Circuit Test Results	
B - Percent Noise Regulation, Clutter-Free Environment	
C - Percent Noise for Weather Samples	
D - Isolated-Hit Performance	
E - Weather False Target Rates	
F - Target Hit Distribution	
G - Video Select Mapping	

LIST OF ILLUSTRATIONS

Figure		Page
1	Block Diagram of RDAS	3
2	Typical Rank-Order Quantizer	5
3	Percent Noise Versus Input Noise Level	9
4	Weather Noise Regulation	10
5	Weather Noise Regulation	11
6	Percent Noise Versus Input Noise Level	12
7	Effect of Target in Zone	15
8	Percent Quantization Versus Target Signal Level, ASR-5 Linear MTI	21
9	Percent Quantization Versus Signal Strength, ASR-7 Log Normal	22
10	Percent Quantization Versus Signal Level, ASR-7 Linear MTI	23
11	Percent Detection Versus False Target Rates ASA Function of Predetector and Final Detector	25
12	Percent Detection Versus False Target Rates for 1/16-nmi Time Interval Sampler and RDAS Hit Processing (ASR-5)	26
13	Percent Detection Versus False Target Rates for Fixed- Position and Flying Targets (ASR-7, Linear Normal)	27
14	Percent Detection Versus P_{fa} for Flying and Fixed- Position Targets (ASR-7 Linear MTI)	278
15	P_D P_{fa} Performance of Double-Hit Function	30
16	P_D P_{fa} Performance of Double-Hit Function	32
17	P_D P_{fa} Performance of Double-Hit Function	33
18	Average Isolated-Hit Count Versus Single-Lab Correlation	35
19	Typical Second-Threshold Control Values Employed for ASR-5 Samples	37
20	Typical Second-Threshold Control Values Employed for ASR-7	38

LIST OF TABLES

Table		Page
1	Summary of Isolated-Hit Results	17
2	ASR-7 PRF Sequence	19
3	Best Set of Video Select Mapping Parameters	42
	A. Clutter Monitor	42
	B. Isolated-Hit Mapping	42
4	Summary of Video Mapping Results for Best Set of Parameters	43
	A. ASR-5 Samples	43
	B. ASR-7 Sample	43

INTRODUCTION

PURPOSE.

The purpose of this activity was to determine the performance characteristics of the radar processing subsystem (RPS) of the All Digital Tracking Level System. The specific objectives of the effort were

1. To compare actual rank-order quantizer effectiveness to that of theoretical expectations.
2. To test two methods of false alarm control based on estimation of clutter correlation.
3. To determine a best set of operating parameters and system configuration for the airport surveillance radars (ASR-5 and ASR-7).

BACKGROUND.

A test and evaluation of an RVD-3, and associated software, was conducted under phase I of the Automated Radar Terminal System (ARTS) Enhancement Program. The results of this investigation are documented in UNIVAC report PX 10027.

This system employed a mean-level type of quantizer and provided for either hardware or software detection of targets. The primary findings of this effort were that software detection with a software predetector was highly inefficient, but was capable of producing detection comparable to that achieved with a hardware detection function. In addition, an excessive number of false targets were experienced in weather clutter environments.

In the interim, a mathematical analysis of radar-signal processing techniques was conducted by the Johns Hopkins Applied Physics Laboratory (APL). The primary problem investigated was control of false target rates in atmospheric disturbances such as rain clutter. The large number of statistical distributions encountered in clutter returns led to the recommendation of a distribution-free (nonparametric) type of quantizer in lieu of a mean-level type.

Specifications for an RPS were developed which included a hardware radar data acquisition subsystem (RDAS) and associated software written for the UNIVAC input/output processor (IOP). A contract was subsequently awarded to UNIVAC Corporation to develop the required software, and the design and fabrication of the RDAS were subcontracted by UNIVAC to Burroughs Corporation. At the same time, steps were taken by the National Aviation Facilities Experimental Center (NAFEC) to design and test a rank-order quantizer. A description of this effort and detailed results were presented in an interim report (reference 1). Briefly, the report delineated detection and false target rates achieved with

a successfully designed rank-order quantizer interfaced with the RVD-3. Performance of the RVD-3, as designed by the contractor, was compared to that achieved with the RVD-3 integrated with a rank-order quantizer and various range bidders. Tests were accomplished for both clutter and clutter-free environments.

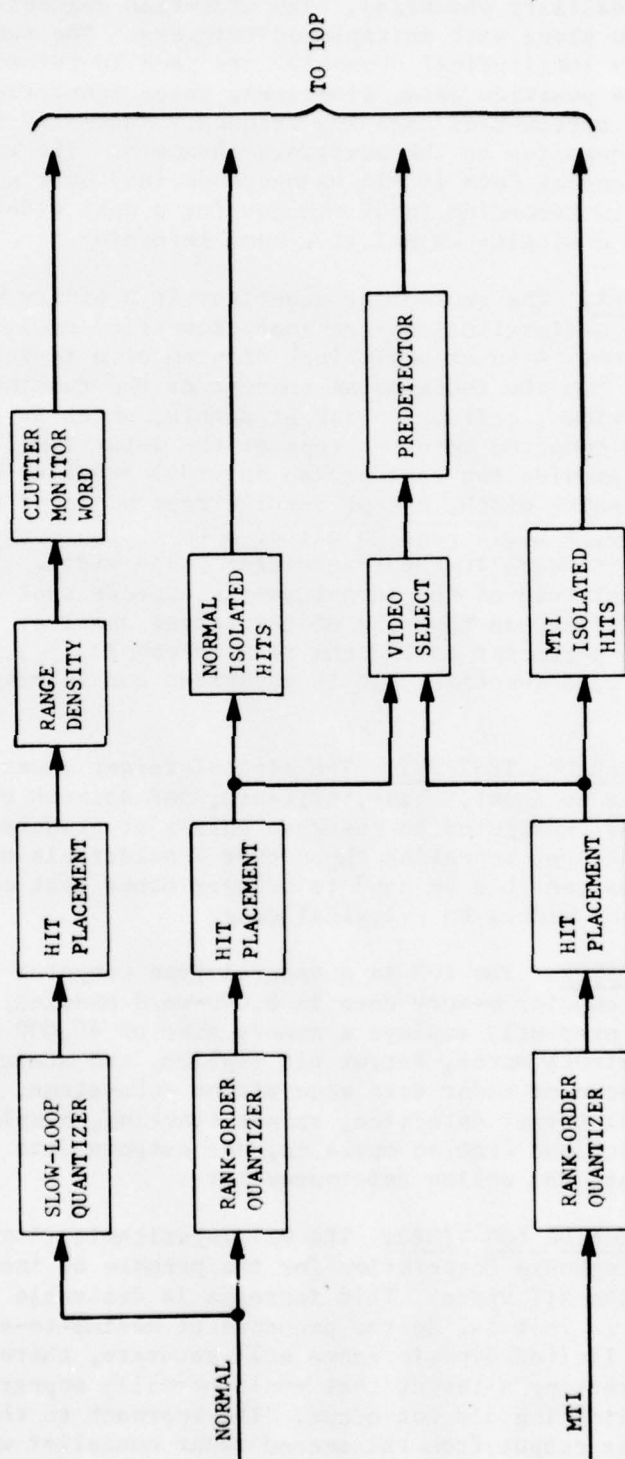
DESCRIPTION OF EQUIPMENT.

The following paragraphs are presented to provide a brief description of the equipment employed to obtain data defining the performance of the RPS:

RADAR PROCESSING SUBSYSTEM (RPS). The RPS consists of a hardware PDAS (figure 1), and associated software that resides in the UNIVAC IOP. The PDAS accepts basic timing information and analog video from the radar. Two rank-order quantizers are employed to convert the analog video into amplitude-quantized binary hits and regulate the percent noise (P_N) to the selected value. One rank-order quantizer is used to process each of the two input videos (normal and moving target indicator (MTI)). Selection of the appropriate video is accomplished via a video switch and is controlled by the IOP. Discrete video selection is accomplished for an area 2 nautical miles (nmi) in range by 32 azimuth change pulses (ACP's). This is hereafter referred to as a zone. A mechanism for identifying clutter is provided by the clutter monitor function. A "clutter monitor word" is transferred to the IOP and is employed to develop the "video select word" that is used to control video selection (normal or MTD). The output of the video switch (either MTI or normal video) is processed by a hardware predetector that is provided to reduce the IOP loading. This hardware predetector provides only an indication of a potential target within a zone. It does not convey to the software detector the discrete range cell of the potential target. The search for the range cell is accomplished by a software predetector prior to final detection. A sliding-window statistical detector is implemented to perform final detection, hit discrimination, and derivation of target azimuth via a center-of-mass technique. A detected target is then passed on to the tracker as a potential track or as an update for an established track.

WESTINGHOUSE RADIOFREQUENCY TEST TARGET GENERATOR. This test target generator is designed to provide simulated targets that have most of the characteristics of live targets such as azimuth-scanning modulation, target pulse-to-pulse scintillation, Doppler, and variable target radiofrequency (RF) levels. The test generator provided a coherent RF test target by sampling a portion of both the radar stable local oscillator (STALO) and coherent local oscillator (COHO) frequencies. The RF test target is injected into the radar system at the radar directional coupler.

AMPEX MODEL FR-950 VIDEO TAPE RECORDER. The FR-950 video recorder is a wide-band, rotary-head, magnetic tape recorder. It is designed to record and reproduce data with a bandwidth of 10 hertz (Hz) to 6 megahertz (MHz) on a direct frequency modulation (FM) carrier with sidebands not extending beyond 3 to 12 MHz. The recorder provides for record/reproduce channels (two wide-band



76-22-1

FIGURE 1. BLOCK DIAGRAM OF RDAS

channels and two auxiliary channels). The wide-band channels are employed to record analog video along with multiplexed triggers. The two narrow-band channels (auxiliary longitudinal channels) are used to record both analog and digital antenna position data, time code, voice annotations, and flutter compensation. The narrow-band data are frequency modulated and multiplexed via subcarrier frequencies on the auxiliary channels. The time-base stability of the reproduced analog data is ± 15 nanoseconds (ns) over a full tape. The length of a data recording is 30 minutes for a dual wide-band recording and 60 minutes for a single-channel wide-band recording.

RANK-ORDER QUANTIZER. The rank-order quantizer is a binary moving window in range that employs a distribution-free (nonparametric) decision process for hit/miss declaration. A functional block diagram of a typical rank order is depicted in figure 2. The fundamental concept of the ranking process is that a sample of radar video, called the target sample, which is the center tap of the delay line, is compared to other taps of the delay line. The tap spacing is established to provide two taps per an interval equal to the approximate radar transmitter pulse width, except for the tape adjacent to the target tap. For this case, a guard band on either side of the center tap is established which is equal to the transmitter pulse width. The number of cases where the amplitude of the target sample exceeds that of the individual noise samples is defined as the rank of the target samples. This rank is compared against a parameter called the rank threshold (T_R). When the target rank exceeds the T_R , a quantized hit is generated and is outputted to range binning logic.

DIGITAL TARGET GENERATOR TEST SET. The digital target generator test set (DTGTS) accepts, as an input, radar, triggers, and azimuth reference pulses (ARP's). It can be configured to generate pulses at predetermined range and azimuth-start locations, repeating these over a selectable number of adjacent sweeps. The pulses can then be used to trigger other test equipment or be applied as a control signal to a logical gate.

INPUT/OUTPUT PROCESSOR. The IOP is a general-type computer that provides for expansion of the computer memory core in 8,000-word modules. The system at NAFEC ASR-5 radar presently employs a memory size of 40,000 (40K) words. The IOP accepts azimuth words, target hit replies, and status information words from the beacon or radar data acquisition subsystems. It is used to perform statistical target detection, target tracking, display functions, and keyboard input functions from an operator, and outputs data functions to the ARTS III display and the online teletypewriter.

MOVING TARGET INDICATOR LOG VIDEO. The MTI logarithmic (log) receiver was developed by Westinghouse Corporation for the purpose of increasing the dynamic range of the MTI video. This increase is desirable to enable super-clutter visibility. That is, in the presence of medium-to-strong clutter, a receiver having a limited dynamic range will saturate, thereby decreasing the probability of detecting a target that would normally appear above the clutter level if limiting did not occur. The approach to this design was to utilize the bipolar output from the second radar canceller which has a 35-

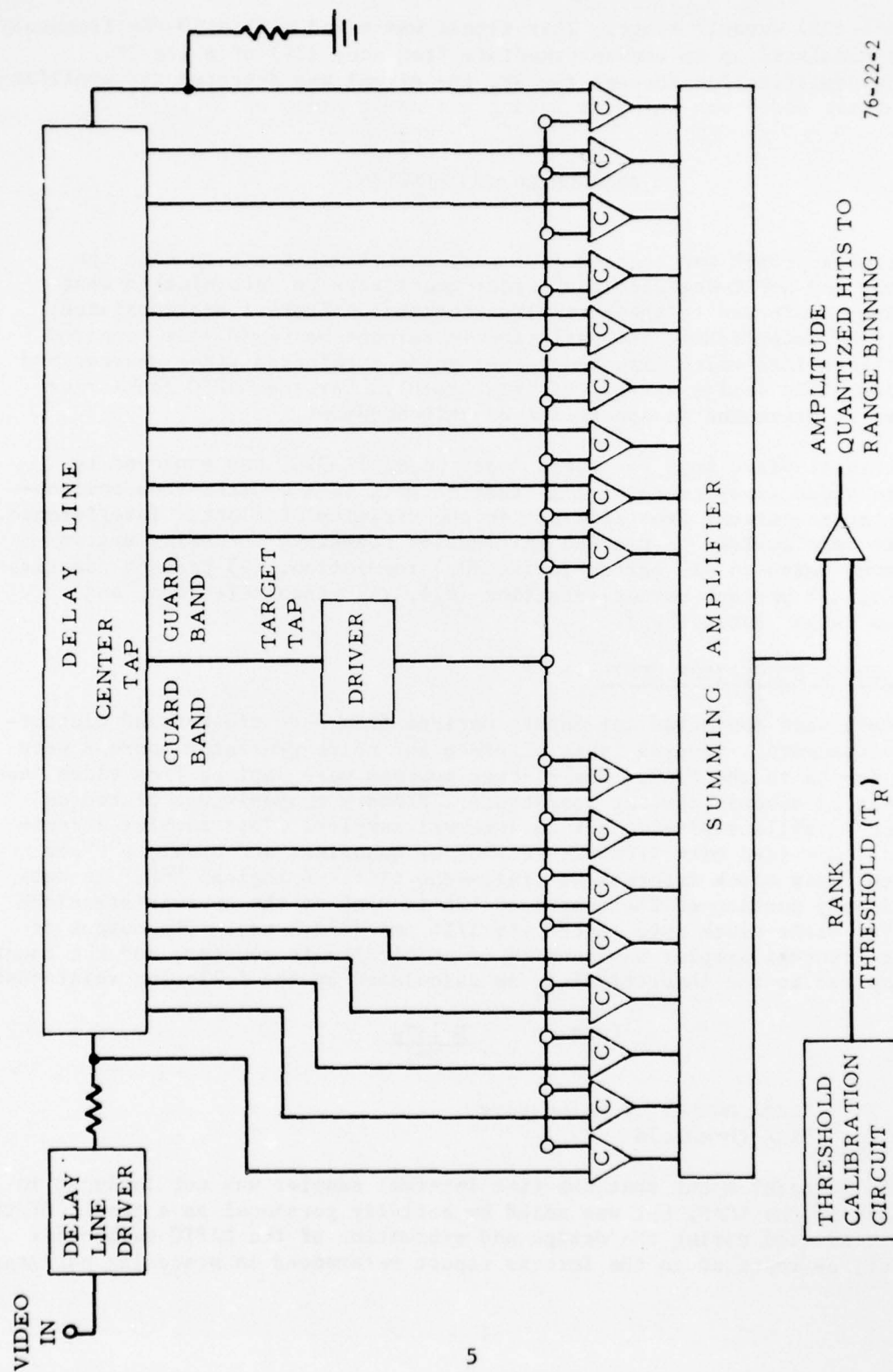


FIGURE 2. TYPICAL RANK-ORDER QUANTIZER

40-decibel (dB) dynamic range. This signal was mixed with a 30-MHz frequency and thus modulated up to the intermediate frequency (IF) of a log IF. Following amplification through the IF, the signal was detected and amplified. The resulting video was unipolar having a dynamic range of 35 to 40 dB.

PROCEDURES AND RESULTS

The initial approach was to conduct a series of bench tests on both the contractor and NAFEC-designed rank-order quantizers to determine to what extent they conformed to theoretical performance. These tests consisted primarily of establishing the variation in percent noise (P_N) as compared to the theoretical value experienced for various selected video sources and amplitudes. The design and circuit test results for the NAFEC rank-order quantizer is presented in appendix A of this document.

A dual-channel video tape recorder, Ampex model FR-950, was employed to reproduce video tapes containing RF test targets in a clutter-free environment or target returns from aircraft in the vicinity of clutter interference. The tests were devised to provide information necessary to define system performance based on (1) percent noise (P_N) regulation, (2) percent quantization (P_Q), (3) percent target detection (P_D), (4) video selection, and (5) false target rates (P_{fa}).

PERCENT NOISE REGULATION TESTS.

These tests were conducted for inputs derived from both clutter and clutter-free environments. Several types of video and noise generator sources were used as inputs to the RDAS. The clutter sources were derived from video tape recordings of several clutter conditions. Primary emphasis was placed on obtaining P_N while employing a time interval sampler. This sampler accepts amplitude-quantized hits from the rank-order quantizer and examines these hits once every clock interval at trail-edge time. A logical "ONE" is outputted if any portion of the quantized hit is high at the appropriate clock time. The basic clock rate tested was 1/16 nmi (772.5 ns). The output of the time interval sampler was counted on an electronic counter, and the counts were compared to the theoretical P_N as calculated by the following relationship:

$$P_N = \frac{N+1-T_R}{N+1}$$

where: N = Total number of noise taps
 T_R = Rank threshold

It should be pointed out that the time interval sampler was not included in the design of the RDAS, but was added by activity personnel as a result of the studies conducted during the design and evaluation of the NAFEC rank-order quantizer, as reported in the interim report referenced in preceding paragraphs

of this document. This design necessitated inclusion of a pulse-width standardizer that established a pulse width of $3/64$ nmi for each sampled hit. This circuit was necessary in order to defeat the operation of the RDAS hit-processing logic that was inherent in the design of the RDAS. This function included a minimum and maximum pulse-width discriminator. Therefore, to minimize the effect of the hit-processing function, a minimum and maximum hit of $1/64$ and $3/16$ nmi were employed, respectively.

CLUTTER-FREE ENVIRONMENT. Several modifications to the contractor-designed rank-order quantizer were accomplished by activity personnel in an attempt to upgrade its performance to that approaching theoretical operation. Tests were conducted prior to any modifications of the circuit design and were repeated after each modification. P_N results were obtained prior to any modification and also following incorporation of each circuit change. However, the results of each intermediate step are not presented in this report.

The following design changes were incorporated:

1. Diode networks were added to the summing function for each tap in order to provide equal transition time for both positive- and negative-going levels.
2. The input video signal to the delay line was alternating current (a.c.)-coupled in order to remove the direct current (d.c.) offset that was propagated down the delay line.
3. The weighting of the delay line taps was changed from a configuration based on d.c. attenuation to one established by measuring the attenuation characteristics for a 500-kilohertz (kHz) random noise source.
4. The analog and digital circuit grounds were isolated from each other to the extent that physical limitations would allow. This was accomplished to isolate the clock noise introduced by the digital circuits from the analog circuits.

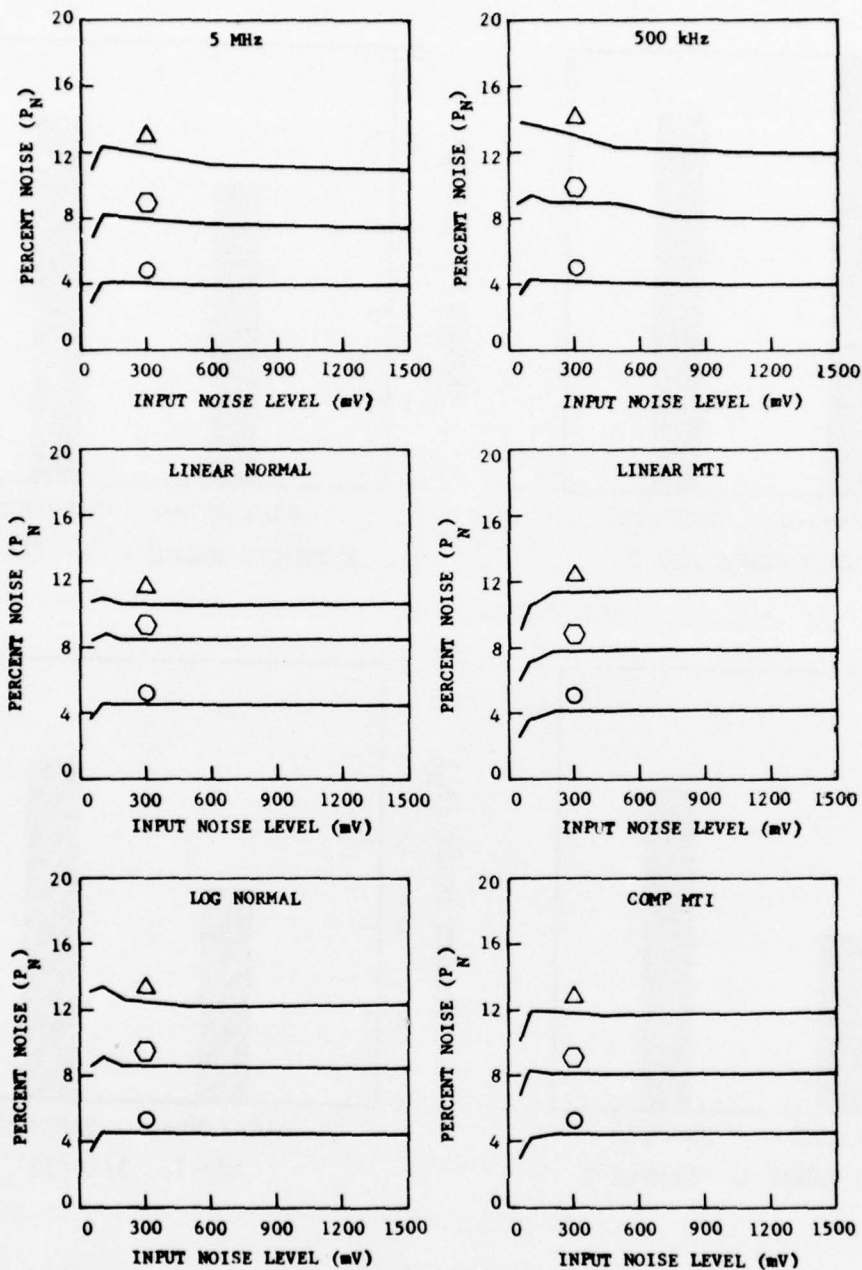
The values of P_N achieved with the contractor-designed quantizer, before and after circuit modifications, are presented along with the results for the NAFEC version for a $1/16$ -nmi time interval sampler in appendix B. Also included for some cases is the P_N achieved while employing the NAFEC rank-order quantizer with the original hit-processing function. The results are displayed as a function of system configuration, input noise source, and selected value of P_N . It is evident from these results that some improvement in P_N regulation for the contractors rank-order quantizer was achieved by incorporating the various modifications listed above. However, a strong dependency on input source still existed for the modified version. This was not the case for the NAFEC design, for which the P_N regulation for each test fell well within 10 percent of the selected value. The limited data for the rank-order quantizer with the RDAS hit processing indicates that a significantly greater deviation in P_N resulted with the RDAS hit processing as compared to that of the time interval sampler.

The next group of tests was conducted to determine P_N regulation as a function of input signal amplitude. These tests were performed for several types of noise sources and input amplitudes ranging from 50 millivolts (mV) to 500 mV. The results are presented in figure 3, as a function of input noise level, selected T_R , and noise source. It is evident from these data that acceptable regulation is achieved for all input levels exceeding 100 mV. For levels less than 100 mV, a rapid decrease is experienced.

CLUTTER ENVIRONMENT. A dual-channel video tape recorder was employed to reproduce several samples of radar returns of weather clutter derived from both the ASR-5 and ASR-7 radar. The ASR-5 video types that were processed included log normal, linear MTI, MTI log, and the extended range MTI. Those derived from the ASR-7 were log normal and digital MTI videos. It should be noted at this time that the digital-to-analog converter from the ASR-7 MTI employs a sample rate of 625 ns. The test environment was similar to that of the clutter-free tests, except that the input signals were derived from the video recorder. The P_N results for various weather samples are depicted in figures 4 and 5 for both a 1/16-nmi time interval sampler and the rank-order quantizer interfaced with the RVD-4 hit-processing function. When available, P_N results for normal and MTI videos are presented. Analyses of this information clearly indicate that the 1/16-nmi time interval sampler provides a lesser deviation from the selected value of P_N than the RVD-4 hit processing approach. Two samples of weather clutter were employed to obtain the relationship between selected and measured P_N over the full range of threshold for the NAFEC rank-order quantizer with a time interval sampler and with the hit-processing function. These results are depicted in figure 6 and indicated that only the time interval sampler approach produces a linear relationship.

P_N results for the total surveillance area which included weather clutter were obtained for both MTI and linear normal videos. The information is depicted in appendix C as histograms for several weather clutter samples. Analyses of these figures indicate that the measured P_N was well within 10 percent of the predicted value for T_R ranging between 17 and 24.

ISOLATED HITS. The initial design of the RPS included a weather monitor function that was designed to estimate azimuth correlation of weather clutter returns over a several-scan interval and then feed back a control signal to the rank-order quantizer to vary P_N on a zone basis. The objective of this function was to control the number of predetections and false targets that were processed by the IOP and subsequently transferred to the tracker. This technique was not formally tested, since initial investigation proved that P_N is not the primary factor in controlling false targets attributed to weather clutter. The principal cause of false targets is the azimuth correlation of the weather returns. Reference 1 indicates that P_{fa} could be controlled if appropriate second-threshold values were employed. In addition, an analytical study performed by APL resulted in findings that the weather monitor function actually worked in the reverse direction for values of single-lag correlation in excess of 0.5. Therefore, the logical approach was to develop a function that would dynamically select the appropriate second threshold, based on hit correlation necessary to achieve a predetermined false target rate.

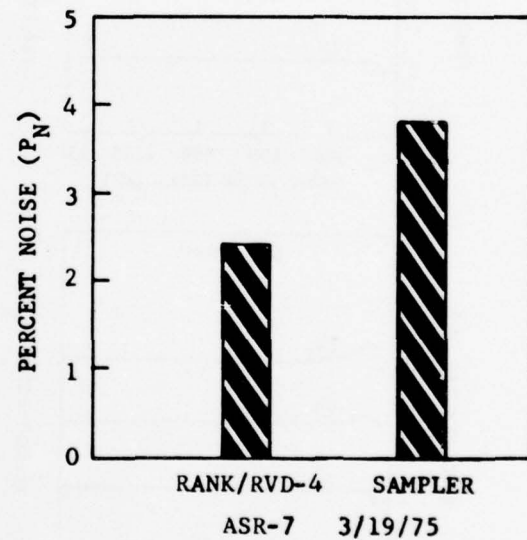
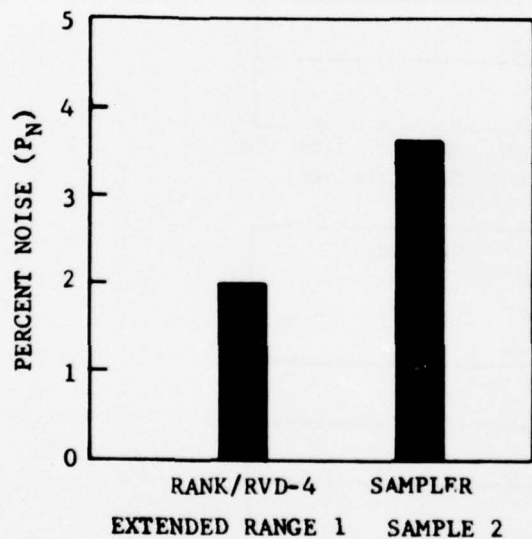
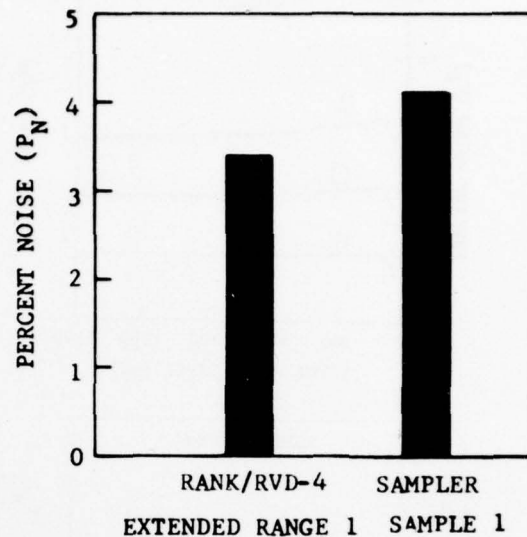
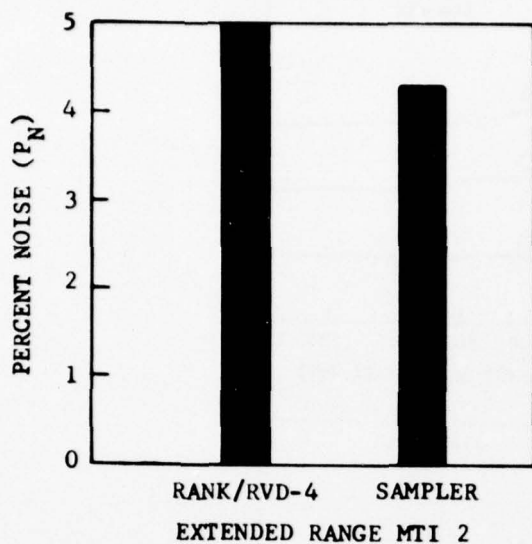


NOTES:
 MINIMUM PULSE-WIDTH DISCRIMINATION
 = $1/64$ NMI
 MAXIMUM PULSE-WIDTH DISCRIMINATION
 = $31/6$ NMI

○ 4% THEORETICAL P_N
 ⬡ 8% THEORETICAL P_N
 △ 12% THEORETICAL P_N

76-22-3

FIGURE 3. PERCENT NOISE VERSUS INPUT NOISE LEVEL



NOTES:

SELECTED $P_N = 4$ PERCENT

MINIMUM PULSE-WIDTH
DISCRIMINATION = $1/64$ NMI

MAXIMUM PULSE-WIDTH
DISCRIMINATION = $3/16$ NMI



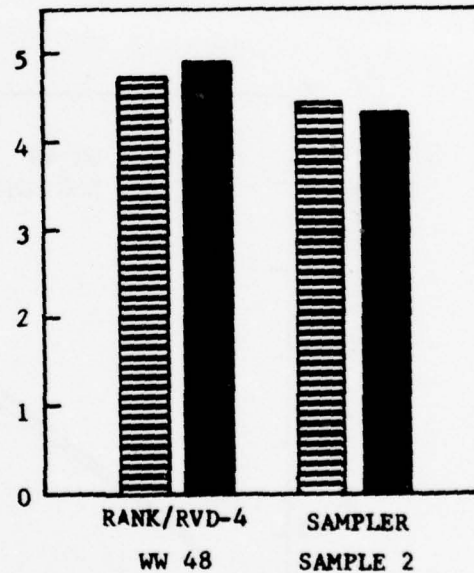
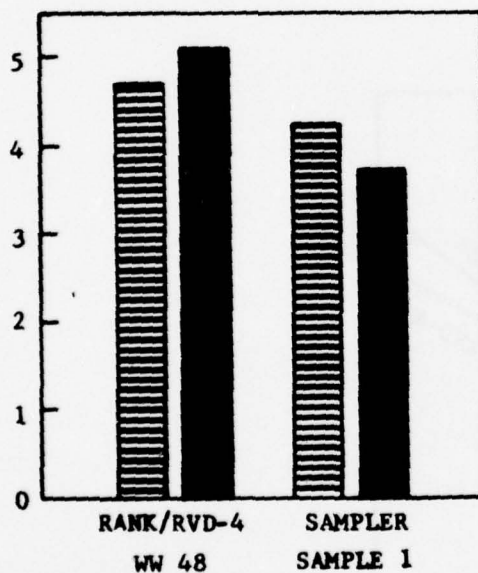
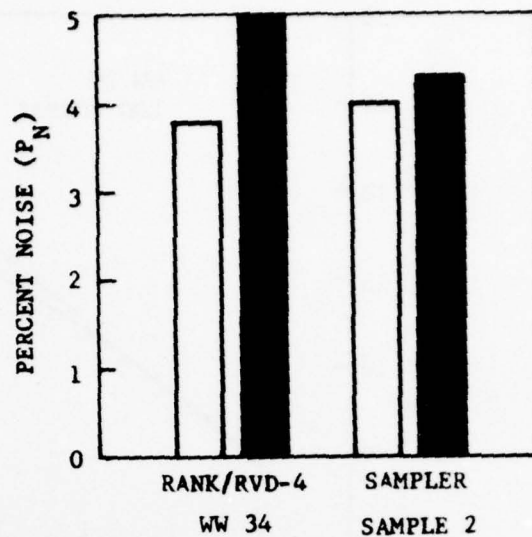
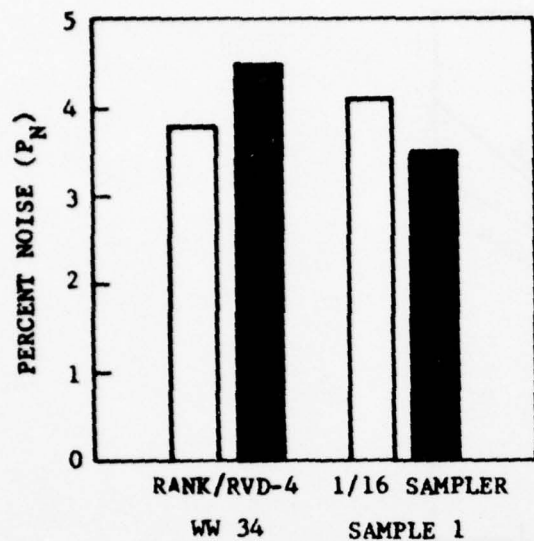
EXTENDED RANGE MTI



ASR-7 MTI

FIGURE 4. WEATHER NOISE REGULATION

76-22-4



NOTES:

SELECTED P_N = 4 PERCENT

MINIMUM PULSE-WIDTH
DISCRIMINATION = 1/64 NMI

MAXIMUM PULSE-WIDTH
DISCRIMINATION = 3/16 NMI

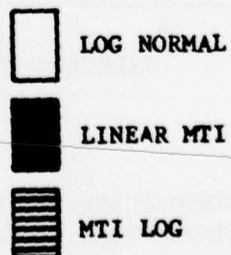
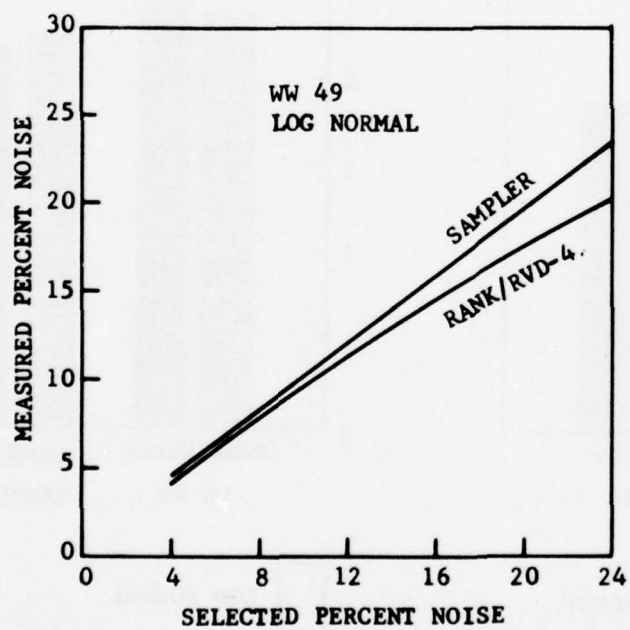
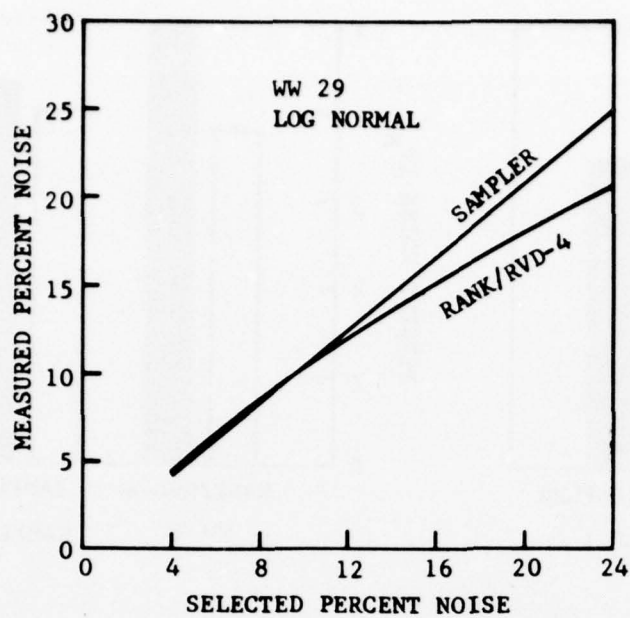


FIGURE 5. WEATHER NOISE REGULATION

76-22-5



NOTES:

MINIMUM PULSE-WIDTH DISCRIMINATION = $1/64$ NMI

MAXIMUM PULSE-WIDTH DISCRIMINATION = $3/16$ NMI

76-22-6

FIGURE 6. PERCENT NOISE VERSUS INPUT NOISE LEVEL

A study performed by UNIVAC Corporation resulted in a technique that established the value of the second threshold by measuring the occurrence of isolated hits within a zone. An isolated hit is defined as one that is not bounded by another hit at the same range cell on the two adjacent neighboring sweeps. The hit pattern for an isolated hit would then be "010." This technique was employed in the RPS by utilizing existing logic originally employed for the weather monitor function.

Utilization of the existing logic limited the accuracy of the isolated-hit count for each zone to only an estimate of the number of occurrences per zone. The actual process involved sensing the occurrence of an isolated hit on a sweep basis for a 2-nmi interval and summing, in azimuth, the number of occurrences for each zone. Recognition of isolated hits, on a sweep basis, is performed in the RDAS, and the azimuth summation is accomplished by the IOP software. Therefore, no more than one isolated hit per sweep, for each zone, can be recognized by the function. This is why the isolated-hit count is considered to be an estimated value. This was recognized as a potential limitation to system performance, and therefore it was deemed necessary to conduct tests that would define the relationship between the estimated and actual isolated hits. These comparisons were performed on a zone basis for several consecutive scans. The question also arose as to whether a more stable measurement could be performed for greater values of P_N . Since the number of predetections resulting from an increased value of P_N were in excess of the processing capability of the IOP program, a direct comparison between actual and estimated counts was not possible. A second reason was that the isolated-hit counter is a five-bit counter with a maximum count of 31. Therefore, for a P_N far in excess of 4 percent, this counter would be at maximum count for practically every zone sampled. The tests were conducted for zones containing hits resulting only from receiver noise, weather clutter, and targets of various signal levels for both normal and MTI video sources. Electronic counters were employed to simultaneously count the actual isolated hits for P_N values of 4 and 32 percent. At the same time, the estimated values of the isolated-hit count for a P_N of 4 percent were acquired via a software subroutine inserted into the RPS program.

Prior to presenting the results of these tests, it seems appropriate to discuss the use of the isolated-hit counts so that the reader may have a better understanding of the importance of these tests. Briefly, the isolated-hit count is employed on a zone basis to develop the appropriate second threshold to be employed in each individual zone. Previous evaluation of radar processors has clearly indicated that false-alarm control is only a problem in weather clutter environments and that MTI video results in a fewer number of false targets within a weather clutter environment than that experienced when employing normal video returns from the same weather clutter zone sampled. As a result, it was decided to operate the RPS in a configuration that would select MTI video in weather clutter areas and apply second-threshold control for those zones within the boundaries of the weather clutter.

With these basic ground rules established, the specifics of the function implemented to perform second-threshold control can be addressed. The isolated hits are employed to derive the required second-threshold value according to the following relationship:

$$T_L = T_O + A(C_O - C)$$

where: $A = \frac{\text{window length} - T_O}{C_O - C_{wl}}$

T_O = Base T_L used in clutter-free environment

C_O = The value of isolated hits for which second-threshold control is enabled

C_{wl} = Value of isolated hit for which T is forced to a value equal to the window length

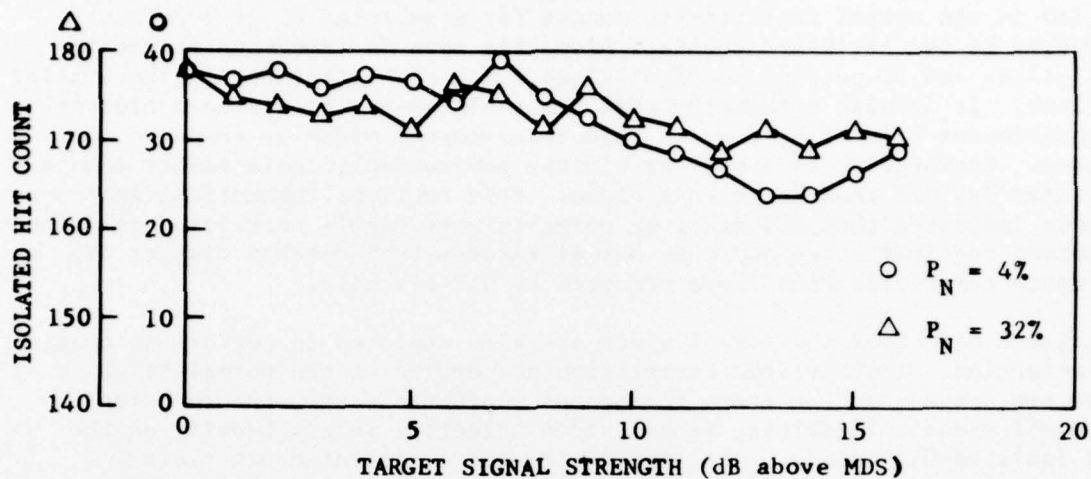
This function is a simple straight-line relationship. The theoretical value of isolated hits, for uncorrelated returns, within a zone is given by:

$$\text{Isolated Hits} = (\text{Range Cells/Zone}) (1 - P_N)^2 P_N$$

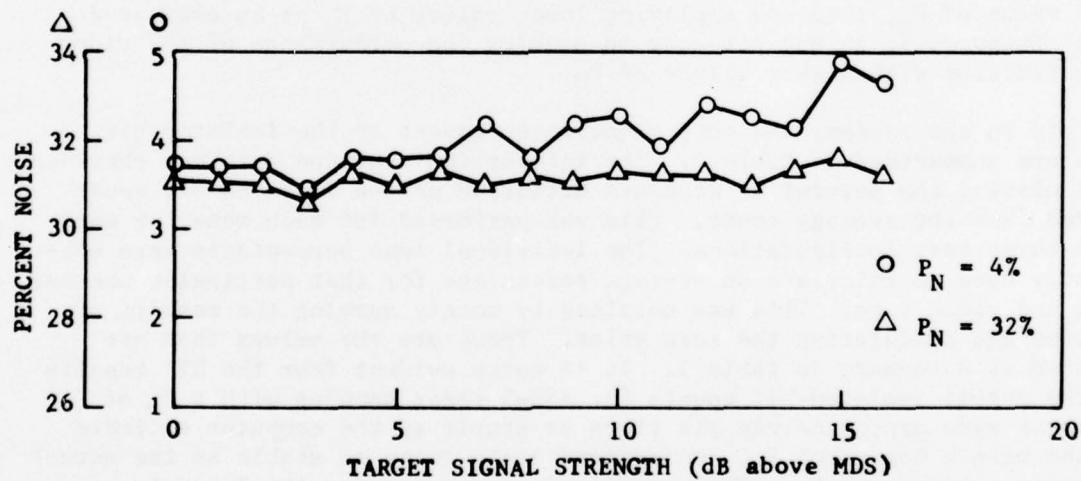
With this in mind, the value of isolated hits is directly proportional to the value of P_N in each zone. The reader should also recall that P_N varied considerably when employing the RDAS hit-processing function. Therefore, it was decided that data would be collected for only time interval sampled rank-order quantized hits for which a fairly constant P_N could be achieved. The main point here is that the second threshold should be established based on correlation properties of the clutter and not variations in P_N . Although isolated-hit data with the RDAS hit-processing function are not presented here, its effect on other aspects of system performance will be discussed in subsequent topics within this document.

From the results of targets on isolated-hit counts (shown in figure 7), the isolated-hit count for either of the configurations is inversely proportional to the signal level. This is particularly true for a selected value of P_N of 4 percent. Specifically, the drop in isolated-hit counts for a 4-percent P_N was approximately 30 percent over the full range of signal levels (0-15 dB above MDS). The corresponding results for a P_N of 32 percent was only a 3-percent change. The effect that target strength had on P_N is indicated by the curves in figure 7B. For a selected P_N of 4 percent, the zone P_N increased from approximately 3.89 to 4.9 percent as the signal level increased from 0 to 15 dB.

This was not the case for the selected value of 32 percent for which no virtual change in measured P_N was experienced.



A. ISOLATED HIT COUNT VERSUS TARGET SIGNAL LEVEL



B. PERCENT NOISE VERSUS TARGET SIGNAL LEVEL

76-22-7

FIGURE 7. EFFECT OF TARGET IN ZONE

Observing the isolated-hit counts for several weather samples shown in appendix D-1 through D-31 indicates that, percentage-wise, there was a lesser deviation in the actual isolated-hit counts for a selected P_N of 4 percent as compared to the estimated counts. Also, the same is true when comparing the actual 4- and 32-percent configurations, with the latter having the smaller deviations. It is also noteworthy that the isolated-hit counts in a clutter-free environment tend to be greater values for normal video as compared to MTI video. Conversely, in a weather clutter environment, isolated-hit counts are greater for MTI than for normal video. This confirms theoretical analyses that have indicated that MTI receiver noise is more highly correlated in azimuth than normal receiver noise and that normal returns from weather clutter are more highly correlated than those produced by MTI circuits.

The isolated hits from the normal video are also employed to perform automatic video selection. That is, the correlation properties of the normal video clutter are sensed, and in those regions of weather clutter, the function selects MTI video. Therefore, proper video selection relies heavily on the normal isolated-hit values. Analyses of the normal isolated-hit plots indicate that the variation in isolated-hit count from scan to scan for the actual counts was less than that achieved for the estimated counts. In addition, the actual counts for a P_N of 32 percent had the least deviation as compared to 4 percent P_N cases. This would tend to indicate that a video selection function based on isolated-hit counts should be more stable, using a high value of P_N , than one employing lower values of P_N or an estimated count. However, it is not possible to predict the performance of the video select function with higher values of P_N .

As an aid to the reader, the most significant aspect of the isolated-hit curves are summarized in table 1. The information provided here was obtained by calculating the percent of standard deviation of the isolated-hit count differed from the average count. This was performed for each zone for each of the three test configurations. The individual zone percentages were subsequently used to calculate an average percentage for that particular weather sample and video type. This was obtained by merely summing the results of each zone and calculating the mean value. These are the values that are presented as a summary in table 1. It is quite evident from the MTI results that the actual isolated-hit counts for ASR-5 radar samples with a P_N of 32 percent were approximately six times as stable as the computer estimate obtained with a 4-percent P_N , and approximately twice as stable as the actual counts for a 4-percent P_N . The corresponding results for ASR-7 samples indicate that the actual 32-percent counts were approximately 2 and 3 times as stable as the 4-percent computer and actual counts, respectively. In general, the normal isolated-hit counts fluctuated approximately 1.4 times as much as those yielded by MTI video.

TABLE 1. SUMMARY OF ISOLATED-HIT RESULTS

Sample	MTI			Normal		
	Actual ISH P _N =32%	Actual ISH P _N =4%	Computer Estimate P _N =4%	Actual ISH P _N =32%	Actual ISH P _N =4%	Computer Estimate P _N =4%
WW29	6%	10.8%	43.7%	10.1%	20.1%	62.1%
Extended Range MTI No. 2	5.1%	11.4%	22%	9.8%	16.7%	48.8%
Angel	5.2%	9.8%	29%	4.2%	11.7%	38.6%
WW34	5.2%	12.2%	30.6%	5.2%	18%	35.2%
WW49	4.7%	11.8%	29.3%	6.5%	14.5%	36.4%
Average ASR-5	5.24%	11.2%	30.9%	7.2%	16.2%	44.2%
3/12/75	4.8%	11.7%	15.1%	5.3%	10.0%	12.3%
4/15/75 A.M.	4.1%	8.7%	23.5%	5.2%	18.5%	48.9%
4/15/75 P.M.	4.7%	9.9%	8.8%	7.6%	13.9%	17.5%
4/3/75	6.9%	15.9%	24.3%	8.9%	18.7%	27.2%
7/14/75 A.M.	5%	9.8%	10.9%			
Average ASR-7	5.1%	11.2%	16.5%	6.7%	15.3%	26.5%

PERCENT QUANTIZATION AND DETECTION TESTS.

These tests were conducted to determine the percent quantization and detection of test targets generated in a clutter-free environment and to define detection of live targets which prevailed in areas of weather clutter. For some cases, data for both a 1/16-nmi time interval sampler and the RDAS bit-processing approach were obtained. The signals employed for these tests were derived from the ASR-5 and ASR-7 radar. To provide repeatability of input data, the Ampex FR-950 video tape recorder was utilized to record and reproduce each source of input video.

CLUTTER-FREE TESTS.

An RF test target generator, having a beam-modulated pattern, was employed to generate targets of various signal levels. Since statistical detection is based on range cells, there are positions relative to cell boundaries that produce optimum to poor detection. For this reason, it was felt that more meaningful data could be obtained if the test targets moved in range by some interval which was not a multiple of the digitizer clock frequency. This was accomplished by employing the moving target feature of the RF test target generator. It was necessary to generate four rings of test targets, each separated in range from the preceding target by approximately 3.75 nmi, to provide an adequate sample size and to permit recording of a full data run of RF levels for a particular video tape. It should be reemphasized at this time that the position of each target was established at a range that was not an interval of the RDAS clock frequency. The velocity of each ring was adjusted for the first optimum phase of the radar under test. The resulting velocities were approximately 75 and 43 knots for the ASR-5 and ASR-7, respectively. The ASR-5 was employed in a nonstaggered mode, while the ASR-7 was configured for a pulse repetition frequency (PRF) stagger. The PRF values and sequence are presented in table 2. An azimuth trigger which occurred 32 times per scan (bit 7 of the RDAS azimuth counter) was used to generate 32 test targets per scan at the same range for each of the four rings. Therefore, for each test target level, 32 samples for each range position were available yielding a total sample size of 128 targets per scan.

The RF test target was injected into the directional coupler of the radar set which was placed offline with the transmitter firing into a dummy load. The type of video under test was then applied as an input to the video recorder. The test target velocity range triggers, radar pretrigger, azimuth change and reference pulses (ACP's and ARP's), and time code were also recorded on tape. The recording consisted of target levels that ranged from 0 to 15 dB above minimum discernible signal (MDS), independently established for each receiver, in 1-dB steps. For each test target level, 15 scans of data were recorded. The velocity range triggers were AND'ed with RVD-3 test target signals to establish azimuth windows having a duration of 18 sweeps centered at the azimuth at which the theoretical peak signal of the RF targets occurred.

TABLE 2. ASR-7 PRF SEQUENCE

<u>PRT</u>	<u>PPF</u>
1403	713
953	1050
893	1120
853	1173
1053	950
833	1200

The reproduced velocity-range triggers were applied to a pulse-delay generator to line up the triggers with the range-binned hits resulting from the test targets. The four range pulses out of the generator were then AND'ed with the range-binned hits to provide percent quantization data. The range extent of each pulse was adjusted to 750 ns (1/16 nmi). The procedure was accomplished for each video source to compensate for differences in system delay. Therefore, each pulse provided a range-azimuth gate centered about the test target in both range and azimuth as it moved radially each scan. An electronic counter was employed to count the output of the gate for each 15-scan test interval. These counts were used to calculate percent quantization (P_Q) for each video and hit-processing scheme. The following relationship was applied to obtain the required information:

$$P_Q = \frac{\text{Actual number of hits in window}}{\text{Maximum possible hits in window}} \times 100$$

Therefore,
$$P_Q = \frac{\text{Number of hits for 32 windows}}{32 \text{ windows} \times 18 \text{ hits/window}} \times 100$$

The number of test target detections that resulted for each test configuration were obtained via a software modification to the IOP RPS program. The average number of targets detected for each target level were printed on the teletype at the end of each run. The program provided for automatic start and termination of each data set. These data were employed to calculate percent detection (P_D) as follows:

$$P_D = \frac{\text{Average number of test targets detected per scan}}{128 \text{ possible targets}} \times 100$$

Prior to collection of detection data, it was necessary to adjust the threshold of the predetector and software sliding-window detector for each test configuration to the value that resulted in a false target rate of approximately 1×10^{-5} . The tests were then conducted for predetection and final-detection thresholds to provide a sufficient number of data points to derive plots of P_D versus false targets.

The video tapes containing the 128 moving targets for each video source were reproduced and both P_Q and P_D were obtained. The various configurations tested were (1) log or linear MTI, (2) rank-order quantizer or thermal noise meter, (3) RDAS hit processing or a 1/16-nmi time interval sampler, and (4) employment of a double-hit generator with the thermal noise meter. It should be noted that the antenna rate for the ASP-5 video sources was approximately 15 revolutions per minute (r/min) and, for the ASP-7 tests, the rate was 12.75 r/min. Additionally, the fixed PRF of the ASP-5 is 1030 pulses per second, and the average PRF for the staggered ASP-7 triggers per ACP was not the same for the two systems. This would result in a different number of expected hits per antenna beam width. With the above in mind, changes to the test target generator were necessary to match the beam shape of the test target to that of a point target in space (a two-way Gaussian return). An additional requirement levied on this activity was to conduct comparison tests between the RPS with inputs derived from the ASP-7 and the moving target detector, developed by Lincoln Laboratories. This system employed an FPS-18 radar set that had an average PRF of 1240. It was decided to conduct the ASP-7 RPS portion of the comparison tests in two ways: (1) match the number of replies per beam width for the two systems, and (2) simulate the actual hit pattern expected from an ASP-7 point source.

The first group of results is presented in figure 8 for which the P_Q -versus-test-target signal level is plotted for the RDAS hit-processing logic, with a 1/64- and 2/64-nmi minimum pulse width criteria for ASP-5 linear MTI video.

The selected P_N was 4 percent, with a resulting P_N of 4.8 and 2.4 percent for a 1/64- and 2/64-nmi minimum pulse width, respectively. These results indicate that there was a 1.5- to 2-dB loss introduced by employing a 2/64-nmi minimum. Unfortunately, no data are available for P_Q while employing a 1/16-nmi sampler. However, sensitivity comparisons for P_D will be presented in subsequent paragraphs.

The P_Q achieved for ASP-7 log normal and linear MTI is presented in figures 9 and 10, respectively. Both the 725 and 825 azimuth step interval results are depicted for a 1/16-nmi time interval sampler. It is evident that approximately a 1- to 2-dB increase in sensitivity is achieved with a step interval of 825 versus that obtained for a 725 interval. The plots also show that MTI video is on the order of 2 dB less sensitive than log normal video. It can also be seen that there is a significant increase in overall sensitivity for the ASP-7 videos as compared to the ASP-5. This is attributed primarily to the increase in the number of hits per beam width generated by the test generator for the slower antenna rotation rate of the ASP-7 signals.

Attention can now be turned to the results obtained to define P_D as a function of predetection and final-detection thresholds, and hit-placement techniques. The first set of results was obtained to define the relationship between P_D and P_{fa} for varying values of T_L and predetection thresholds. A more exact comparison as performed between the various configurations can be accomplished by plotting P_D versus false target rates for specific signal levels. More than one point is obtained by plotting the false target rate

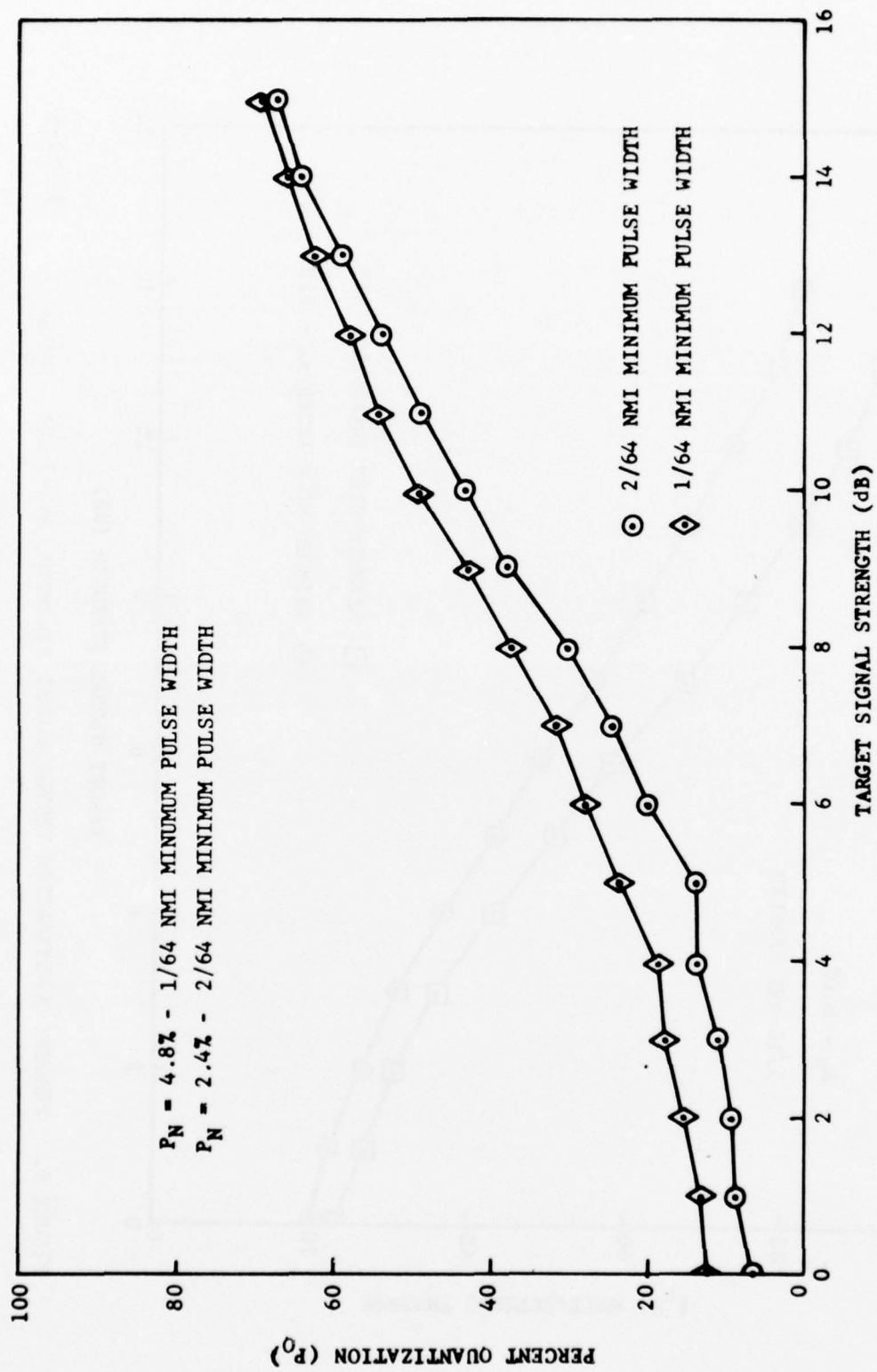


FIGURE 8. PERCENT QUANTIZATION VERSUS TARGET SIGNAL LEVEL, ASR-5 LINEAR MTI

76-22-8

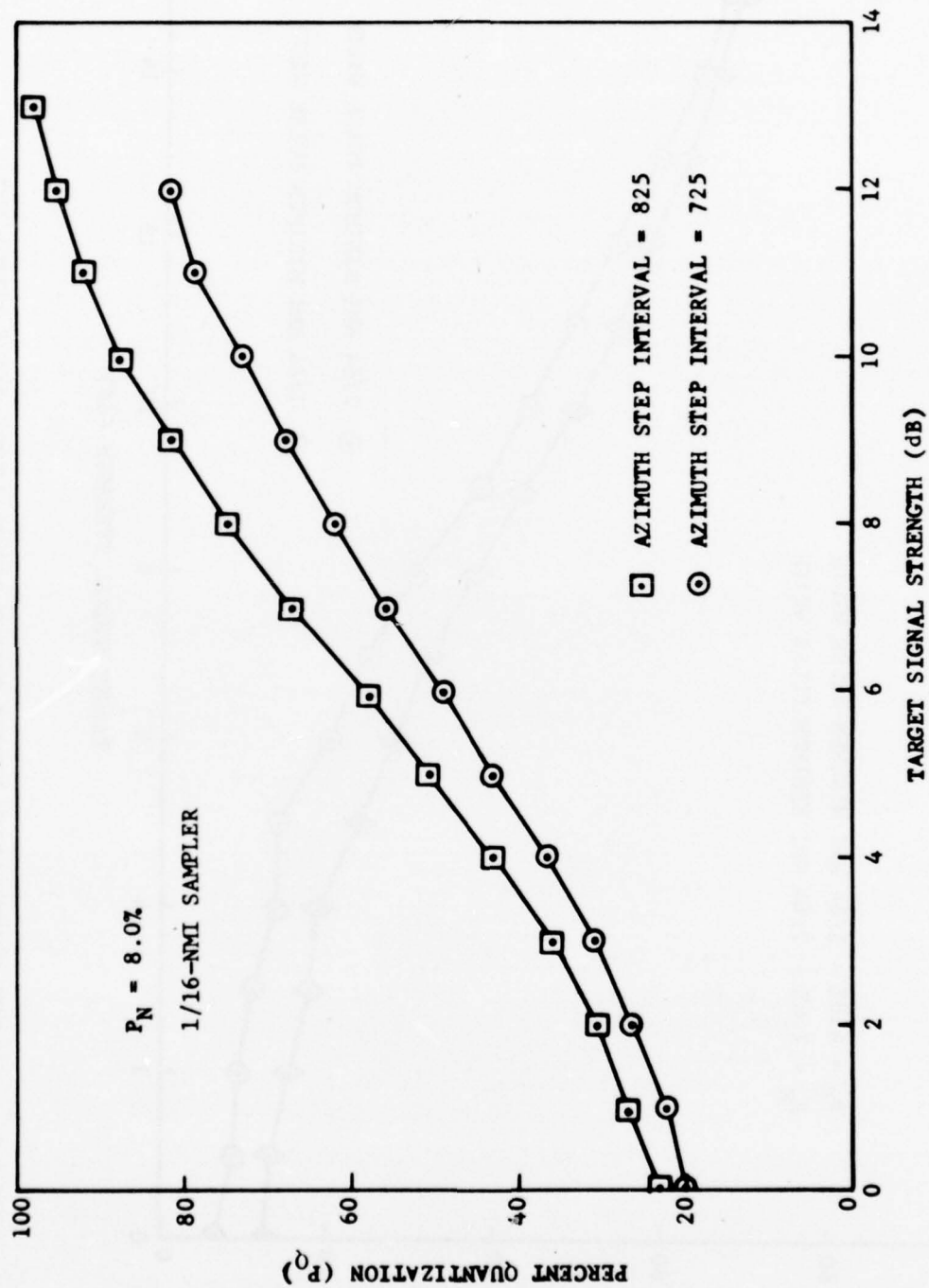
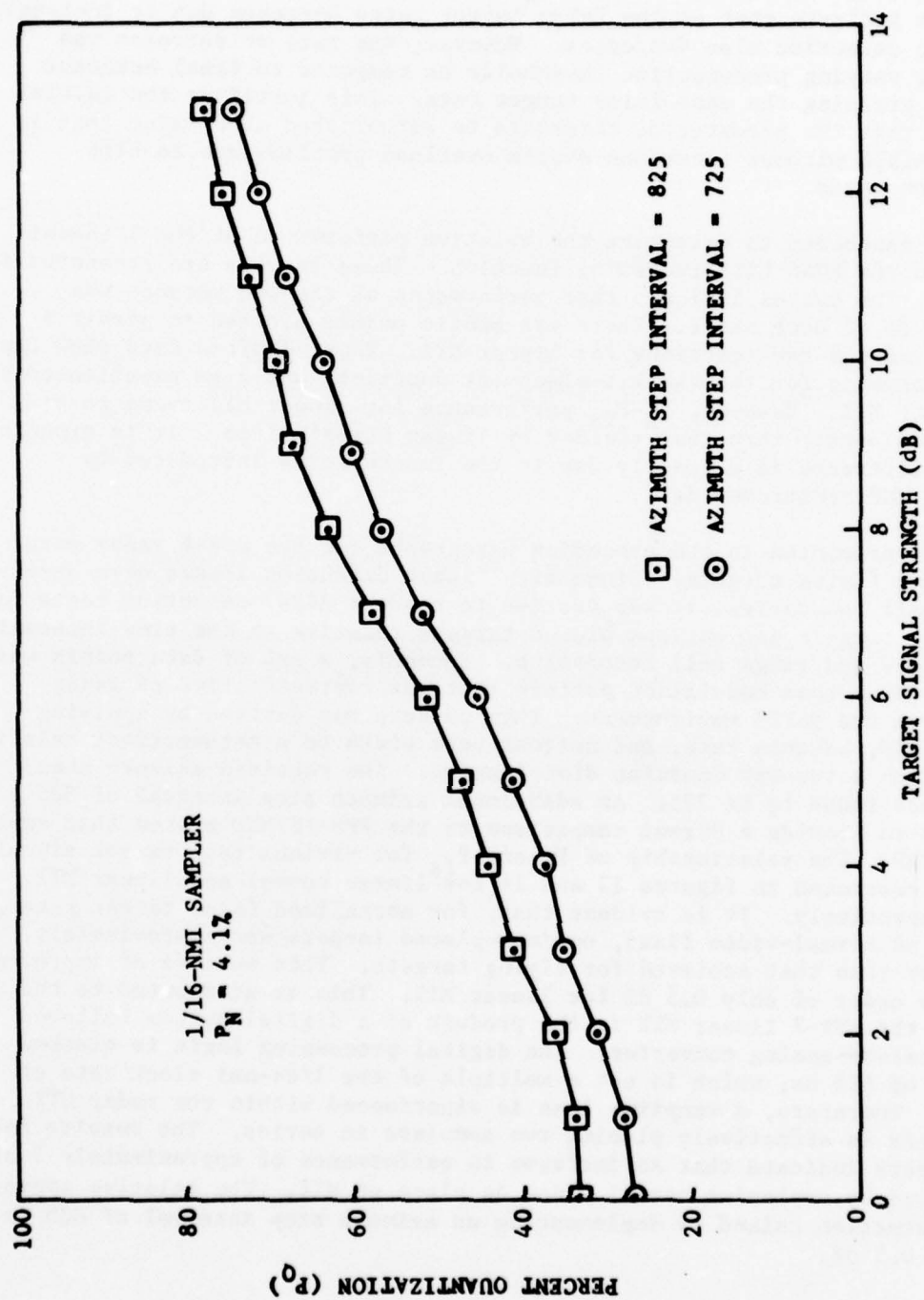


FIGURE 9. PERCENT QUANTIZATION VERSUS SIGNAL STRENGTH, ASR-7 LOG NORMAL

76-22-9



76-22-10

FIGURE 10. PERCENT QUANTIZATION VERSUS SIGNAL LEVEL, ASR-7 LINEAR MTI

and P_D for several values of T_L or predetection threshold for the same signal level. The P_D - P_{fa} results are plotted in figure 11 for ASR-5 log normal video. The data were obtained for a P_N of 8 percent with the 1/16-nmi sampler. The results indicate that as the false target rates decrease due to increasing thresholds, detection also decreases. However, the rate of decrease was greater for varying predetection thresholds as compared to final detector thresholds yielding the same false target rate. This justifies the initial philosophy that the predetector threshold be established at a value that is the lowest possible without incurring system overload problems due to high predetection rates.

Tests were conducted to determine the relative performance of the 1/16-nmi sampler and the RDAS hit-processing function. These results are presented in figure 12. The curves indicate that performance of the two methods was within 0.5 dB of each other. There are single points plotted to permit a comparison of the two functions for linear MTI. These limited data show that equal performance for the two hit-placement functions was also experienced for ASR-5 linear MTI. However, P_D - P_{fa} performance for linear MTI seems to be about 1.5 dB better than that yielded by linear normal video. It is expected that the difference is primarily due to the inaccuracies introduced by performing MDS measurements.

The results presented in the preceding paragraphs for the ASR-5 radar were obtained for flying targets. Since significant detection losses were observed at range cell boundaries, it was decided to conduct ASR-7 detection tests for both flying targets and optimum placed targets relative to the time interval sampler clock and range cell boundaries. Secondly, a set of data points was collected for a beam modulation pattern that was representative of radar returns from the NAFEC environment. This pattern was derived by applying the radar PRF, antenna rate, and antenna beam width to a mathematical relationship based on a two-way Gaussian distribution. The required azimuth step interval was found to be 725. An additional azimuth step interval of 825 was tested to provide a direct comparison to the FPS-18/MTD system that employed a higher PRF. The relationship of P_D and P_{fa} for various test target signal levels is presented in figures 13 and 14 for linear normal and linear MTI, video, respectively. It is evident that, for normalized false target rates, detection of normal-video fixed, optimum-placed targets was approximately 2 dB better than that achieved for flying targets. This measure of improvement was on the order of only 0.5 dB for linear MTI. This is attributed to the fact that the ASR-7 linear MTI is the product of a digital system followed by a digital-to-analog converter. The digital processing logic is clocked at a rate of 625 ns, which is not a multiple of the 1/64-nmi clock rate of the RDAS. Therefore, a sampling loss is experienced within the radar MTI logic. This is effectively placing two samplers in series. The results for fixed targets indicate that an increase in performance of approximately 2 dB was achieved by employing normal video in place of MTI. The relative improvement in detection gained by implementing an azimuth step interval of 825 is less than 0.5 dB.

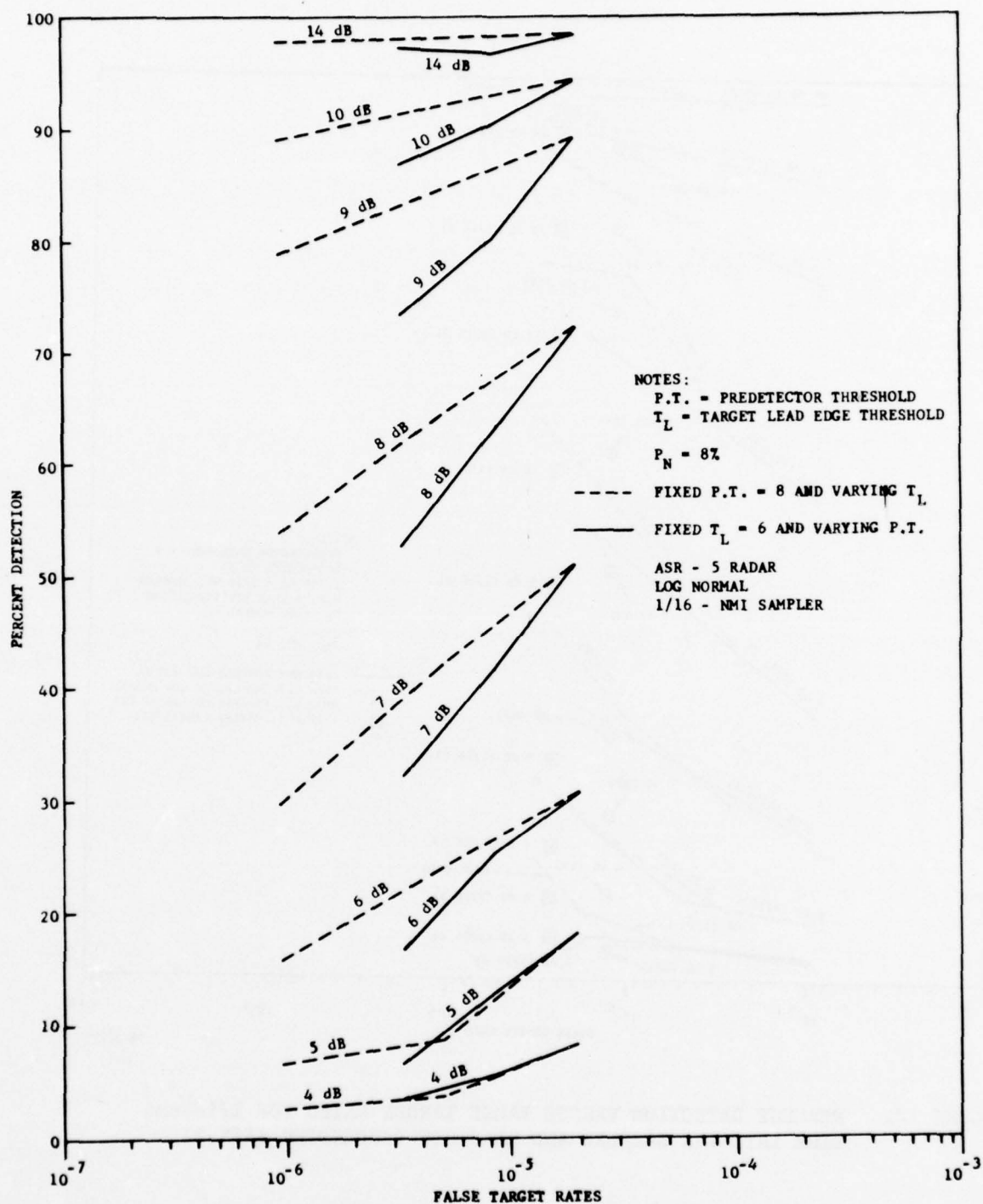


FIGURE 11. PERCENT DETECTION VERSUS FALSE TARGET RATES AS A FUNCTION OF PREDETECTOR AND FINAL DETECTOR

76-22-11

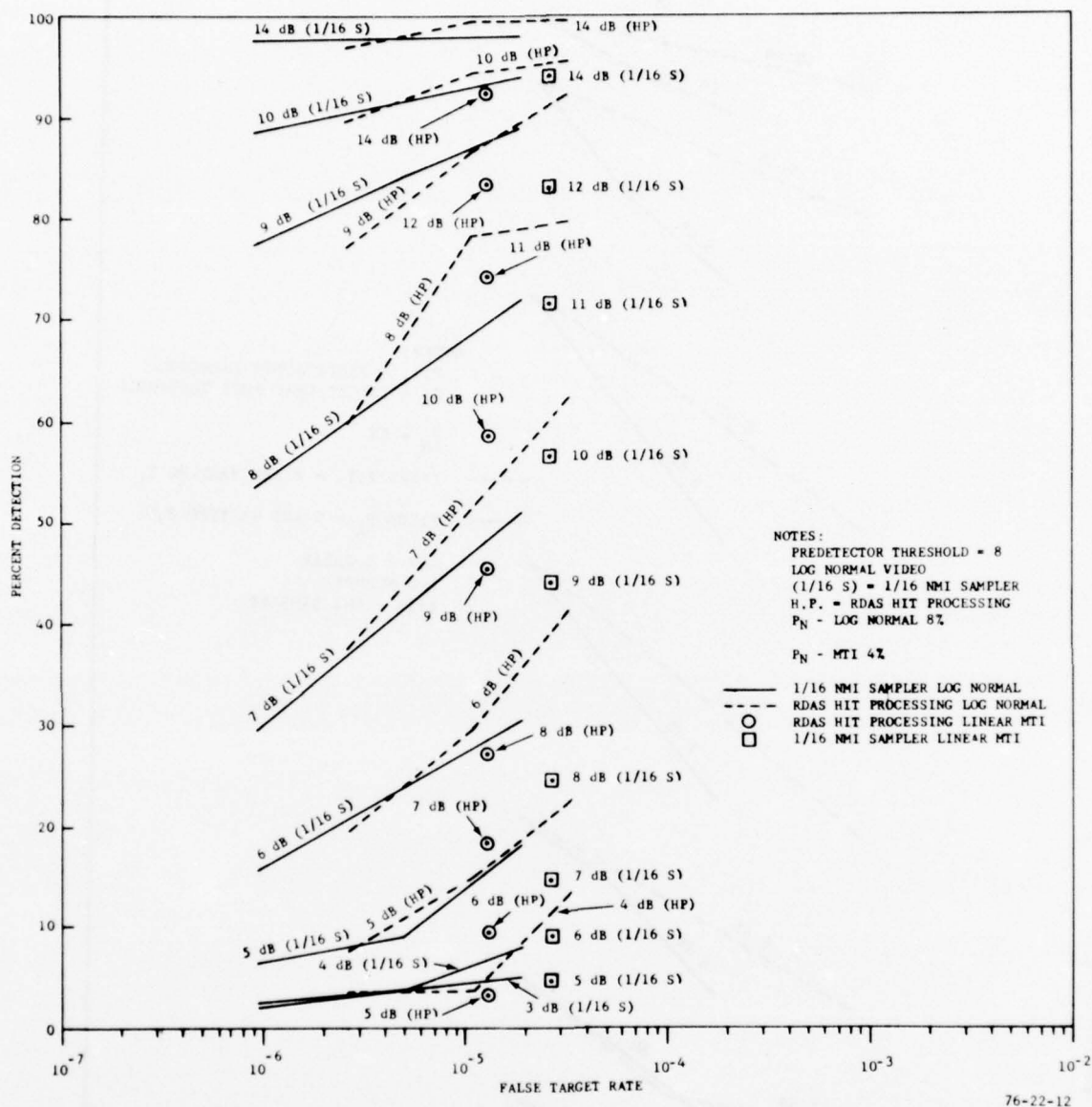


FIGURE 12. PERCENT DETECTION VERSUS FALSE TARGET RATES FOR 1/16-nmi TIME INTERVAL SAMPLER AND RDAS HIT PROCESSING (ASR-5)

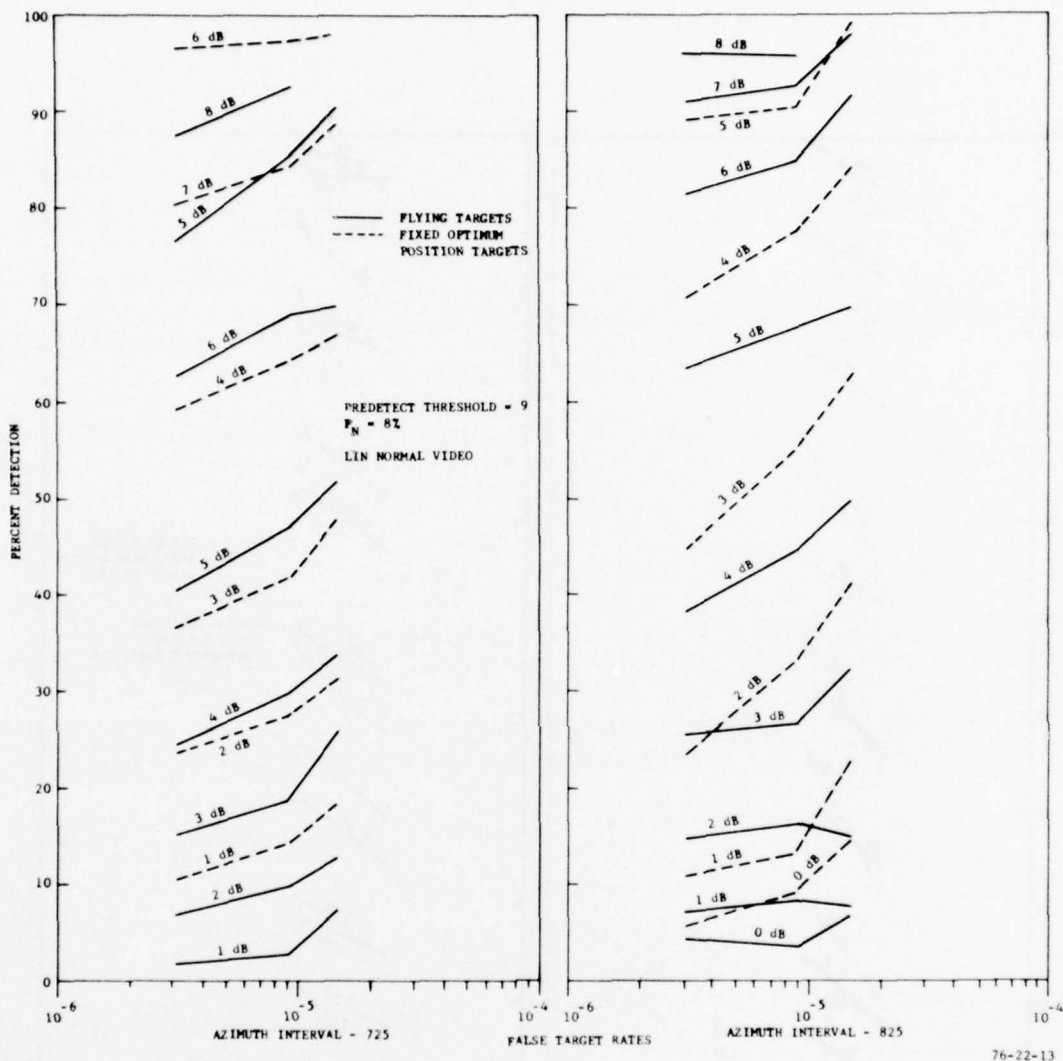


FIGURE 13. PERCENT DETECTION VERSUS FALSE TARGET RATES FOR FIXED-POSITION AND FLYING TARGETS (ASR-7, LINEAR NORMAL)

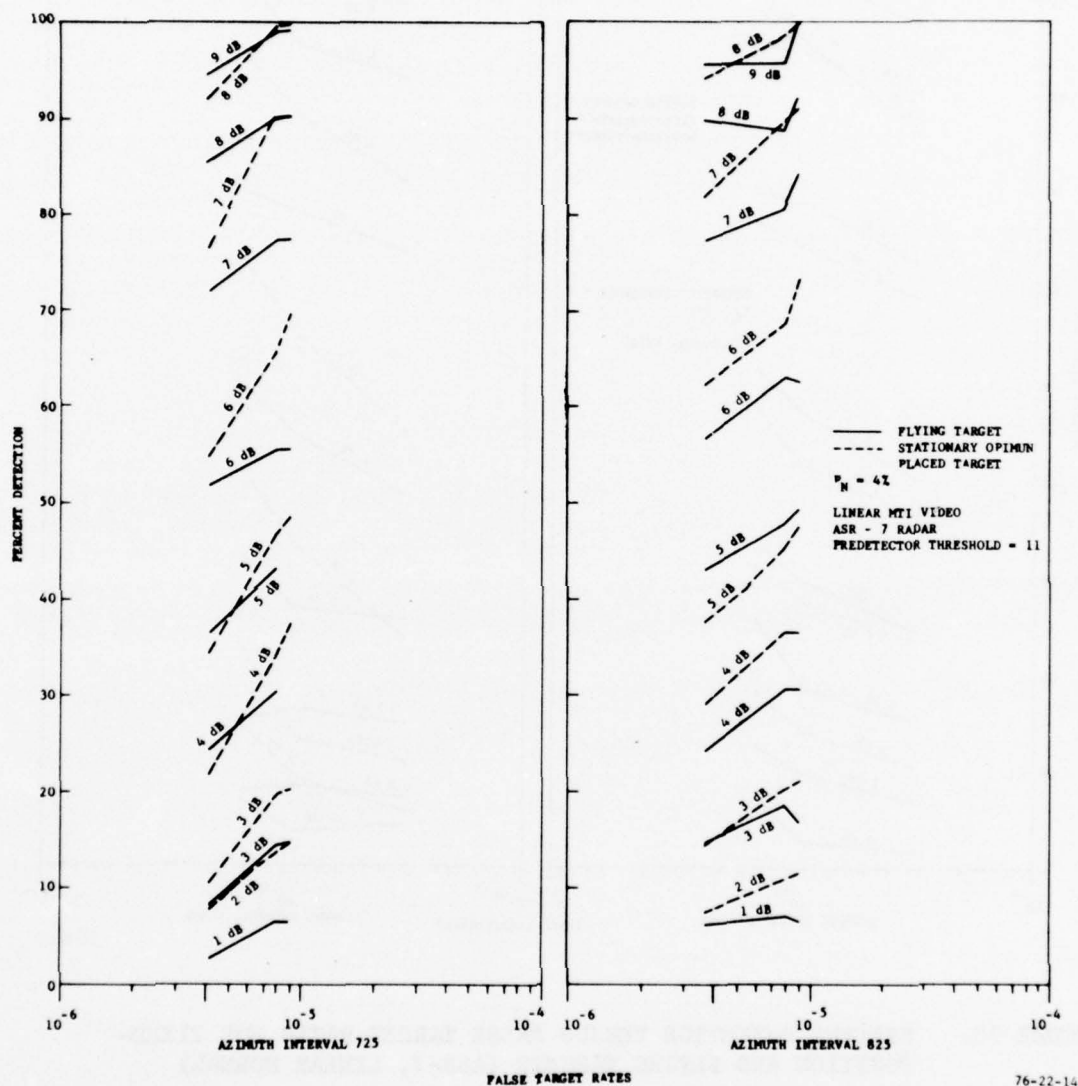
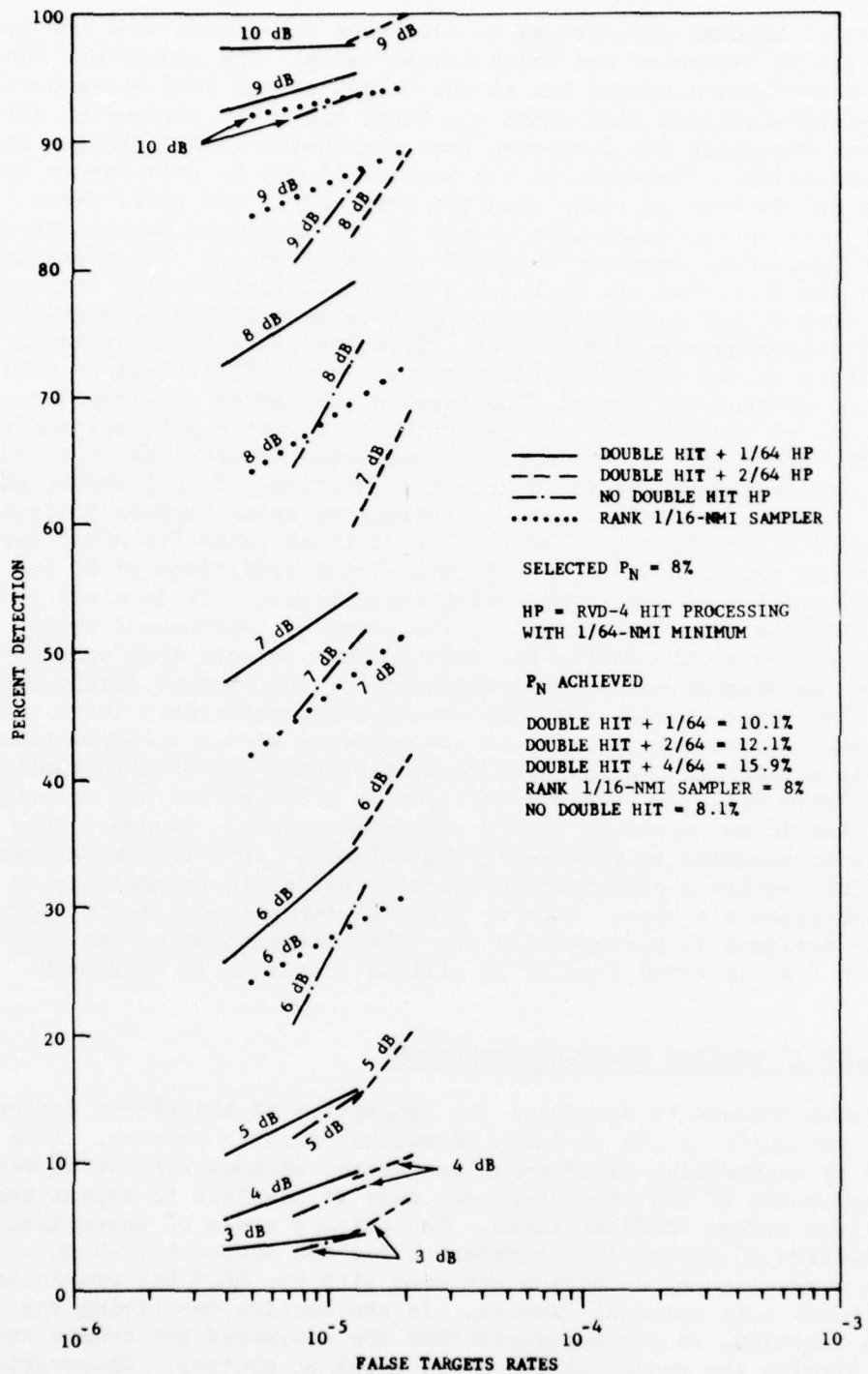


FIGURE 14. PERCENT DETECTION VERSUS P_{fa} FOR FLYING AND FIXED POSITION TARGETS (ASR-7, LINEAR NORMAL)

The next phase of testing was devised to determine the effect that the double-hit function had on detection and false target rates. The double-hit function is provided to generate a second hit at the output of the RDAS hit-processing logic at some predetermined time after the first hit. The purpose of this function is to compensate for detection loss attributed to hit sharing at range-cell boundaries. Placement of the second hit may be selected to 1/64, 2/64, or 4/64 nmi further in range than the first hit. The tests were conducted for each of the selectable values of hit placement except for the 4/64-nmi position, since computer overload was experienced. The overload was attributed to the fact that the double-hit function synthetically increases P_N . The measured P_N for a selected value of 8 percent with a 4/64-nmi hit-placement was approximately 15.9 percent. This indicates that for each legitimate hit, a second synthetic hit occurred in an adjacent range cell. It should be noted that the target finalization subprogram combines two targets into one if the range of the two targets is within 1/16 nmi and their center azimuths are within 11 ACP's. This mechanism is provided to reduce the number of splits introduced by the double-hit function. Establishment of false target rates is accomplished by measuring the false targets following this range/azimuth correlation. The results of these tests for ASR-5 log normal inputs are depicted in figure 15 as a direct comparison of P_D and P_{fa} for a selected P_N of 8 percent. Observing these results, it is clear that when normalizing the false target rates, the level of improvement in P_D achieved when employing the double-hit function was no more than approximately 0.5 dB. This improvement was only experienced for test target levels between 6 and 8 dB. For other levels, the improvement was considerably less. In addition, a more pronounced improvement was achieved with a 2/64-nmi placement as compared to a 1/64-nmi condition. The primary drawback of this function is that the effective value of P_N was significantly greater than the selected value, resulting in an excessive number of predetections. However, this problem could be overcome by performing the detection function in hardware which would not require a predetection function and could be designed to handle the increased hit rate. Another problem with the double-hit approach is that it is designed to perform with the RVD-4 hit-processing technique and not a discrete time interval sampler as will be clarified in following paragraphs.

DETECTION TESTS IN WEATHER CLUTTER ENVIRONMENT.

These tests were devised to determine the capability of the RPS to detect targets of opportunity in the vicinity of weather clutter returns. This was accomplished by reproducing video tapes containing various samples of weather clutter. Employment of the video recorder made it possible to repeat test runs for various system configurations. The primary areas of investigation were the selection of appropriate parameters for the second-threshold control function and comparison of detection achieved with the RDAS hit processing versus a 1/16-nmi time interval sampler. In the section describing the isolated-hit function, it was explained that the estimated hit counts are employed to develop the second threshold in areas of clutter. Observation of false target rates, while employing second-threshold control, indicated that the usable range of values for the CW_0 parameter (point at which the dynamic



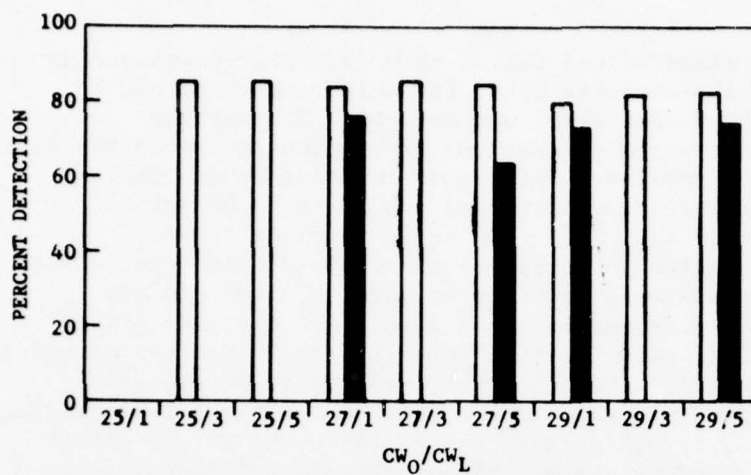
76-22-15

FIGURE 15. P_D P_{fa} PERFORMANCE OF DOUBLE-HIT FUNCTION

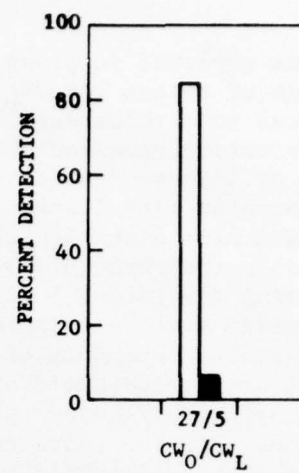
T_L is employed in place of a fixed value) was 25 thru 29. The corresponding range of values for CW_L (the isolated-hit count for which the threshold is forced to a value equal to the window size) was zero thru 5. Further observation revealed that there was a severe loss of receiver noise on the tail end of intense weather clutter returns. This is an inherent radar problem associated with linear receiver recovery time and was found to be more predominant with the ASR-5 radar set. With the above in mind, it was anticipated that this loss in noise would reduce the isolated-hit count, thus raising the target lead-edge threshold in areas in which clutter did not actually exist. Additionally, previous experience revealed that the higher frequency components of receiver noise were rejected by the RDAS hit-processing minimum-hit threshold of 1/64 nmi. This, however, was not as severe when employing a 1/16-nmi-range time interval sampler in place of the hit-processing logic. For the above reasons, it was decided to determine the actual effect that second-threshold control parameters and hit-placement techniques had on detection of targets of opportunity in the proximity of weather clutter. Several target samples were obtained, and the results are shown in figures 16 and 17. Analyses of these results indicate that a remarkable improvement in detection was achieved for some targets when employing the 1/16-nmi time interval sampler as compared to the RDAS hit-processing logic. An improvement was not always realized; in fact, for several cases, a slight loss with the 1/16-nmi time interval sampler was experienced. The greatest loss was approximately 11 percent. However, this loss was well compensated for by improvements as great as 78 percent. A study of the results also indicates that detection tended to decrease as parameter CW_L was increased and CW_0 decreased in value. Final selection of these parameters was accomplished in the next section in which false target rates are discussed.

WEATHER CLUTTER TESTS, FALSE TARGET RATES.

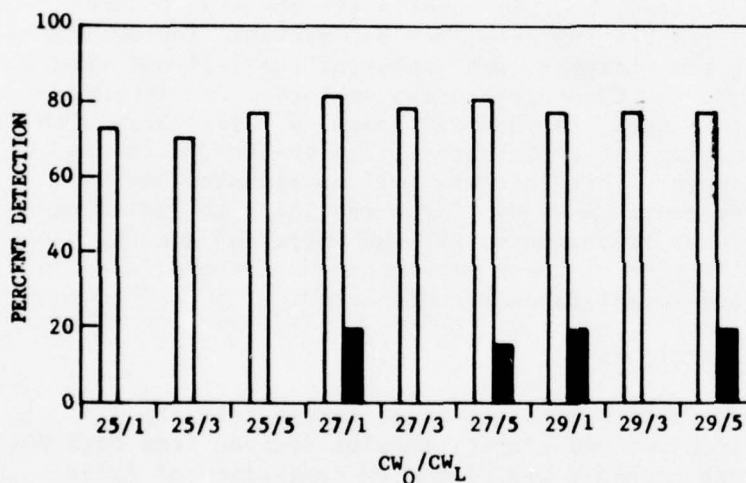
The purpose of these tests was to determine the false target rate (P_{fa}) achieved when processing various weather clutter samples derived from both the ASR-5 and ASR-7 radar. Primary emphasis was placed on comparison of false target rates within weather clutter when employing MTI video. This decision was based on the results of a previous test and evaluation conducted under the ARTS III Enhancement Program. The results of that effort are delineated in reference 1. It was indicated in that document that in a weather clutter environment a normal type of video resulted in a significantly larger number of false targets as compared to results achieved when employing an MTI-type video. The false target results presented in this section were obtained with a P_N of 4 percent and a basic detection threshold of 6. The method of second-threshold control, employing isolated-hit counts as previously detailed under the topic ISOLATED HITS, was employed to select the best parameter values for CW_0 and CW_L . Recalling that for isolated-hit counts less than CW_0 but greater than CW_L , the value of the second threshold is based on the isolated-hit count given by a linear relationship. For isolated-hit counts greater than CW_0 , the base T_L is employed, and for counts less than CW_L , the threshold is forced to a value equal to the size of the basic detection window. In the tests described herein, the window size was maintained to a length of 17 sweeps. When available, data were presented for both the RDAS hit-processing logic and the 1/16-nmi time interval sampler.



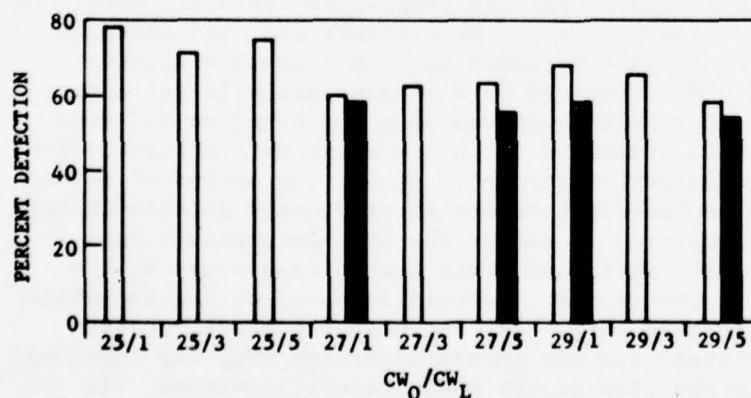
A. SAMPLE 1



B. SAMPLE 2



C. SAMPLE 3



D. SAMPLE 4

1/16-NMI SAMPLER

RDAS HIT PROCESSING

FOR $CW_0 < 27$ FALSE

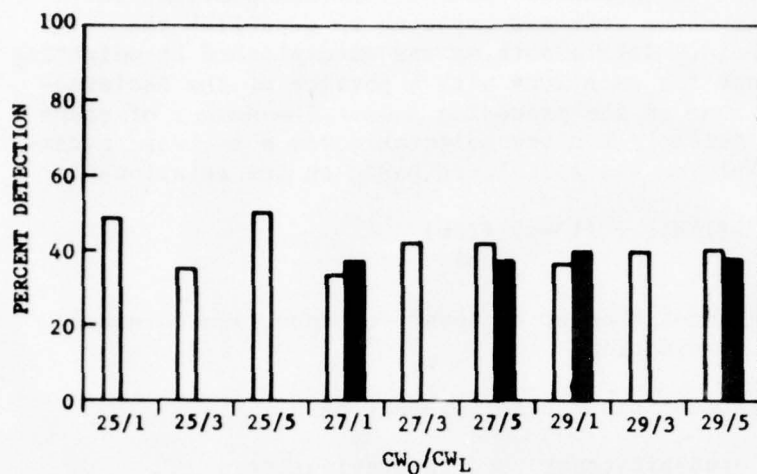
TARGET RATES EXCESSIVE

$P_N = 4\%$

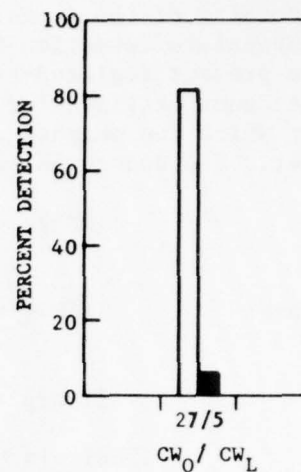
ASR-5 RADAR

FIGURE 16. P_D P_{fa} PERFORMANCE OF DOUBLE-HIT FUNCTION

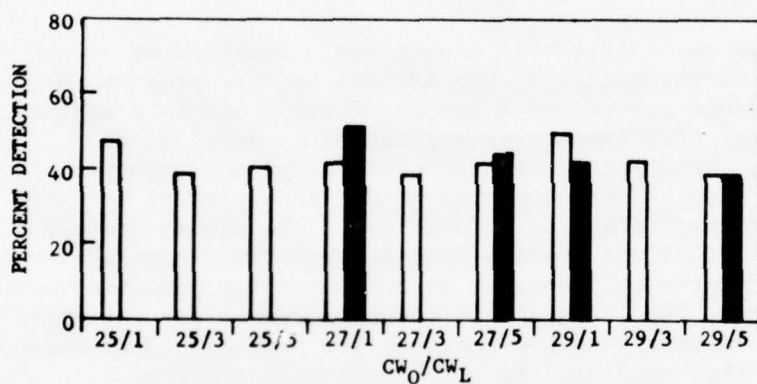
76-22-16



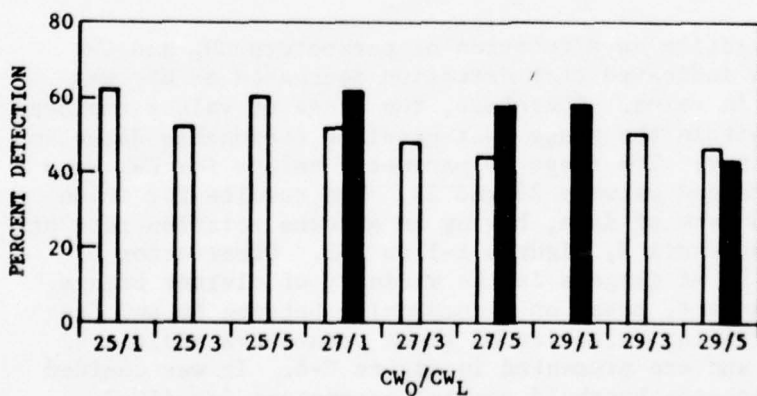
E. SAMPLE 5





F. SAMPLE 6



G. SAMPLE 7



H. SAMPLE 8

 1/16-NMI SAMPLER
 RDAS HIT PROCESSING

FOR $CW_0 < 27$ FALSE
 TARGET RATES EXCESSIVE
 $P_N = 4\%$
 ASR-5 RADAR

FIGURE 17. P_D P_{fa} PERFORMANCE OF DOUBLE-HIT FUNCTION

76-22-17

The original design of the second-threshold control function provided for smoothing of the isolated-hit count that was employed to establish the appropriate detection threshold. This smoothing was accomplished by weighting the present isolated-hit count for each zone with a portion of the isolated-hit count utilized for that zone on the preceding scan. The number of scans for which the weighting was accomplished was selectable via a software parameter. The count that was employed was calculated based on the relationship:

$$(ISH)_T = 1/\alpha (ISH)_P + (1 - \alpha) (ISH)_{old}$$

where: $(ISH)_T$ = Isolated-hit count employed for detection threshold selection

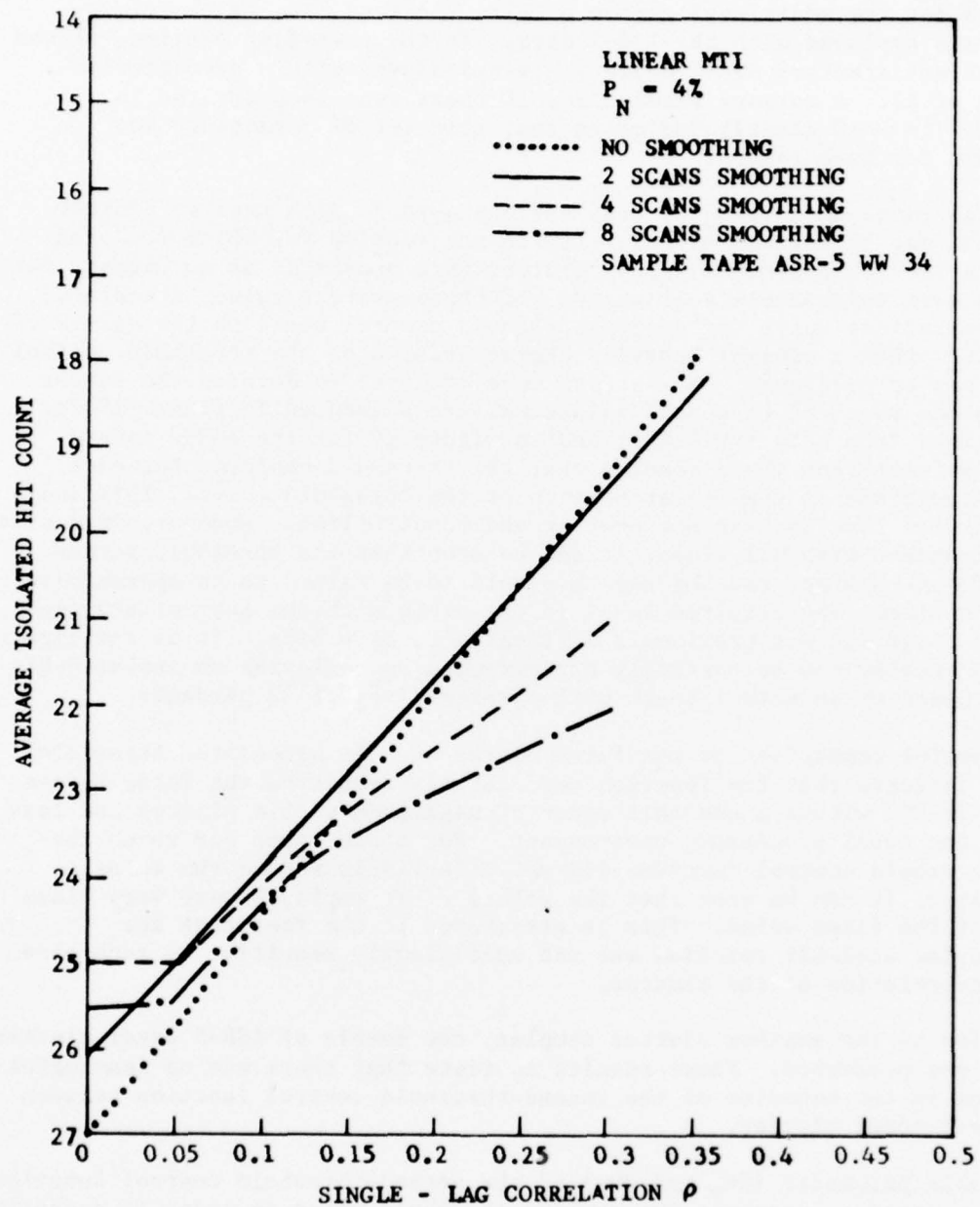
$(ISH)_P$ = Isolated-hit count for present scan

$(ISH)_{old}$ = Isolated-hit count used on previous scan

α = Scan smoothing factor

The effect that smoothing had on isolated-hit counts was determined by employing the radar data extractor module of the RPS operational program to record hit data and isolated-hit counts for a number of zones within a weather clutter environment. The extractor tapes were applied as an input to a reduction program which summarized single-lag correlation (α) and smoothed isolated-hit counts. These results were employed to derive a plot of isolated-hit counts versus single-lag correlation as a function of the number of scans for which the counts were smoothed. A typical plot is shown in figure 18 for weather sample WW 34. It is quite evident that as the smoothing parameter increases from zero to 8 scans, the isolated-hit count decreases for increasing α . Since an increasing value of α would increase the probability of false target rates, it is evident that smoothing is not a desirable function. In accordance with these results, all subsequent tests were conducted with no smoothing.

In the previous section, detection as a function of parameters CW_O and CW_L was delineated. The results indicated that detection decreased as CW_L was increased and CW_O decreased in value. Therefore, the range of values employed for false target tests was within the range that provided reasonable detection in proximity of weather clutter. The range of parameter values for CW_O were 1 and 5, and for CW_L , they ranged between 23 and 29. The results for these sets of parameters for ASR-5 type of data, having an antenna rotation rate of 15 r/min, are presented in appendix E, figures E-1 to E-5. Observation of these results and those for P_D of targets in the vicinity of clutter brings one to select a set of parameters, based on a compromise between P_D and P_{fa} of $CW_O = 27$ and $CW_L = 5$. Following selection of these parameters additional ASR-5 samples were obtained and are presented in figure E-6. It was decided to utilize the same set of second-threshold control parameters for ASR-7



76-22-18

FIGURE 18. AVERAGE ISOLATED-HIT COUNT VERSUS SINGLE-LAB CORRELATION

inputs. As previously noted, a predetection threshold of 11 was necessary to compensate for the additional number of hits received, due to the slower antenna rate employed with the ASR-7 data. In the preceding section, it was shown that satisfactory ASR-7 detection was achieved with a predetection threshold of 11. A cursory examination of these results presented in figures E-7 to E-10 clearly indicates that this set of parameters was appropriate for both radars.

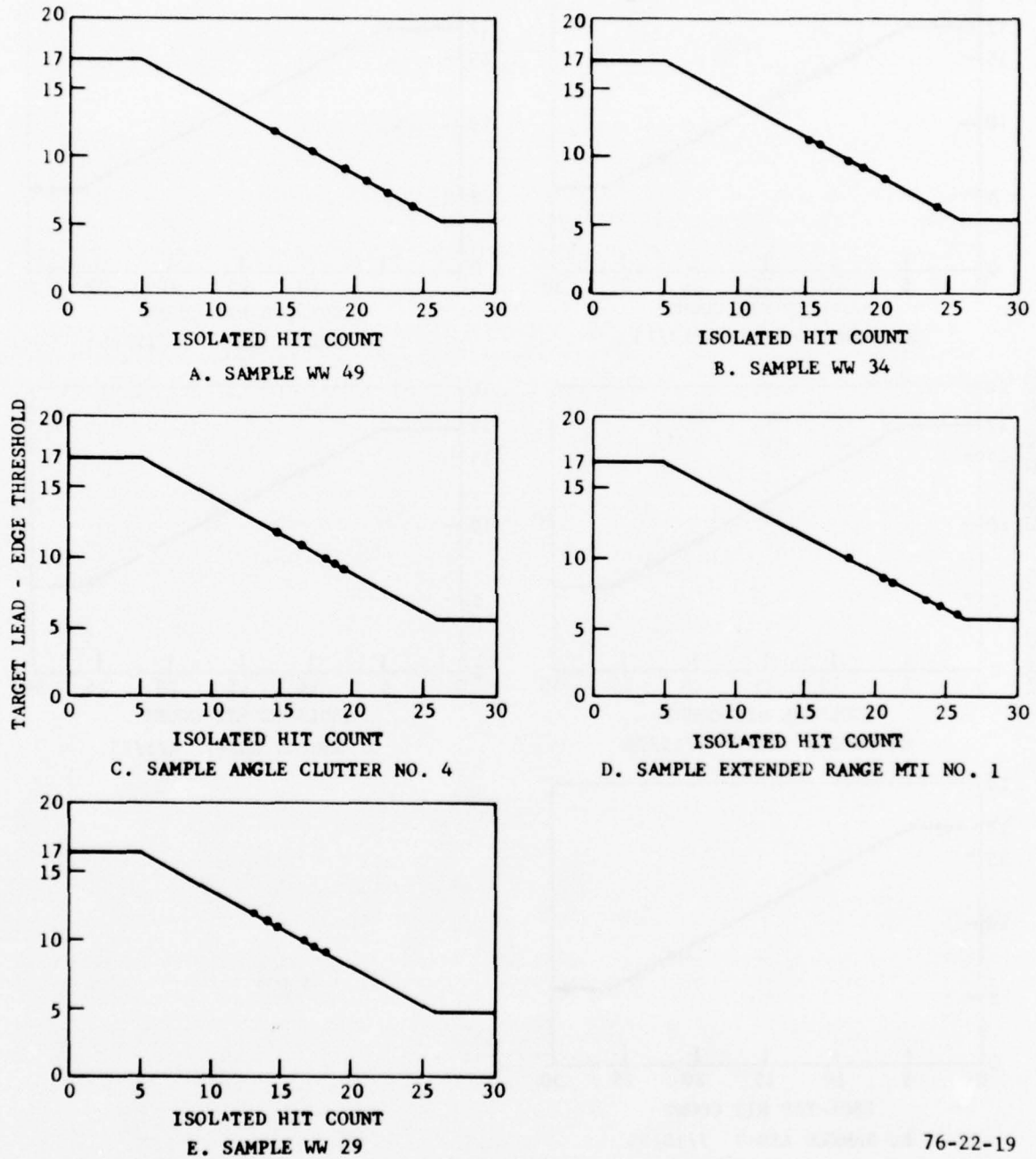
The general range of thresholds that was employed in each weather clutter environment may be derived by referring to the section for which isolated-hit counts for several zones within clutter were presented as an average for each zone over approximately 10 scans. If these average values are placed on the theoretical curve for second-threshold control based on the values of CW_0 and CW_L , then a general behavior characteristic of the threshold control function can be developed. These data were employed to develop the curves depicting the range of threshold values and are presented in figure 19 for video derived from both the ASR-5, and in figure 20 for the ASR-7 radar. It is quite evident from these results that the threshold employed for each weather sample was on the linear portion of the threshold curve. This indicated that the function was not over or undercontrolling. However, in a clutter-free environment with MTI video, it can be seen that the threshold seemed to be overcontrolling, causing the threshold to be raised to an approximate level of 8 hits. The required level in the clear with the appropriate predetection threshold was previously delineated to be 6 hits. It is anticipated that this problem can be partially circumvented by employing an isolated-hit function based on an actual count with a selected P_N of 32 percent.

A more careful comparison of the false alarms and the associated thresholds employed indicate that the function successfully regulated the false target rates to 1×10^{-5} within a one half order of magnitude within clutter and less based on the total processing environment. For those cases for which the second-threshold control function did not effectively reduce the false target rates, it can be seen that the values of T_L employed were very close to that of the fixed value. This is attributed to the fact that the estimated isolated-hit function was not sufficiently sensitive to recognize the low correlation of the clutter.

In addition to the weather clutter samples, one sample of ASR-5 angel clutter activity was processed. These results indicate that there was no meaningful difference in the behavior of the second-threshold control function between weather and angel clutter.

The variable parameter (CW_0 and CW_L) of the second-threshold control function could be changed to increase the applied threshold value in order to decrease the number of false targets. However, as delineated in the PERCENT DETECTION section of this document, target detection of targets in the vicinity of clutter would be degraded.

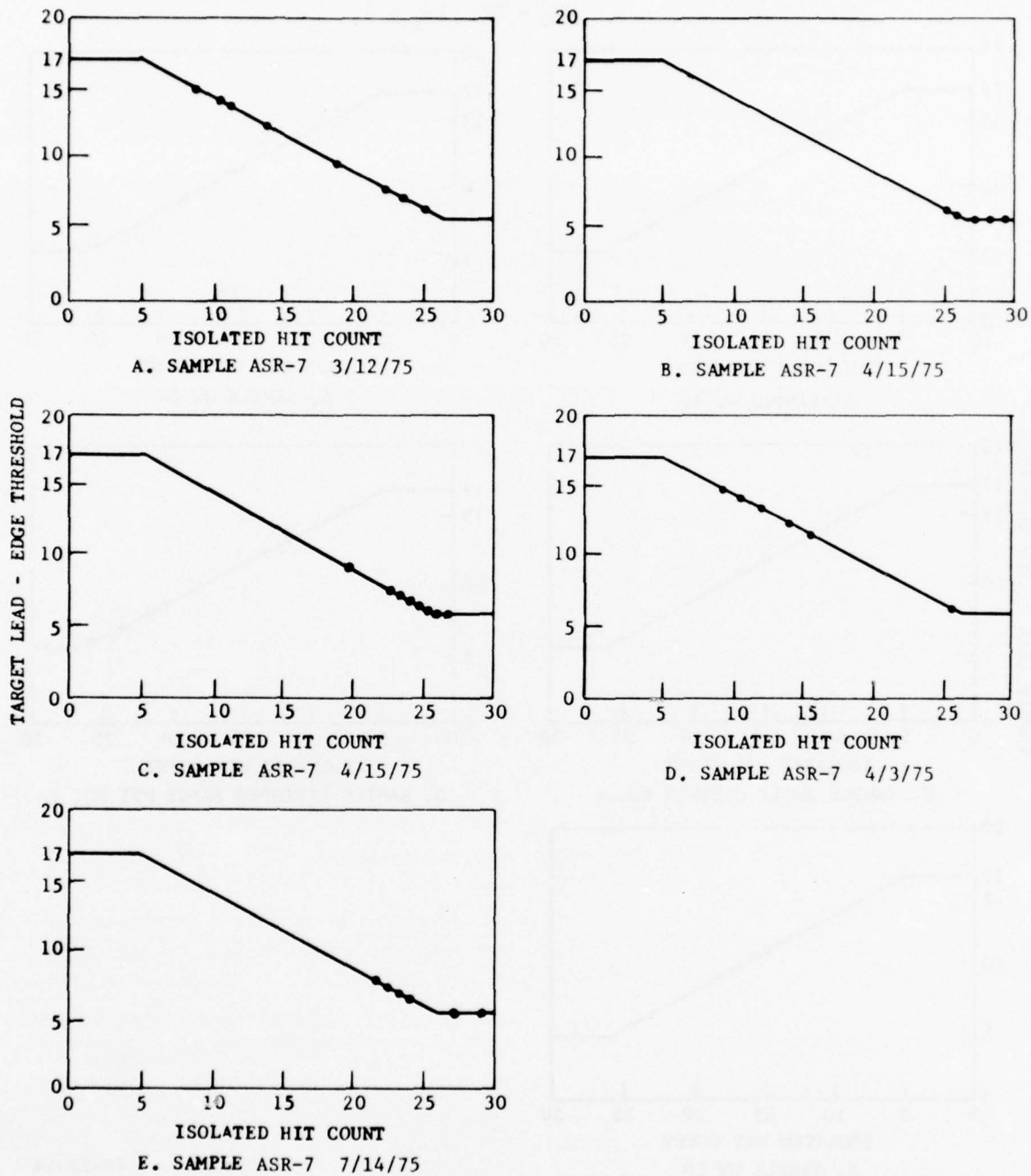
● = AVERAGE ISOLATED HIT COUNT FOR SAMPLE ZONES
 $CW_0 = 27$; $CW_L = 5$



76-22-19

FIGURE 19. TYPICAL SECOND-THRESHOLD CONTROL VALUES EMPLOYED FOR ASR-5 SAMPLES

• = AVERAGE ISOLATED HIT COUNT FOR SAMPLE ZONES
 $CW_0 = 27$; $CW_L = 5$



76-22-20

FIGURE 20. TYPICAL SECOND-THRESHOLD CONTROL VALUES EMPLOYED FOR ASR-7

HIT DISTRIBUTION TESTS.

This category of tests was conducted to determine the distribution of false target hits that resulted primarily from MTI weather clutter returns and secondly the distribution attained for the total MTI environment. It should be recognized that any real targets encountered are included in the data. However, the number of true targets within the weather clutter areas is negligible.

Data were collected for several samples of weather clutter derived from both the ASR-5 and ASR-7 radar. The results are presented graphically as a plot of the percentage of total targets having each hit count. These results are shown in appendix F, figures F-1 to F-3 for the ASR-5, and the corresponding results for the ASR-7 are depicted in figures F-4 to F-6. The hit counts were obtained with the second-threshold control function enabled and disabled. It should be kept in mind that these curves are in percentages and that the average number of targets per scan are not the same for the two states of the second-threshold control function. Examination of these results indicate that the general shape of the distribution for the ASR-5 and ASR-7 inputs is similar for both the map and total processing areas. In most cases, the second-threshold control function reduced the number of short run length targets, with a corresponding reduction in false target rates. Referring to the plots of the estimated threshold values employed for each clutter sample, it is evident that the threshold was normally raised to values that would reject detection of short run length targets. For the case for which the hit distribution did not effectively change when employing second-threshold control, it can be seen that the values of T_L applied by the function were practically the same as that of the fixed threshold. In general, the predominant number of false targets had hit counts of 12 or less with a slight increase occurring at the 20-hit or more data point.

VIDEO SELECT MAPPING TESTS.

A brief description of the philosophy of the video select function was presented earlier in this document. For the convenience of the reader, the operation of this function will be detailed prior to presenting test results. Actually, two mapping techniques were tested. The first method, called "clutter monitor" was included in the RPS design as delivered by the contractor. This function consisted of a 2-nmi range density window which summed hits from a slow-loop self-regulating quantizer and compared this sum to an established threshold. The 2-nmi intervals for each sweep coincided with zone boundaries. Therefore, if a threshold crossing occurred on a sweep within a zone, a logical ONE would be placed in the range density word for that zone. At the end of the sweep, the range density word was transferred to the IOP. The clutter monitor subroutine, residing in the IOP, summed the number of range density threshold crossings per zone. This value was then compared to a preestablished threshold. If this threshold was exceeded, a flag was raised indicating that clutter was potentially sensed in that zone for the current scan. The azimuth threshold crossings were used each scan to increment or decrement an up/down counter. If clutter was sensed on a given scan, the

counter would be up-counted by a parametric value. If clutter was not sensed, the count was decremented. For each scan, the count for each zone was compared to a scan threshold. A successful comparison would cause the MTI quantizer to be selected, and second-threshold control would apply for that zone on the next scan. The counter was continuously updated on successive scans to provide for current clutter sensing. Following establishment of a map defining the zones for which MTI video should be selected, there was a provision to extend the map in range and/or azimuth by one or more zones. This extension is called soaking. Initial tests indicated that the fringes of ground clutter, within the normal video were composed of numerous small run-length targets that were not included in the video select map. Additionally, it was observed that in the vicinity of weather clutter, only one zone of soaking in both range and azimuth was necessary. In line with the above observations, it was decided to extend the capability of the soaking feature. This change consisted of adding a selective range boundary for which all ranges less than the boundary would provide for additional range soaking, and for ranges greater than the established boundary, the basic value of range soaking would prevail.

The second mapping technique was developed to attempt to utilize the normal isolated-hit counts. It was felt that if this function were successful, it would reduce the hardware necessary to develop a video map. More specifically, the slow-loop quantizer and range density counter would be eliminated. The mechanism of the isolated-hit technique was such that only an isolated-hit counter and threshold had to be established in the software. The scan smoothing and soaking functions were the same as described for the clutter monitor.

Prior to processing weather clutter samples it was necessary to establish the additional range soaking that was necessary within the NAFEC ASR-5 ground clutter region. This was accomplished using weather-clutter-free environments and monitoring the false target rates at the fringes of ground clutter. The best configuration that resulted from these tests was a boundary range of 20-nmi, with an additional soaking of two zones within that range boundary. Therefore, the total range soaking within the ground clutter areas was set to three zones.

Following these tests, several video tapes containing weather clutter returns from ASR-5 and ASR-7 were processed using both mapping techniques. Fifty scans of target report data were collected on various mapping parameters. The procedure consisted of forcing selection of MTI video and, at a specific time, enabling the mapping function. Two minutes were allowed for the map to be formulated and then the false target rates were obtained. The results of these tests are delineated in appendix G, tables G-1 through G-5 for ASR-7 inputs, and in tables G-6 through G-8 for ASR-5 returns. The criterion for selecting a best set of parameters was the lowest false target rate while minimizing mapping of clear or target areas. The results indicate that the best set of parameters for the ASR-5 and ASR-7 were not the same for isolated-hit mapping. This is attributed to the fact that the antenna rates

for the two data sets were not the same. Of utmost importance is the fact that comparable performance was achieved with both mapping techniques. The best set of parameters for each method of mapping was as listed in table 3 for the ASR-5 and ASR-7 radar inputs. The results clearly indicate that a one-zone soaking in azimuth is necessary in weather clutter environments.

As stated in earlier paragraphs, the isolated-hit technique requires much less digital logic than that of the clutter monitor approach, and no analog circuitry at all. Therefore, it seems reasonable from the above results that isolated-hit mapping is the preferred approach.

For the convenience of the reader, the results for the best set of parameters for each weather sample are presented in table 4 to provide a quick reference for false target rates. It should be emphasized that the false target rates for all mapping data include real targets and therefore are higher than the actual rate. What is important here is the comparison of rates between the isolated-hit and clutter monitor techniques.

TABLE 3. BEST SET OF VIDEO SELECT MAPPING PARAMETERS

A. Clutter Monitor Technique

Radar	Slow Loop <u>P_N</u>	Range Density <u>Threshold</u>	Azimuth Threshold	Scan Increment	Scan Decrement	Scan Threshold	Sweeps Per Zone	Range	Soaking Added Range	Azimuth
ASR-5	3%	2	12	2	1	5	27	1	2	1
ASR-7	3%	2	12	2	1	5	27	1	2	1

B. Isolated-Hit Mapping

Radar	Isolated Hit <u>Threshold</u>	Increment	Decrement	Scan Threshold	Sweeps Per Zone	Range	Soaking Added Range	Azimuth
ASR-5	29	1	1	10	31	1	2	1
ASR-7	31	2	1	7	31	1	2	1

TABLE 4. SUMMARY OF VIDEO MAPPING RESULTS FOR BEST SET OF PARAMETERS

A. ASR-5 Samples

Sample	False Target Rate	
	<u>Clutter Monitor</u>	<u>Isolated Hit</u>
ASR-5 WW 49	2.6×10^{-5}	2.38×10^{-5}
ASR-5 WW 34	3.5×10^{-5}	3.35×10^{-5}
ASR-5 WW 29	6.76×10^{-5}	5.78×10^{-5}

B. ASR-7 Samples

Sample	False Target Rate	
	<u>Clutter Monitor</u>	<u>Isolated Hit</u>
ASR-7 MTD #6 Comparison	2.75×10^{-5}	2.99×10^{-5}
ASR-7 7/14/75 A.M.	4.22×10^{-5}	4.59×10^{-5}
ASR-7 4/15/75 A.M.	2.16×10^{-5}	2.55×10^{-5}
ASR-7 4/15/75 P.M.	2.02×10^{-5}	2.52×10^{-5}
ASR-7 3/12/75 P.M.	2.98×10^{-5}	3.81×10^{-5}

SUMMARY OF RESULTS

The results of the tests conducted to determine the performance of the radar processing subsystem of the All Digital Tracking Level System are summarized below:

1. Percent noise regulation for the rank-order quantizer designed by the contractor displayed a strong dependency on input source.
2. The NAFEC design of a rank-order quantizer regulated percent noise within 10 percent of the selected value.
3. The time interval sampler produced a linear relationship between selected and actual percent noise independent of input content. This was not true for the RDAS hit-processing function.
4. Acceptable percent noise regulation was achieved for all input levels exceeding 100 mV with the NAFEC-designed rank-order quantizer and a time interval samples.
5. The drop in isolated-hit counts within a zone was approximately 30 percent over a range of target levels between zero and 15 dB above MDS and a percent noise of 4 percent. The corresponding change for a P_N of 32 percent was only 3 percent.
6. The presence of a 15-dB target within a zone resulted in a P_N change of approximately 25 percent of the selected P_N value of 4 percent. However, virtually no change was experienced for a selected P_N of 32 percent.
7. An improvement in isolated-hit stability of a factor of 2 was achieved by employing a 32-percent noise value in place of a 4-percent noise value when counting actual occurrences. The estimated-count technique had fluctuations that were in excess of 6 times as great as those yielded by the 32-percent P_N actual counts.
8. The variations in estimated isolated-hit counts for the ASR-5 were in excess of 1.5 times as great as those for the ASR-7 radar samples.
9. A minimum pulse-width criterion of 2/64 nmi introduced a loss of approximately 1.5 to 2 dB in percent quantization as compared to a 1/64-nmi setting.
10. A 1- to 2-dB increase in percent quantization was achieved with an azimuth step interval of 825 as compared to a step interval of 725.
11. An increasing predetection or final detection threshold results in a decrease in false target rates and detection. However, for equal false target rates, an increasing predetection threshold produced a greater reduction in detection than that introduced by varying the final detection threshold.

12. The detection-false target performance of the hit processing function and the 1/16-nmi sampler were within 0.5 dB of each other for clutter-free environments.

13. Approximately a 2-dB increase in the detection-false target performance for normal video was achieved for stationary targets, optimally placed relative to range cell boundaries, as compared to flying targets which crossed range cell boundaries.

14. The measure of improvement of detection-false target performance for ASR-7 MTI stationary versus moving targets was only 0.5 dB. This was attributed to the digital sampling accomplished in the ASR-7 MTI circuits.

15. A double-hit placement function employing a 2/64-nmi placement criterion produced improved-detection false target performance as compared to a 1/64-nmi placement. However, as compared to no double-hit function, the measure of improvement for the 2/64-nmi condition was less than 0.5 dB.

16. The 1/16-nmi sampler, as compared to hit-processing function, provided detection improvements as great as 78 percent for targets in the vicinity of weather clutter.

17. Detection decreased as second-threshold control parameter CW_L was increased and CW_O was decreased in value.

18. A final detection parameter of 6 was selected for use with all videos derived from the ASR-5 and ASR-7 radars. However, the predetection parameters that were selected differed for the two radars. The best set was as follows:

<u>ASR-5</u>		<u>ASP-7</u>	
<u>Normal</u>	<u>MTI</u>	<u>Normal</u>	<u>MTI</u>
8	10	9	11

19. The second-threshold control function successfully regulated the false target rates to 1×10^{-5} , within a one-half order of magnitude for values of $CW_O=27$ and $CW_L=5$.

20. Fluctuations of the estimated isolated-hit counts tend to indicate that improved performance in the second-threshold control function could be achieved if actual counts were employed with a P_N of 32 percent.

21. The single set of results obtained for angel clutter activity displayed similar behavior as those obtained for weather clutter.

22. The majority of the false targets had hit counts of 12 or less with a slight increase occurring at the 20-hit or more data point.

23. A one-zone azimuth soaking was required for development of an acceptable video selection map.

24. Range soaking of three zones was necessary in the vicinity of ground clutter to compensate for the inability of the video select map to adequately recognize short runlength returns introduced by broken ground clutter.

25. The range soaking required for weather clutter environments was found to be one zone.

26. The video select maps developed by the clutter monitor function and the normal isolated-hit technique were effectively equal. However, the isolated-hit approach required significantly less hardware components.

27. Contractor studies of the weather monitor function indicated that the function did not perform effectively.

CONCLUSIONS

It is concluded that:

1. The NAFEC-designed rank-order quantizer performs to theoretical expectations. This is not true for the contractor's version.
2. A time interval sampling technique for hit placement is superior to the RDAS hit-processing approach.
3. For typical levels of receiver noise, the rank-order quantizer, with a time interval sampler, is insensitive to variations in input amplitude.
4. The weather monitor is not an effective means of regulating false targets within weather clutter.
5. The isolated-hit count within a zone is inversely proportional to the signal level of a target within that zone. The variations are far greater for a P_N of 4 percent as compared to 32 percent.
6. The zone P_N is insensitive to targets for a 32-percent selected value of P_N .
7. The isolated-hit counts for a P_N of 32 percent have less deviation than any other configuration tested.
8. Increasing the minimum pulse-width threshold of the hit-processing function results in a significant decrease in percent quantizations.
9. Detection is more severely degraded by varying the predetection threshold than by increasing the final detection threshold.
10. The 1/16-nmi sampler produces superior overall performance as compared to the hit-processing function.
11. Approximately 2-dB sampling loss is experienced for nonstationary targets as compared to those that are stationary relative to range cell boundaries.
12. The double-hit placement function does not improve detection-false target performance.
13. Selection of the appropriate values of the second-threshold control parameters CW_O and CW_L is a compromise between P_D and P_{fa} .
14. The second-threshold control function is an effective means of regulating false target rates within clutter.
15. The performance of the second-threshold control function could be improved if the actual isolated-hit counts for a P_N of 32 percent were employed.

16. The second-threshold control function reduced the number of short-runlength false targets.
17. The video select map requires both azimuth and range soaking.
18. The most deficient function in the RPS is the video select map.
19. The normal isolated-hit video select mapping technique is superior to the clutter monitor approach, based on cost and performance.

RECOMMENDATIONS

It is recommended that initiative be undertaken to:

1. Implement a rank-order quantizer as the first level of detection in future radar-processing systems.
2. Employ actual isolated-hit counts for a 32-percent noise to control false target rates within clutter and a P_N of 4 to 8 percent for detection of the targets.
3. Employ a time interval sampler to accomplish hit-placement (time quantization).
4. Not utilize a double-hit placement function.
5. Develop an improved method of performing the video select mapping function. As an interim technique, a video select map based on actual normal isolated-hit counts for a selected P_N of 32 percent is recommended.

REFERENCE

1. Holtz, Martin H. and Wapelhorst, Leo J., Evaluation of Distribution-Free Quantizer, Several Range Binning Techniques, and an Extended Range Moving Target Indicator Video, Report No. FAA-RD-75-185.

APPENDIX A

NAFEC RANK-ORDER QUANTIZER DESIGN AND
CIRCUIT TEST RESULTS

APPENDIX A

LIST OF ILLUSTRATIONS

Figure		Page
A-1	Frequency Response of Input Buffer and Delay-Line Driver	A-2
A-2	Example of Delay-Line Weighting	A-3
A-3	Delay Line Tap Weighting as Referenced to Center Tap	A-5
A-4	Schematic Diagram of Diode Summer	A-7
A-5	Schematic Diagram of Rank Threshold Circuit	A-8
A-6	Logic Diagram of Sampler Circuit	A-9

APPENDIX A

NAFEC RANK-ORDER QUANTIZER DESIGN AND CIRCUIT TEST RESULTS

RANK-ORDER QUANTIZER BENCH TESTS.

These tests were designed to define the performance of each function composing the NAFEC rank-order quantizer. Each function will be discussed separately, and the parameters for each function that affect rank-order performance will be detailed in depth.

DELAY-LINE DRIVER. The delay-line driver is required to furnish sufficient gain to compensate for delay-line insertion loss and line loss. The gain must be established such that it does not exceed the common mode voltage of the delay-line comparators. The line driver was designed for a gain of 3 and a 3-dB bandwidth in excess of 8 MHz. A frequency response curve for the input buffer and delay-line driver is depicted in figure A-1. The most significant requirement was to assure that there was no direct current (d.c.) offset at the output of the driver. A wide variation in percent noise (P_N) regulation as a function of input noise level was encountered if a d.c. offset was present particularly for low-level noise.

DELAY-LINE COMPARATORS. The function of the delay-line comparators is to compare each tap (noise tap) to the target tap (center tap) and provide a logical ONE output to the summing amplifier if the level at the center tap exceeds that of the noise tap. Since the delay-line loss increases as the signal propagates down the delay line, it is necessary to weight each tap equally with resistor voltage dividers. Actually, the weighting in this design is accomplished by weighting the center tap input to each comparator. The series resistor at each noise tap is the same value. Therefore, the impedance at each noise tap is the same. An example of this weighting technique is shown in figure A-2. The attenuation values used are not actual, but are used merely to illustrate the technique of weighting.

Assume a noise sample at point "A" with an amplitude of one unit. Propagation of the signal down the delay line will result in values of 0.7 at point "B," 0.5 at the center tap, and 0.3 at point "D" due to the attenuation characteristics of the delay line. A system with these attenuation characteristics requires a center-tap signal gain of 2 in order to yield a signal with an amplitude equal to 1.0 at the center-tap amplifier output, point "E." If we neglect the input bias currents of the comparators, points "F" and "G" will "see" a signal of amplitude equal to one unit. The signal at point "H" is 0.7 requiring that the voltage divider R_1 - R_2 yield 0.7 at point "I." The signal at point "J" is 0.3, and the voltage divider R_3 - R_4 yields 0.3 at point "K." Thus, all taps are compensated and are equally weighted at the comparator inputs. The parallel equivalent of each voltage divider, as seen from the comparator input, must be equal to R to prevent drift of the comparator thresholds.

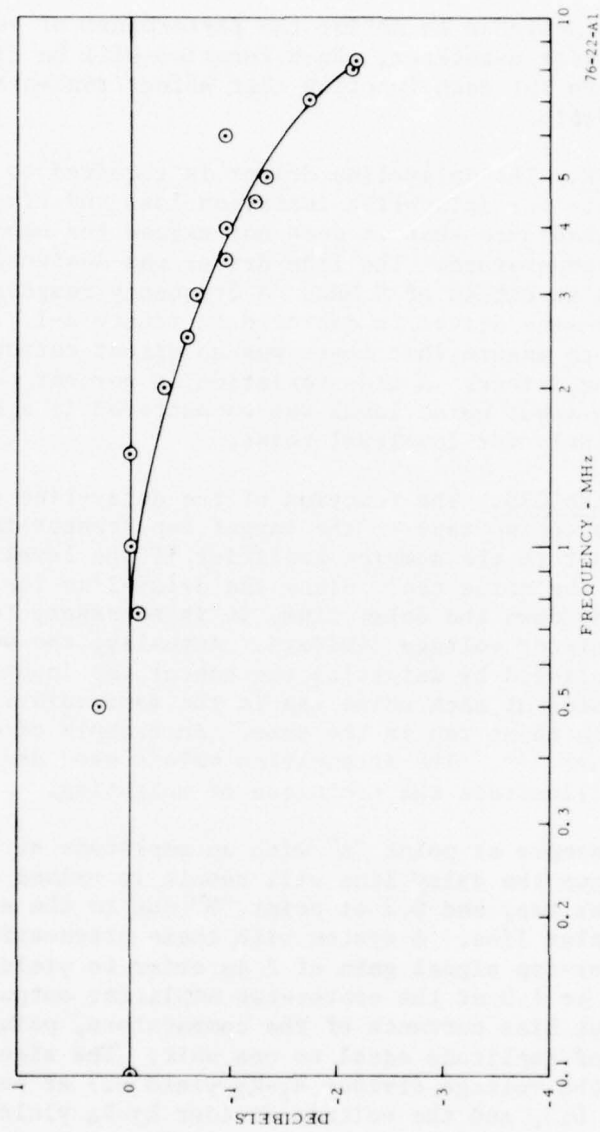
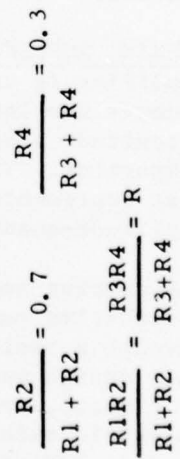


FIGURE A-1. FREQUENCY RESPONSE OF INPUT BUFFER AND DELAY-LINE DRIVER



76-22-A2

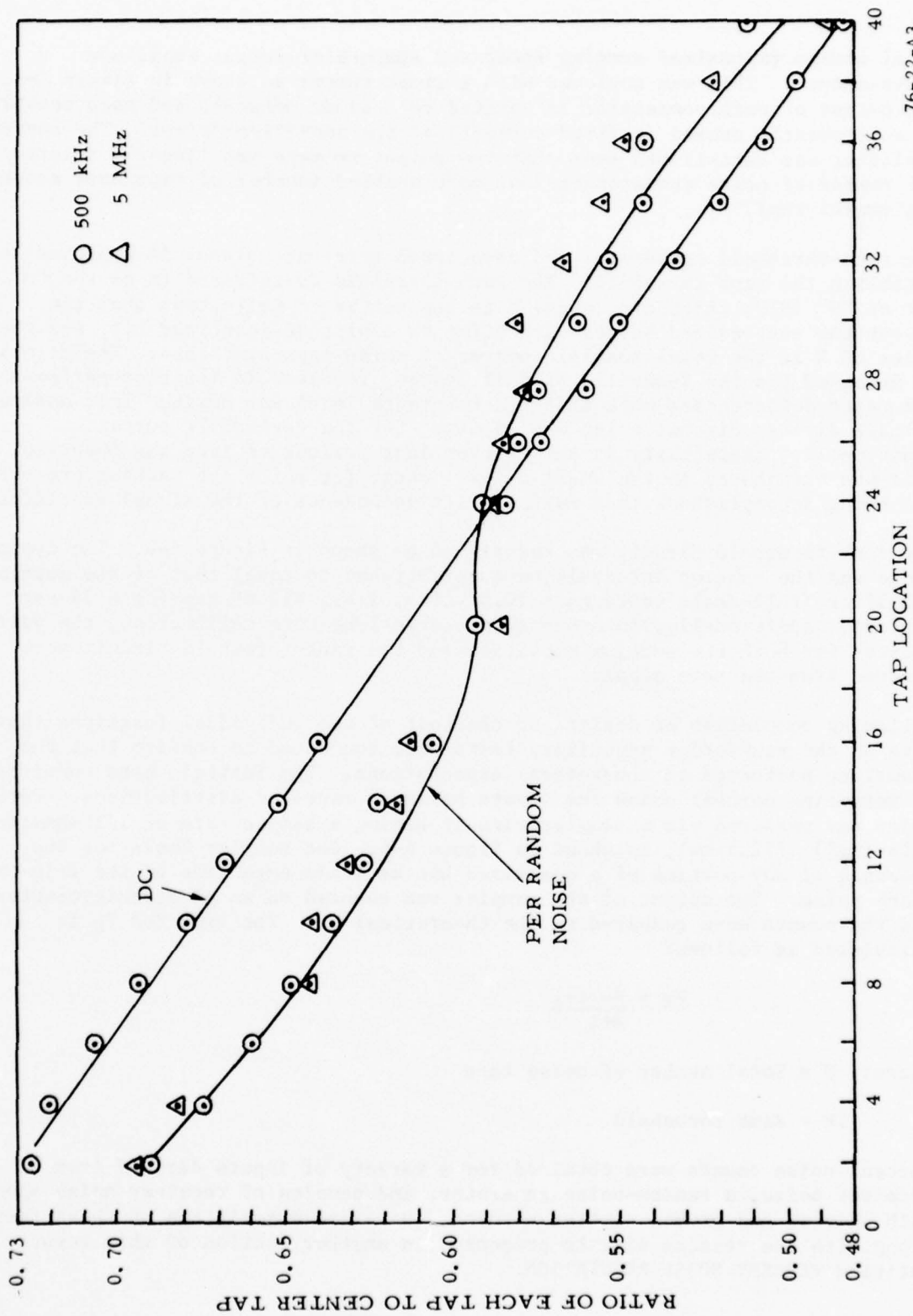
There were three major factors to be considered in selecting the comparator to be employed. These were (1) sufficient speed, (2) sensitivity, and (3) input bias current. The first two items were readily met with the original comparators that were incorporated in the design of the Knoxville quantizer. However, the input bias current was sufficient to cause a voltage drop across the comparator input series resistor. This condition resulted in the quantizer being sensitive to input video levels. That is, percent noise at the output of the quantizer varied as a function of input signal level. Additionally, for a specific input level, the probability of the center tap exceeding the adjacent taps was not stable because of the excessive input bias currents.

The aforementioned weighting of each noise tap by the Knoxville design was found to be based on direct current (d.c.) propagation losses of the delay line. Since the alternating current (a.c.) and d.c. characteristics of the delay line were different, nonlinearity of percent noise resulted as a function of selected rank thresholds. This necessitated selection of resistors for each voltage divider to produce the proper a.c. weighting at each noise tap. Random noise sources having frequency bandwidths of 500 kHz and 5 MHz were applied at the delay-line input. The characteristics of the noise was such that its response was flat from a very low frequency to a sharp cutoff that occurred at the upper frequency of its bandwidth. The signal level for each of the noise taps and their corresponding center-tap sample were measured with a highly accurate RF room mean square (rms) meter. The values of the voltage dividers were calculated to match the noise attenuation characteristics shown in figure A-3.

CENTER-TAP AMPLIFIER. The center-tap amplifier is required to provide the necessary drive to the comparators at each of the delay-line taps. The center-tap amplifier was designed to provide for unity gain and zero output bias. The amplifier was designed to have a bandwidth in excess of 8 MHz to preclude variations in performance of the quantizer as a function of video frequency content.

SUMMING AMPLIFIER AND RANK-THRESHOLD COMPARATOR. The function of the summing amplifier is to sum the number of events for which the center-tap signal exceeds the level at a surrounding noise tap. The sum of these events is outputted as an analog voltage and applied as one input to the rank-threshold comparator. The second input to the comparator is an analog reference voltage that represents the rank threshold that must be exceeded in order to output an amplitude-quantized hit.

The summing amplifier, as designed for the Knoxville quantizer, was basically a resistive summing circuit in which the output of each comparator was summed through a resistor to a common amplifier-driver. The basic deficiency in this design was that the output voltage from the comparators varied as much as 20 percent, resulting in an unreliable summation for comparison to the rank-threshold reference. This basically introduced nonlinearity into the system. An intermediate design of a current summer was explored, but aborted because initial test results indicated that sufficient speed could not be obtained, which resulted in incorrect comparisons at the rank-threshold comparators.



76-22-A3

FIGURE A-3. DELAY-LINE TAP WEIGHTING AS REFERENCED TO CENTER TAP

Final design emphasized summing speed and comparator output amplitude independence. This was achieved with a diode summer as shown in figure A-4. The output of each comparator is applied to a diode network, and each network is subsequently summed (a fixed current) at the amplifier-driver. The summing amplifier was established such that the output voltage was linearly related to the number of noise comparators that were enabled (number of taps that exceeded the center tap).

The rank-threshold comparator and associated reference signal is employed to establish the rank threshold. The rank threshold is referred to as the "M" out of "N" (M/N) threshold, where M is the number of noise taps that the center tap must exceed before outputting an amplitude-quantized hit, and the value of N is the total possible number of noise taps available. The circuits, as designed for the Knoxville ARTS II system, resulted in inferior performance. The major deficiencies were that the reference level was derived from analog voltage divider circuit which was adjusted for the desired P_N output. Additionally, instability in the P_N over long periods of time was observed. This was attributed to the small dynamic range for which the ranking process was being accomplished, thus making drift components of the signal significant.

The rank-threshold circuit was redesigned as shown in figure A-5. The dynamic range and the ranking intervals were established to equal that of the summing amplifier (full-scale voltages = 10.0 volts, i.e., 417 mV/tap for a 24-tap system). Additionally, in order to preserve long-term calibration, the voltage sources for both the summing amplifier and the rank-threshold circuit were derived from the same supply.

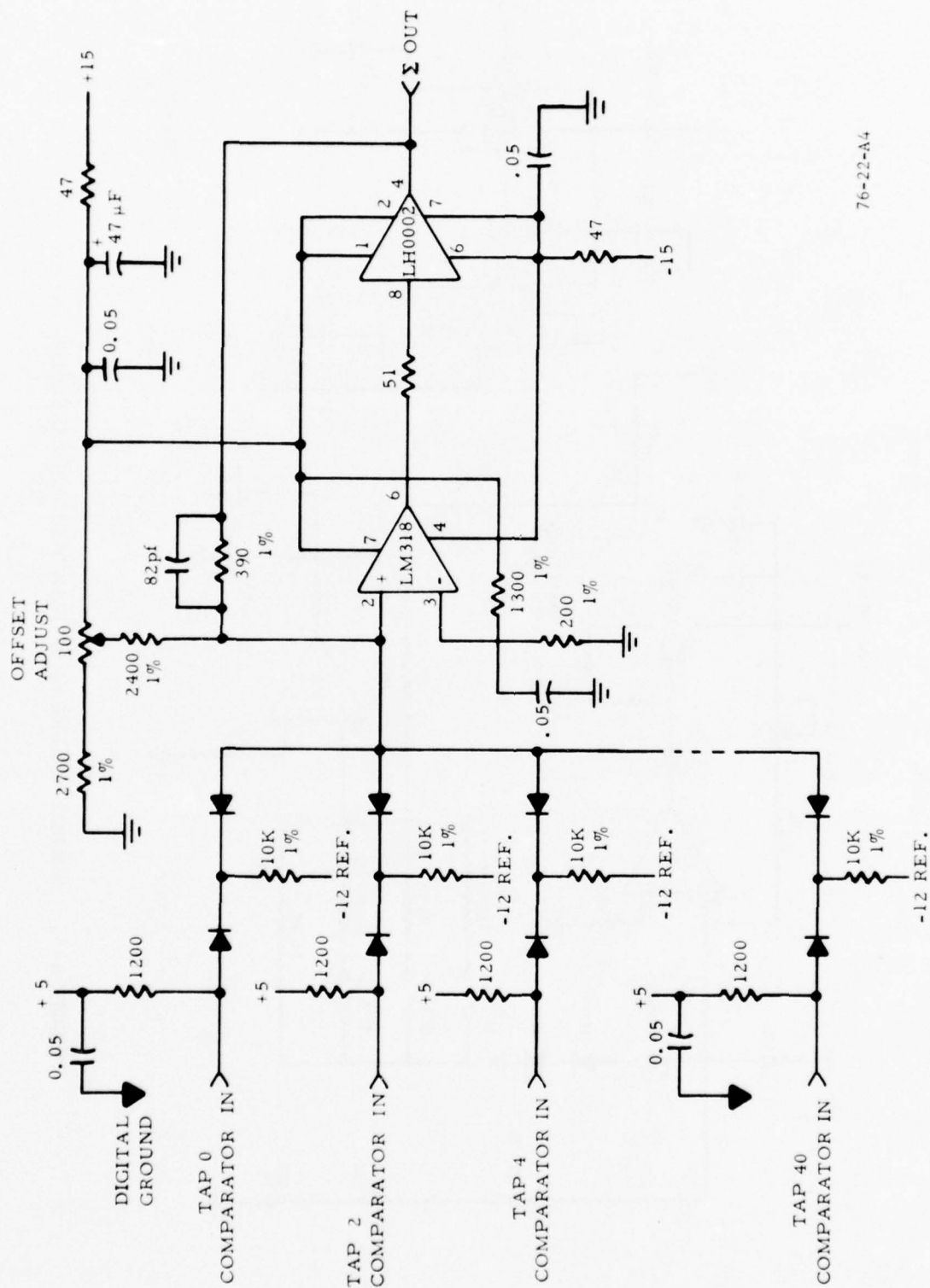
Following completion of design and checkout of the individual functions that make up the rank-order quantizer, tests were conducted to confirm that the quantizer performed to theoretical expectations. The initial tests consisted of measuring percent noise for inputs having a range of distributions. Percent noise was measured via a sampler circuit having a sample rate of 1/16-nautical mile (nmi) (772.5 ns), as shown in figure A-6. The sampler looks for the presence of any portion of a quantized hit at train-edge time of the 1/16-nmi clock pulse. The output of the sampler was counted on an electronic counter, and the counts were compared to the theoretical P_N . The expected P_N is calculated as follows:

$$P_N = \frac{N-TR+1}{N+1}$$

where: N = Total number of noise taps

TR = Rank threshold

Percent noise counts were obtained for a variety of inputs derived from receiver noise, a random-noise generator, and samples of receiver noise along with weather and ground clutter returns. Detailed description of these tests along with the results will be presented in another section of this report entitled PERCENT NOISE REGULATION.



76-22-A4

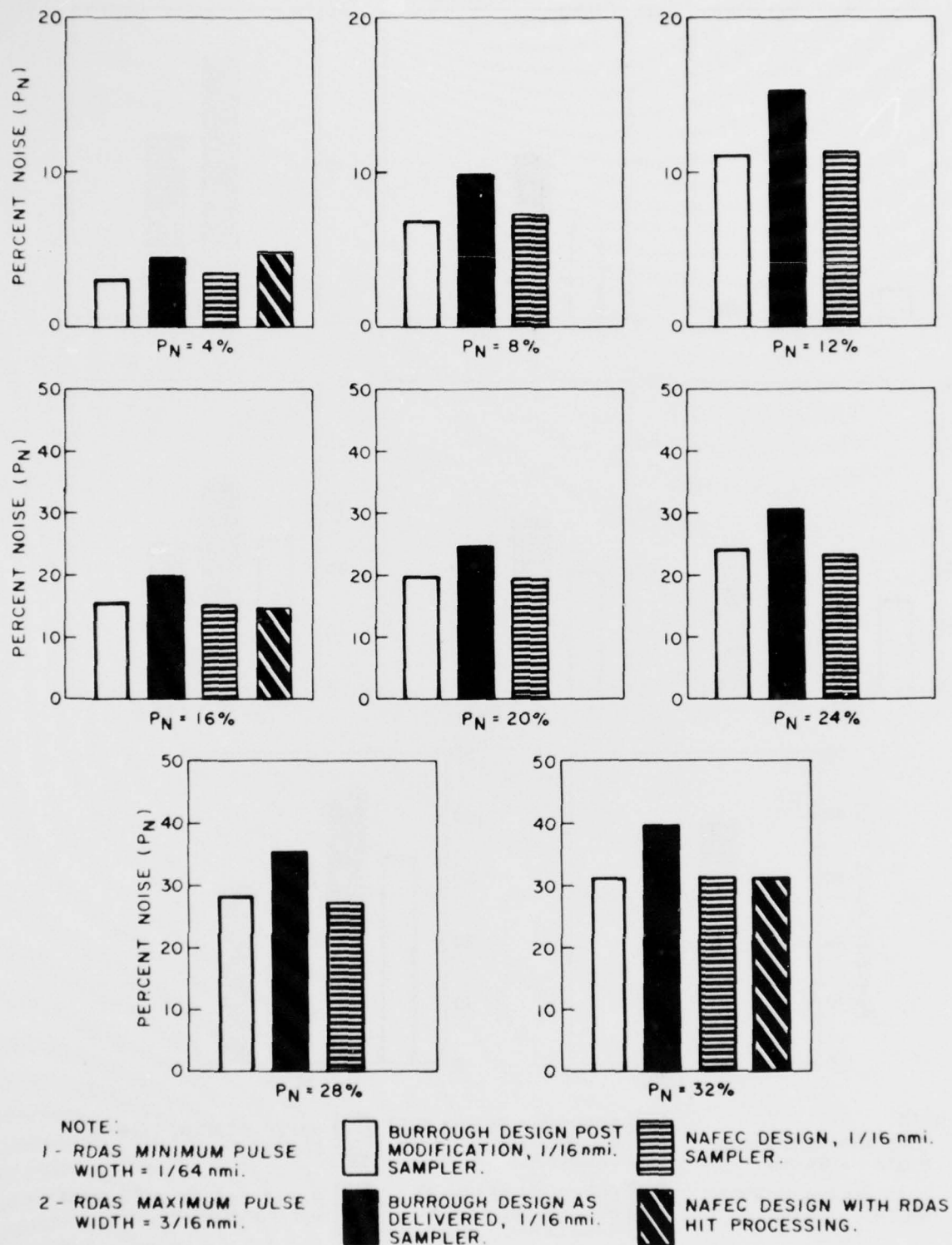
FIGURE A-4. SCHEMATIC DIAGRAM OF DIODE SUMMER

APPENDIX B

PERCENT NOISE REGULATION,
CLUTTER-FREE ENVIRONMENT

APPENDIX B
LIST OF ILLUSTRATIONS

Figure		Page
B-1	Percent Noise Regulation (500 kHz)	B-1
B-2	Percent Noise Regulation (5 MHz)	B-2
B-3	Percent Noise Regulation (Linear Normal)	B-3
B-4	Percent Noise Regulation (Linear MTI)	B-4
B-5	Percent Noise Regulation (Log Normal)	B-5
B-6	Percent Noise Regulation (Extended Range MTI)	B-6
B-7	Percent Noise Regulation (MTI Log)	B-7



76-22-B1

FIGURE B-1. PERCENT NOISE REGULATION (500 kHz)

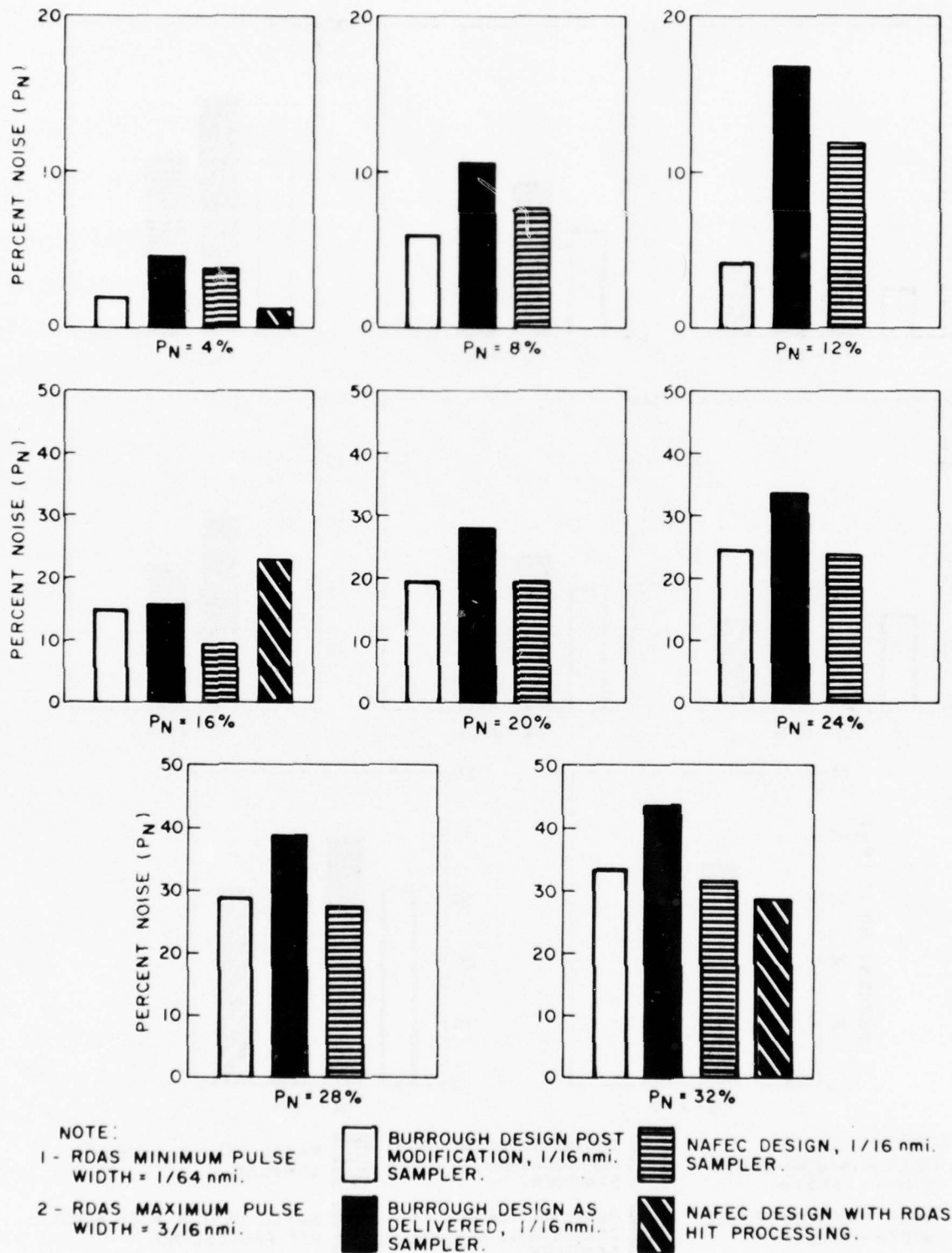
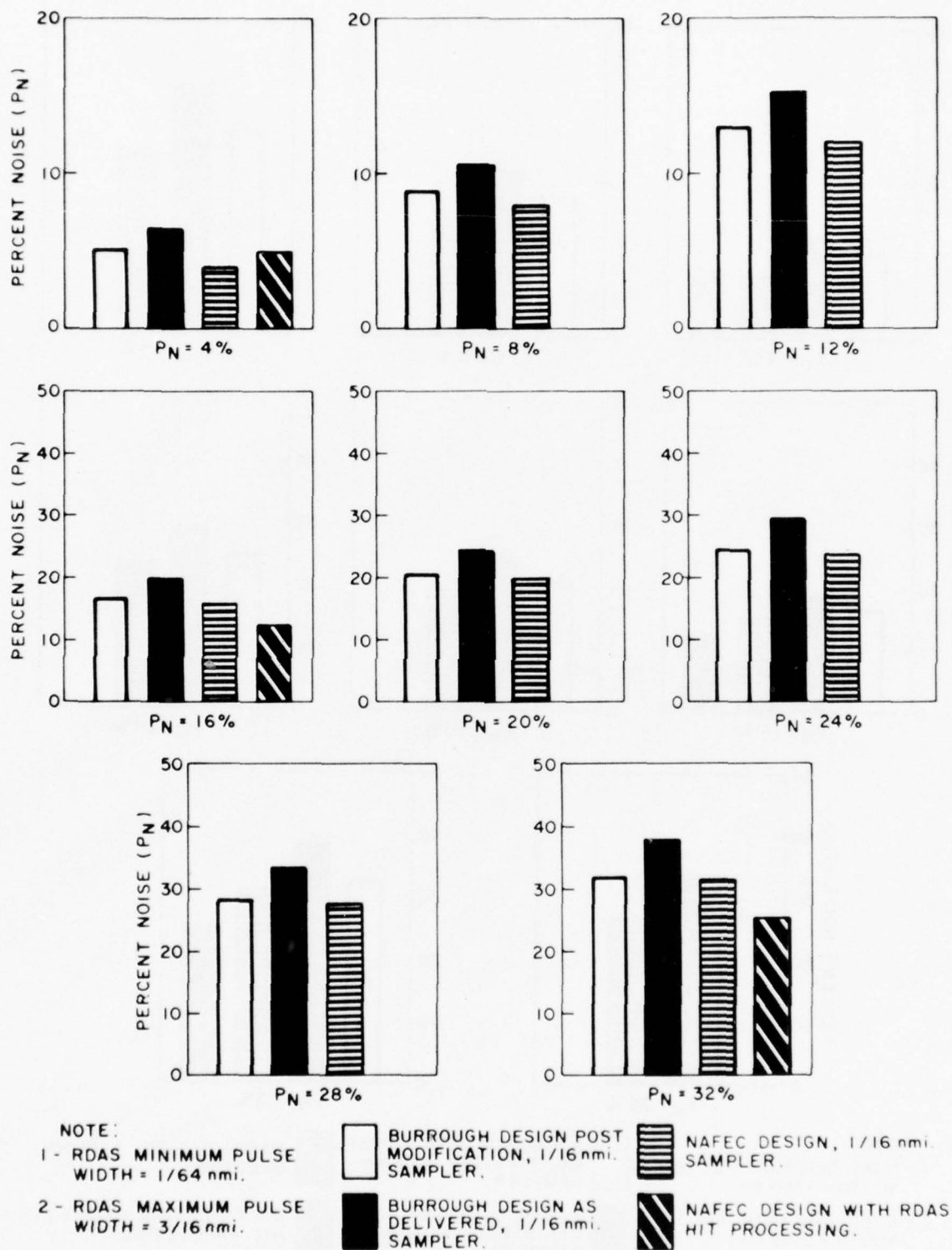


FIGURE B-2. PERCENT NOISE REGULATION (5 MHz)

76-22-B2



76-22-B3

FIGURE B-3. PERCENT NOISE REGULATION (LINEAR NORMAL)

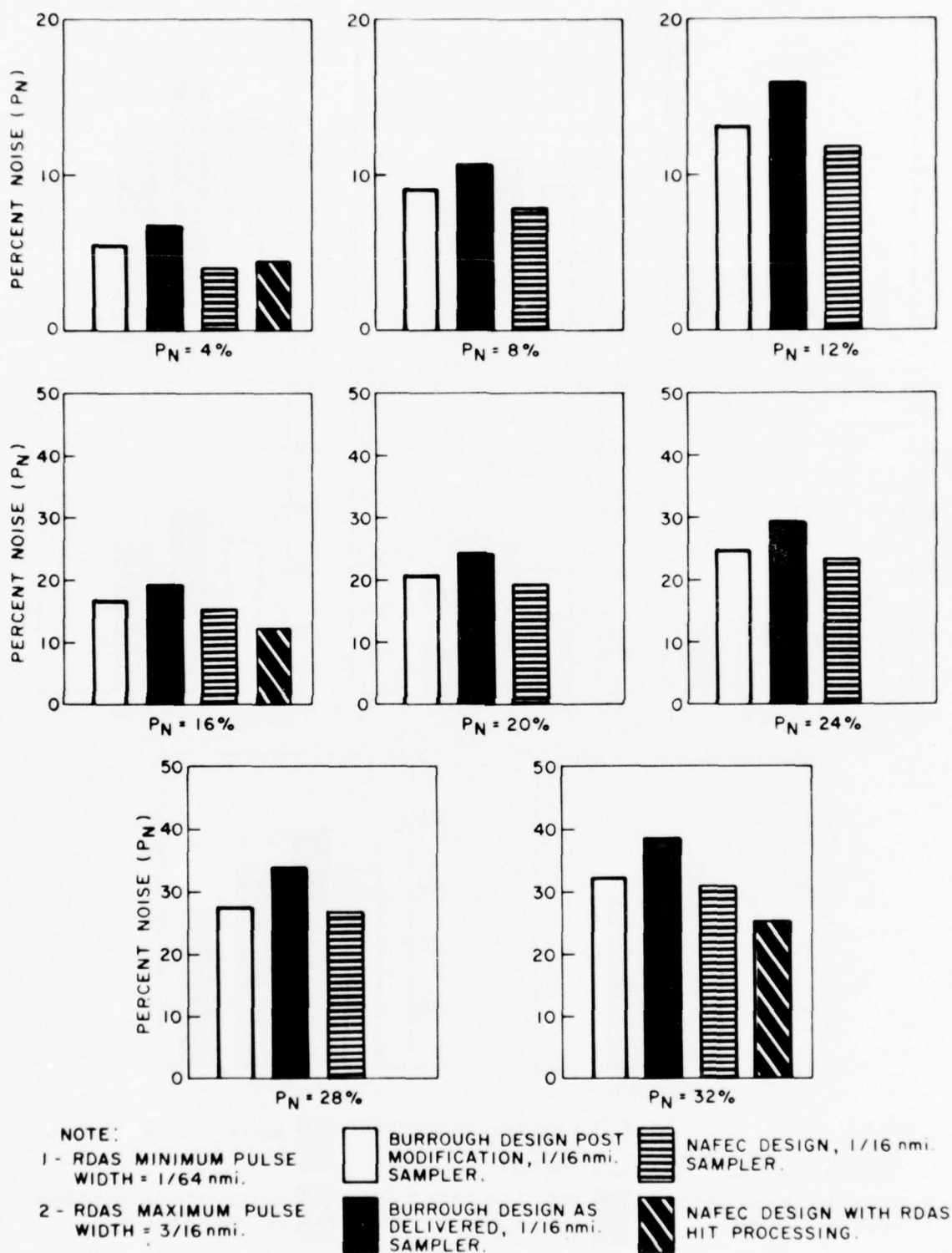
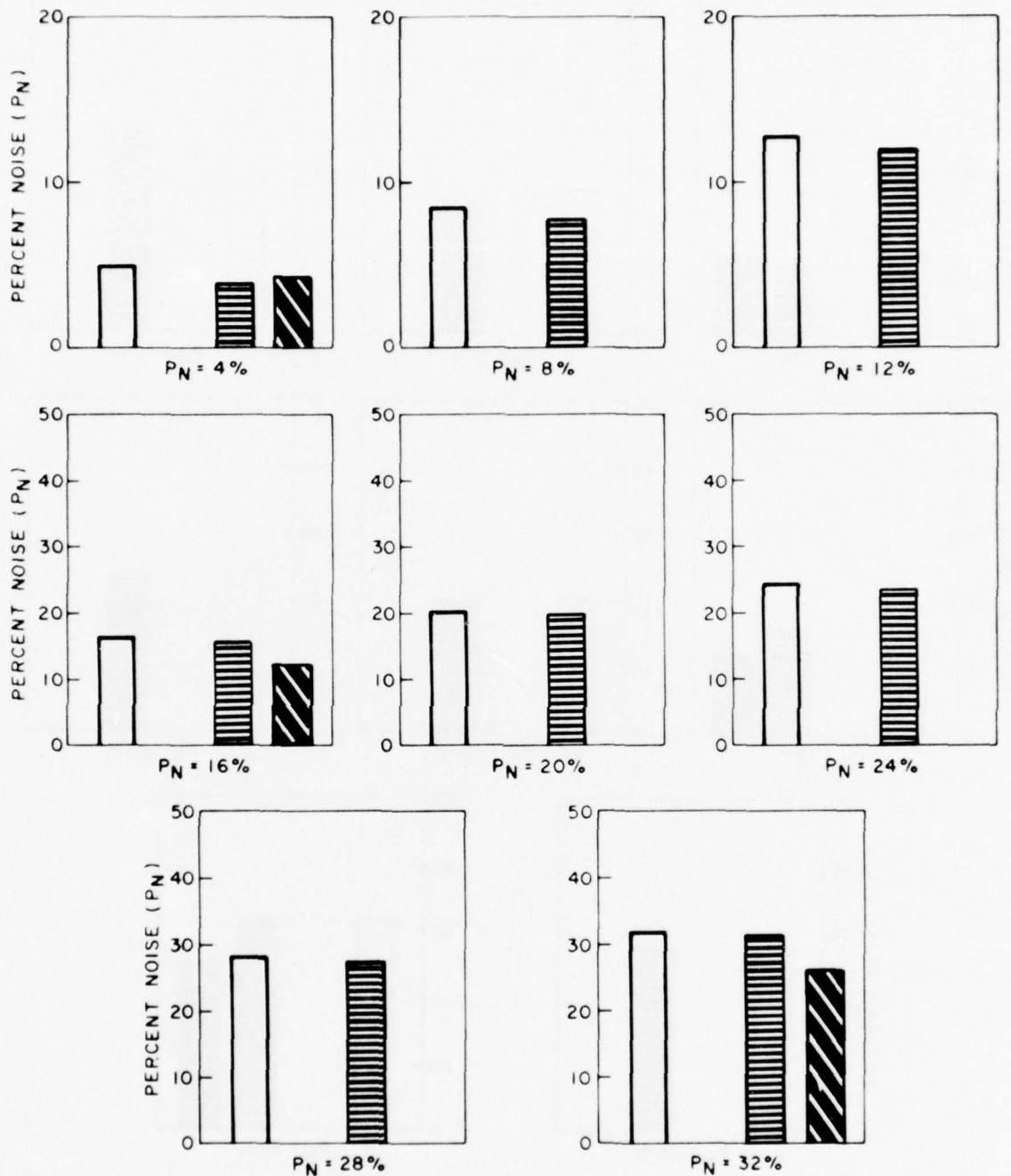


FIGURE B-4. PERCENT NOISE REGULATION (LINEAR MTI)

76-22-B4



NOTE:
 1 - RDAS MINIMUM PULSE WIDTH = 1/64 nmi.
 2 - RDAS MAXIMUM PULSE WIDTH = 3/16 nmi.

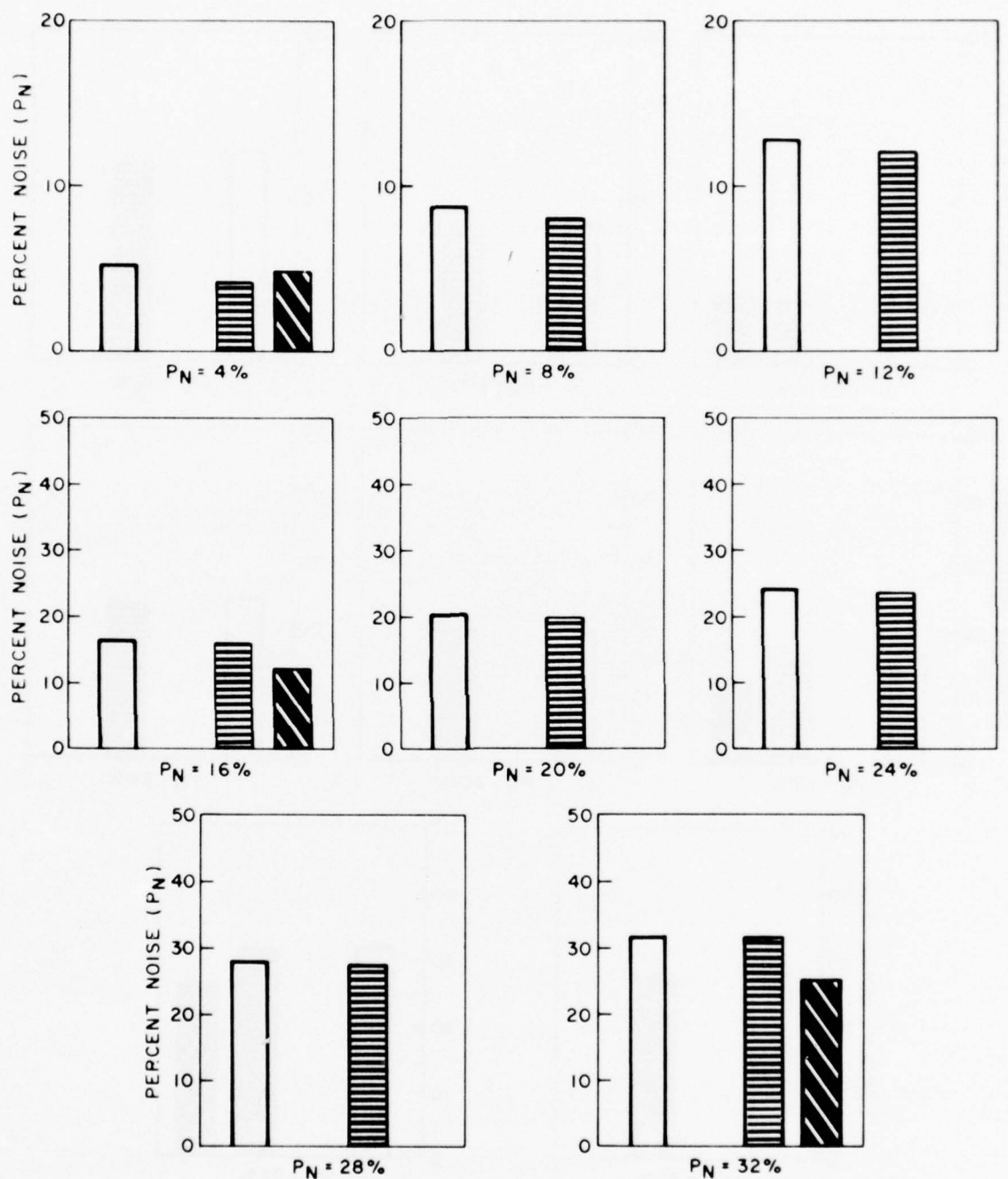
BURROUGH DESIGN POST MODIFICATION, 1/16 nmi. SAMPLER.

NAFEC DESIGN, 1/16 nmi. SAMPLER.

NAFEC DESIGN WITH RDAS HIT PROCESSING.

76-22-B5

FIGURE B-5. PERCENT NOISE REGULATION (LOG NORMAL)



NOTE:
 1 - RDAS MINIMUM PULSE
 WIDTH = 1/64 nmi.
 2 - RDAS MAXIMUM PULSE
 WIDTH = 3/16 nmi.

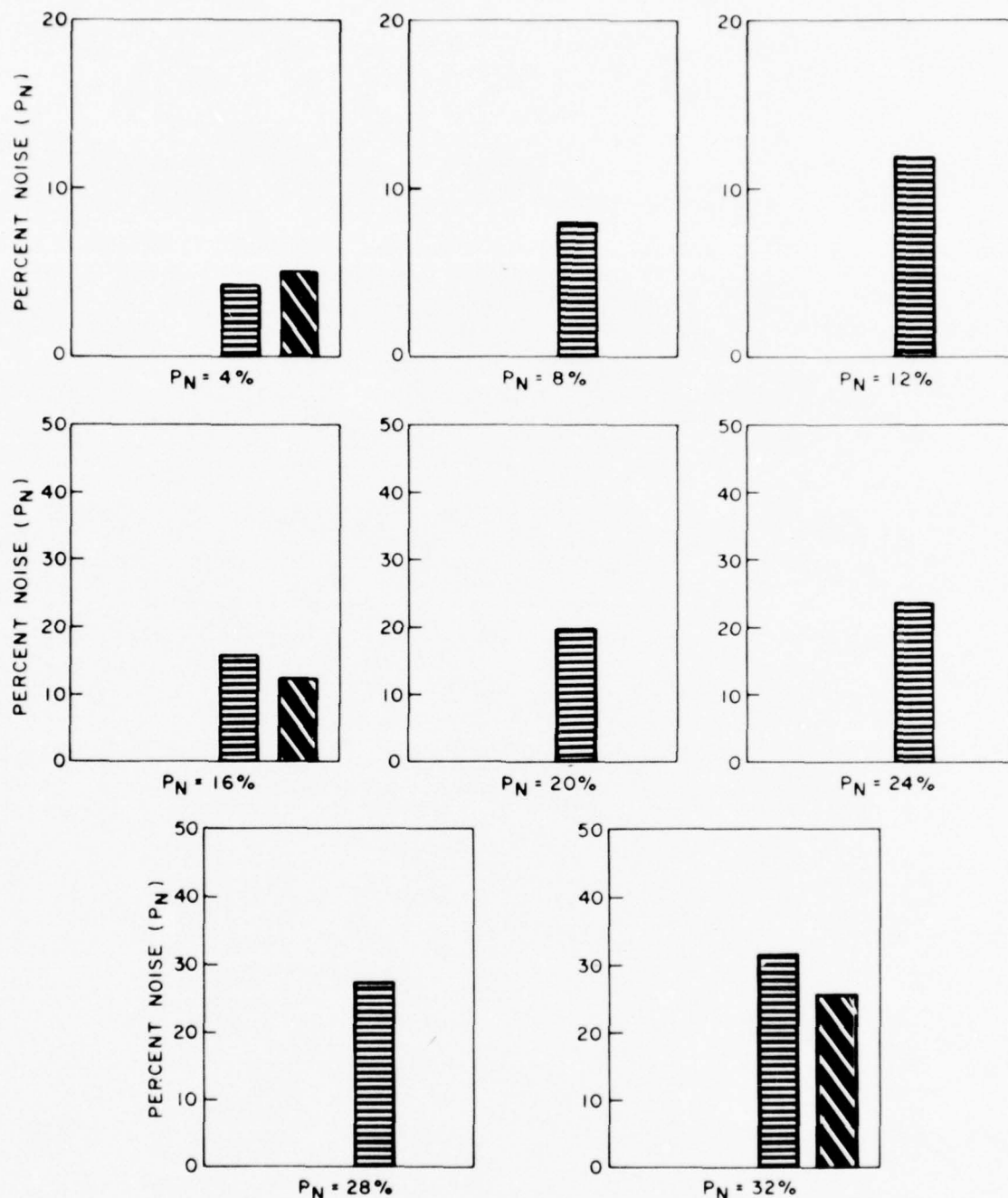
□ BURROUGH DESIGN POST
 MODIFICATION, 1/16 nmi.
 SAMPLER.

▨ NAFEC DESIGN, 1/16 nmi.
 SAMPLER.

▩ NAFEC DESIGN WITH RDAS
 HIT PROCESSING.

FIGURE B-6. PERCENT NOISE REGULATION (EXTENDED RANGE MTI)

76-22-B6



NOTE:
 1 - RDAS MINIMUM PULSE
 WIDTH = 1/64 nmi.
 2 - RDAS MAXIMUM PULSE
 WIDTH = 3/16 nmi.

NAFEC DESIGN, 1/16 nmi.
 SAMPLER.
 NAFEC DESIGN WITH RDAS
 HIT PROCESSING.

FIGURE B-7. PERCENT NOISE REGULATION (MTI LOG)

75-22-B7



The following table shows the number of cases of the several diseases reported in the city of New York during the years 1910, 1911, and 1912. The diseases are arranged in the order in which they appear in the accompanying charts. The number of cases is given in the column headed "Number of Cases." The total number of cases for each year is given in the column headed "Total."

The following table shows the number of cases of the several diseases reported in the city of New York during the years 1910, 1911, and 1912. The diseases are arranged in the order in which they appear in the accompanying charts. The number of cases is given in the column headed "Number of Cases." The total number of cases for each year is given in the column headed "Total."

APPENDIX C

PERCENT NOISE FOR WEATHER SAMPLES

APPENDIX C

LIST OF ILLUSTRATIONS

Figure		Page
C-1	Clutter P_N Regulation Sample ASR-5 WW 29	C-1
C-2	Clutter P_N Regulation Sample ASR-5 Extended Range MTI No. 1	C-2
C-3	Clutter P_N Regulation Sample ASR-5 Angel Clutter No. 4	C-3
C-4	Clutter P_N Regulation Sample ASR-5 WW 34	C-4
C-5	Clutter P_N Regulation Sample ASR-5 WW 49	C-5
C-6	Clutter P_N Regulation Sample ASR-7 4/15/75 AM	C-6
C-7	Clutter P_N Regulation Sample ASR-7 4/3/75	C-7
C-8	Clutter P_N Regulation Sample ASR-7 4/15/75 PM	C-8
C-9	Clutter P_N Regulation Sample ASR-7 7/14/75	C-9

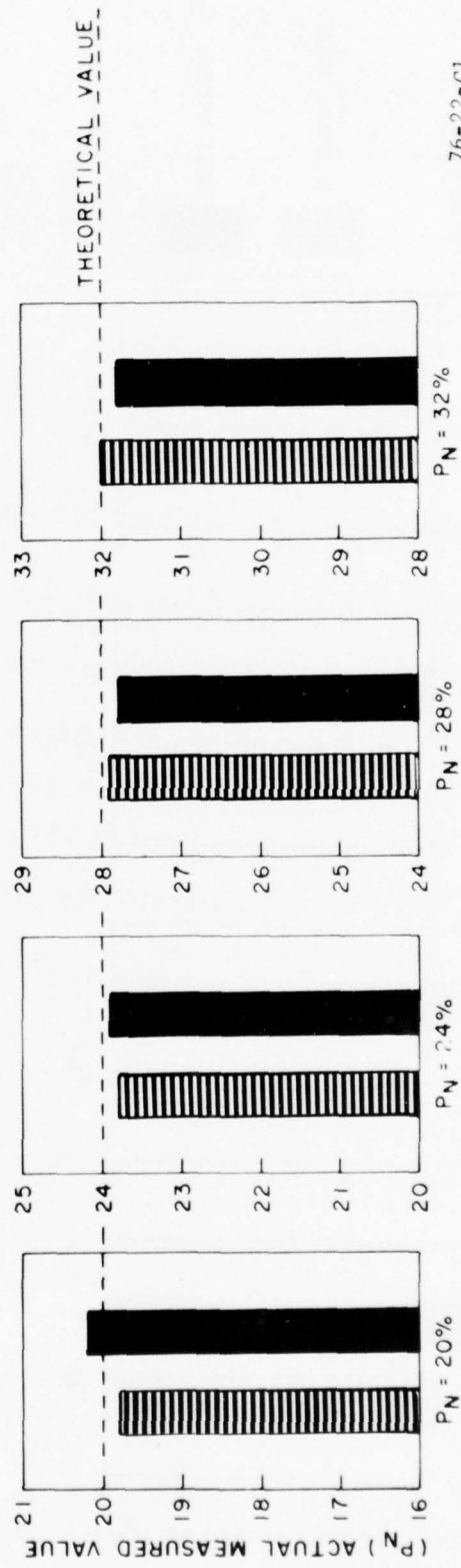
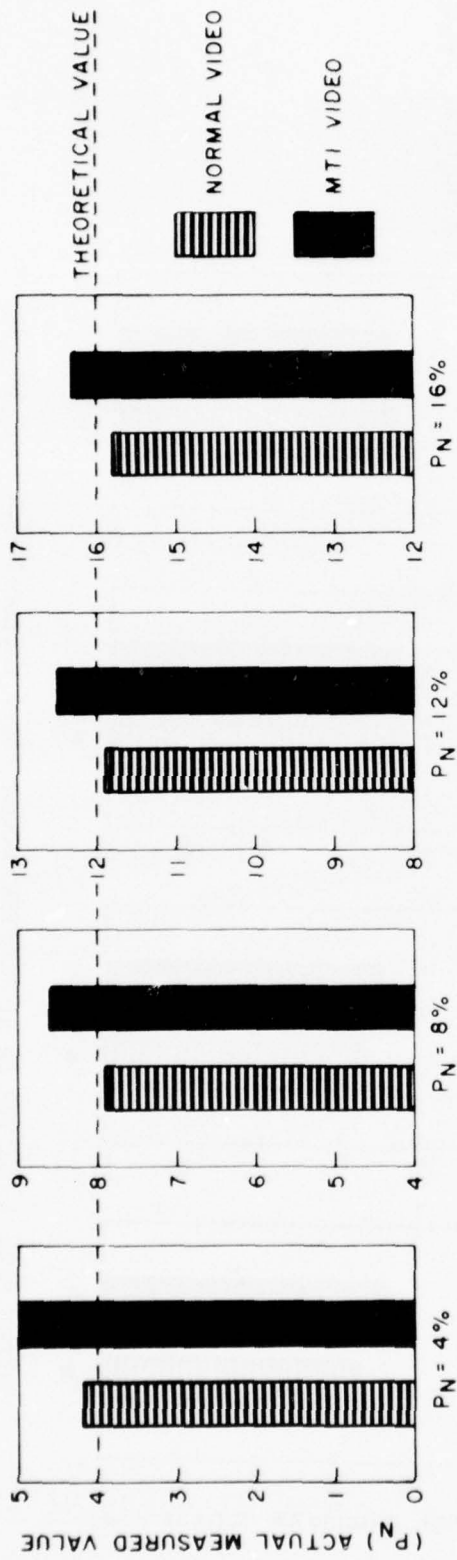


FIGURE C-1. CLUTTER P_N REGULATION SAMPLE ASR-5 WW 29

76-22-C1

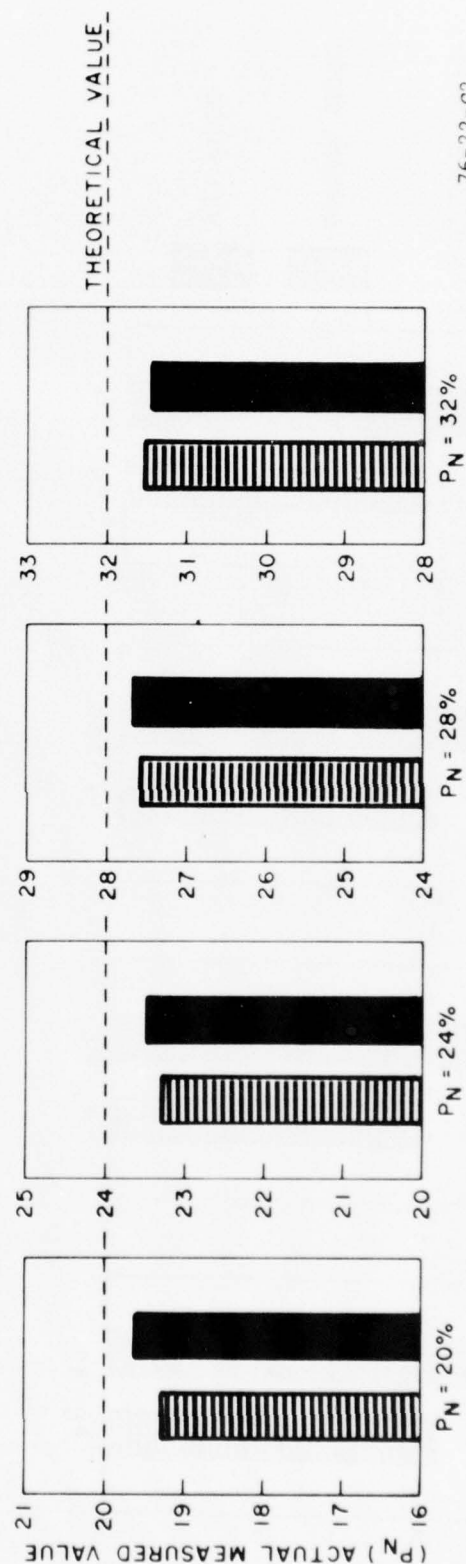
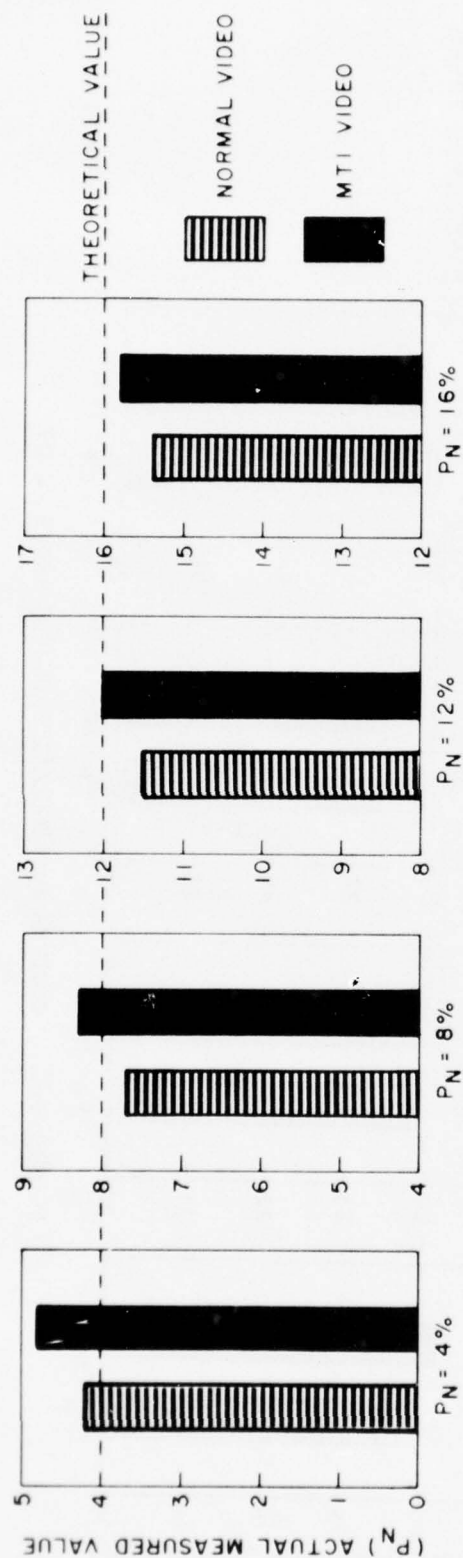


FIGURE C-2. CLUTTER P_N REGULATION SAMPLE ASR-5 EXTENDED RANGE MTI NO. 1

76-22-C2

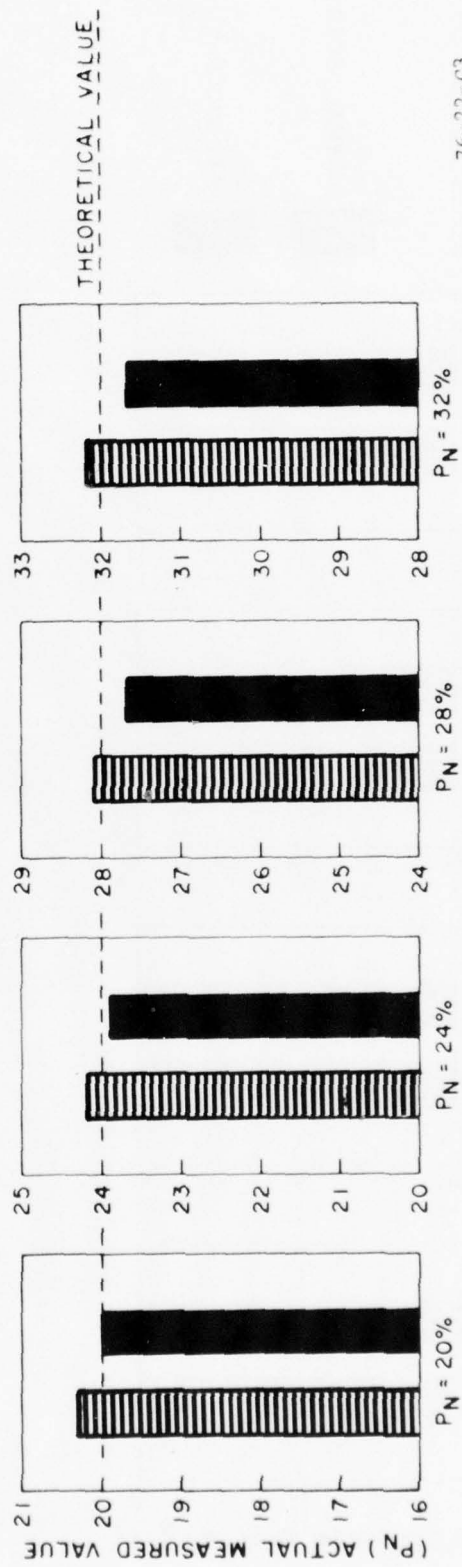
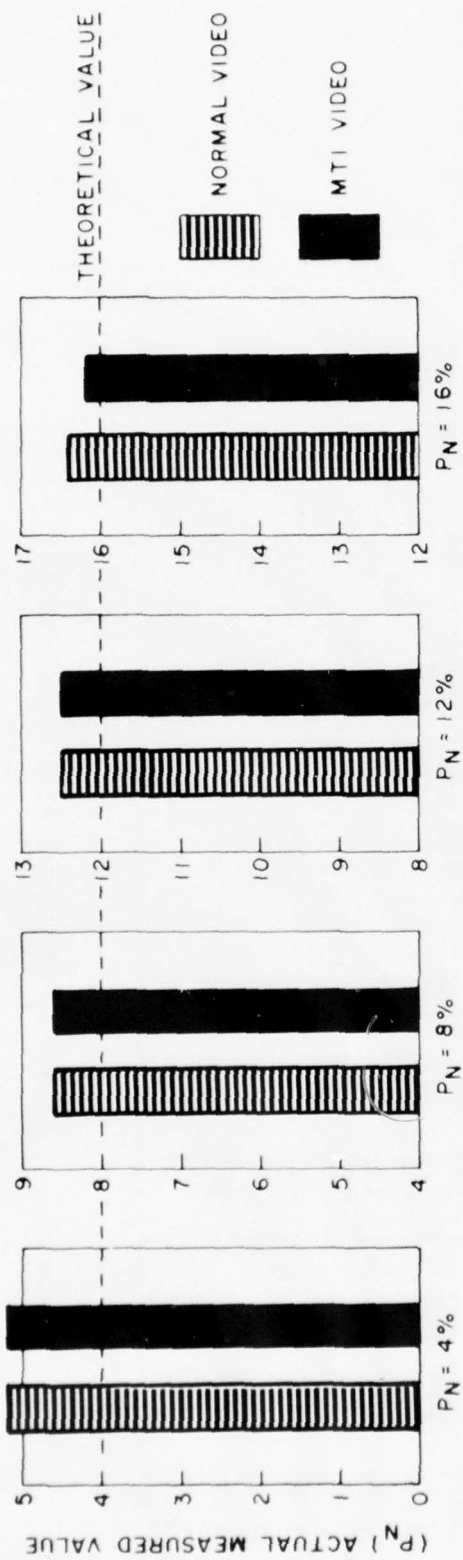


FIGURE C-3. CLUTTER P_N REGULATION SAMPLE ASR-5 ANGEL CLUTTER NO. 4

76-22-C3

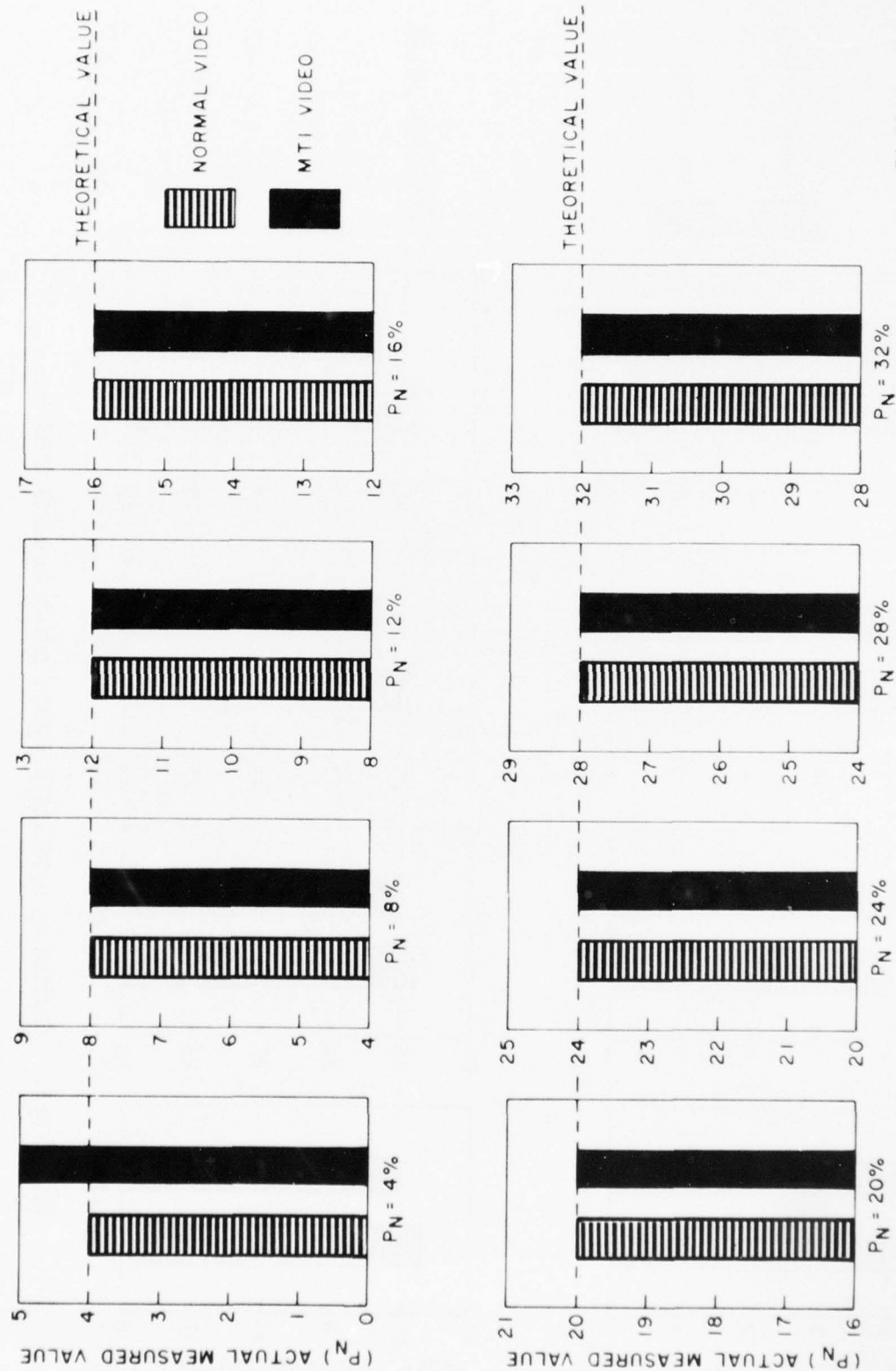


FIGURE C-4. CLUTTER P_N REGULATION SAMPLE ASR-5 WW 34

76-22-C4

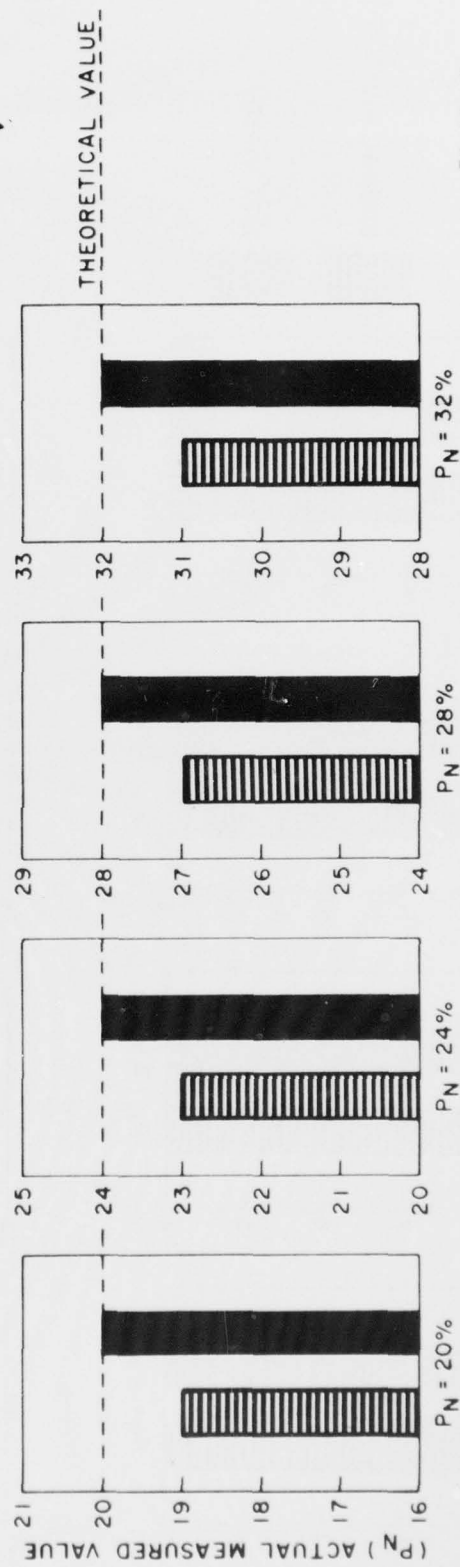
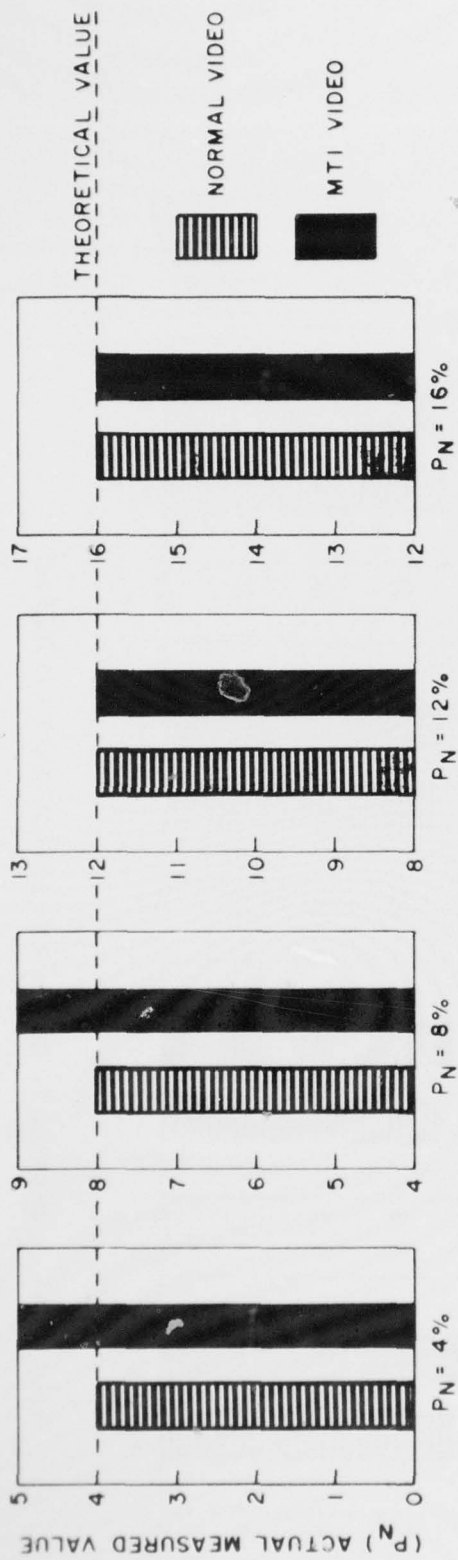


FIGURE C-5. CLUTTER P_N REGULATION SAMPLE ASR-5 WW 49

76-22-C5

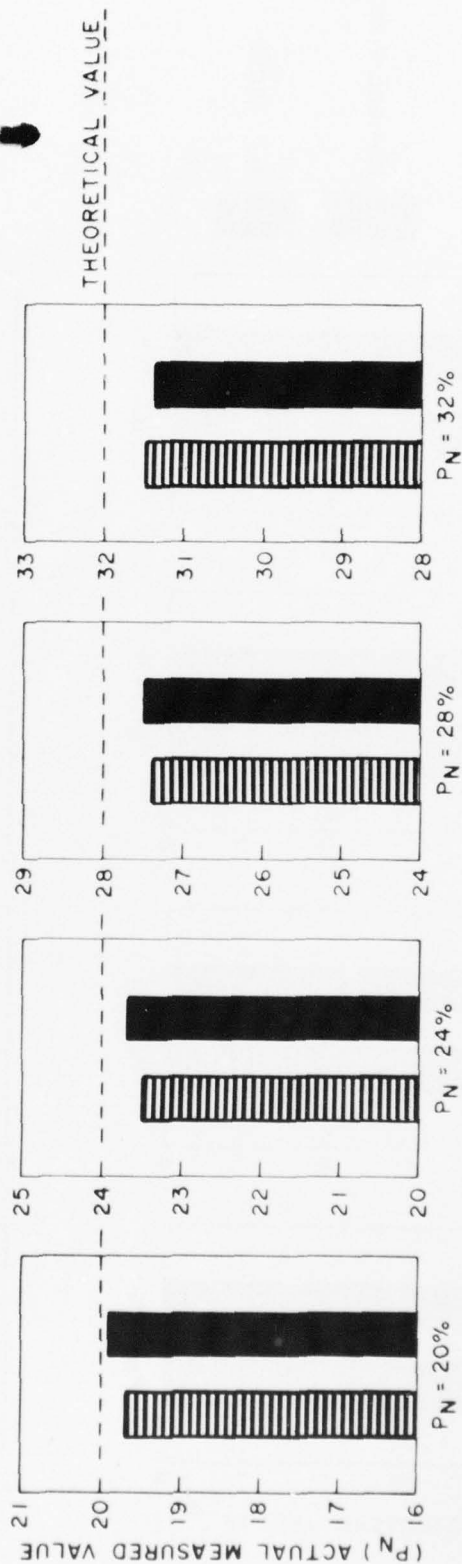
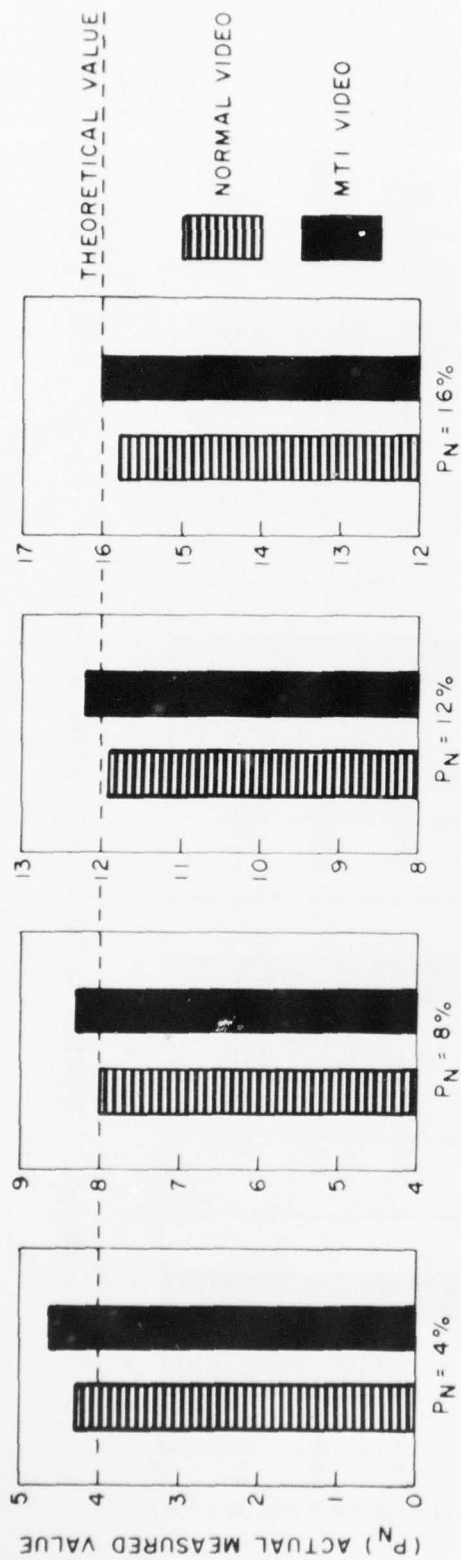


FIGURE C-6. CLUTTER P_N REGULATION SAMPLE ASR-7 4/15/75 AM

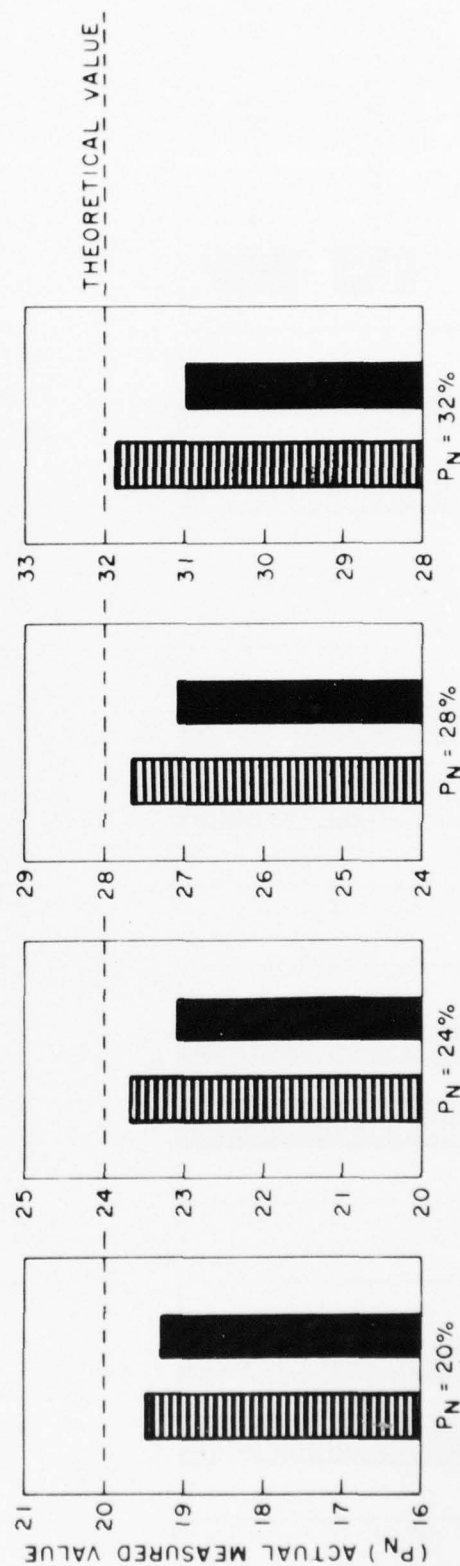
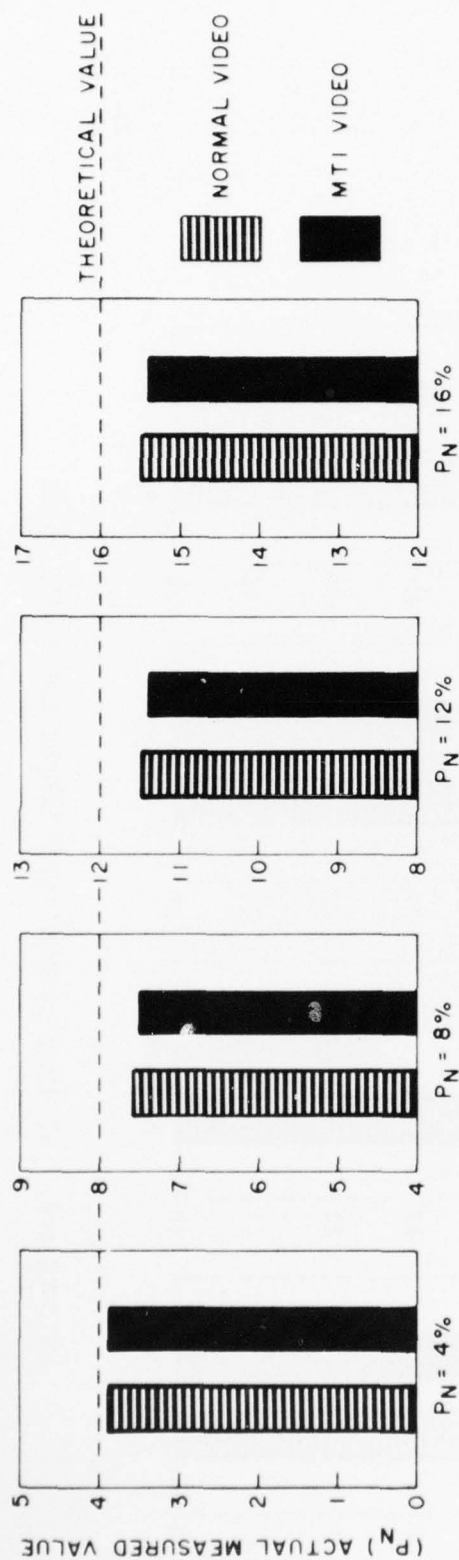


FIGURE C-7. CLUTTER P_N REGULATION SAMPLE ASR-7 4/3/75

76-22-C7

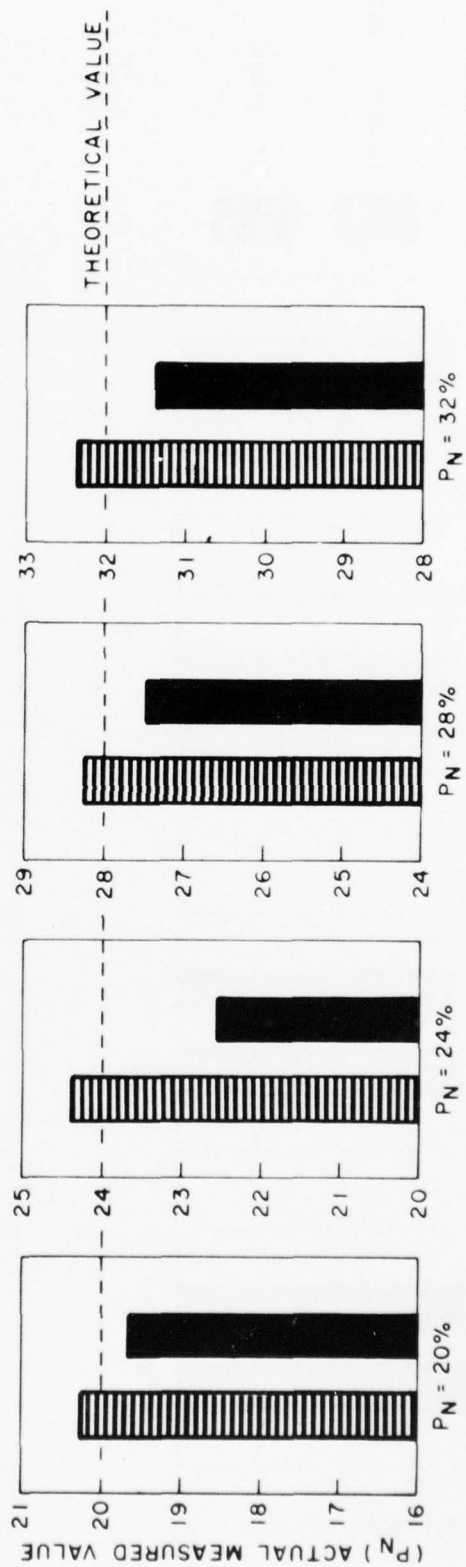
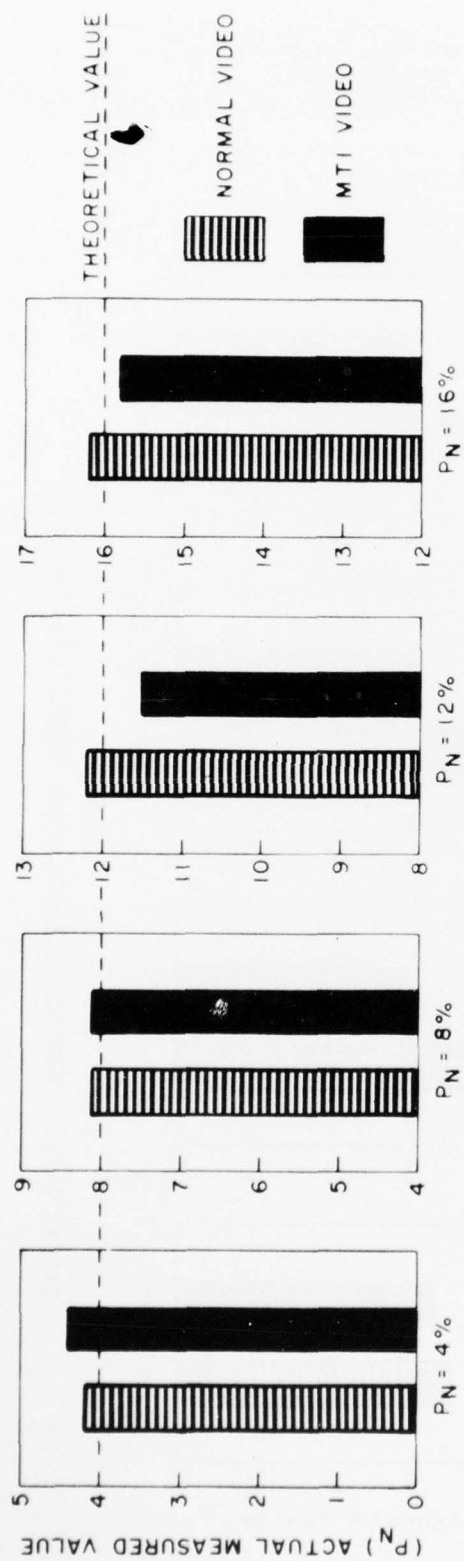
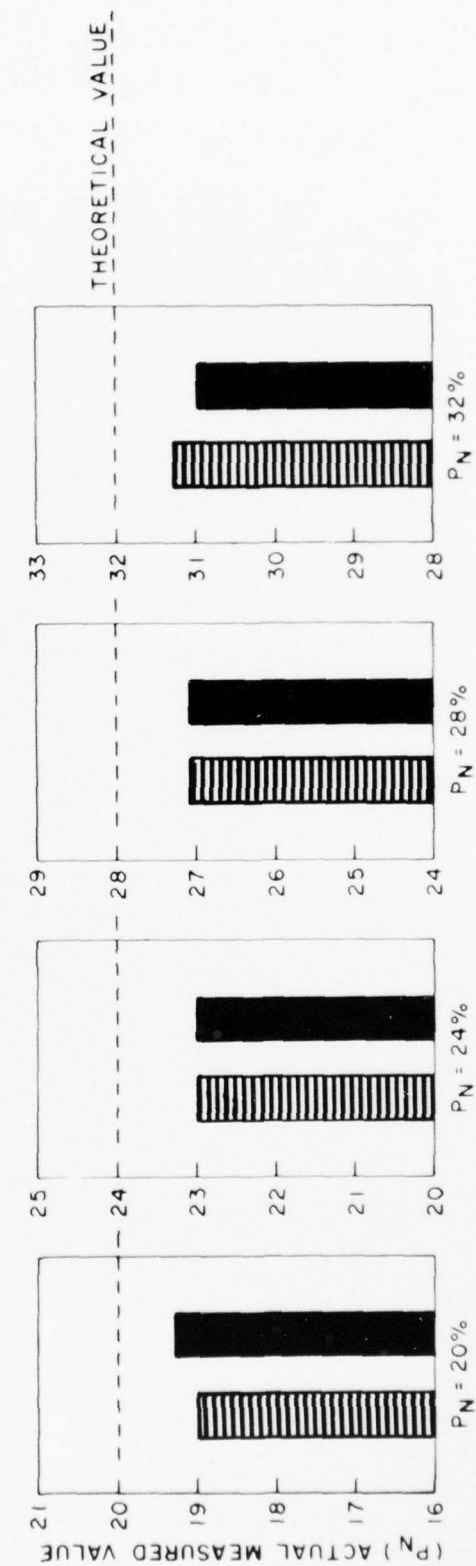
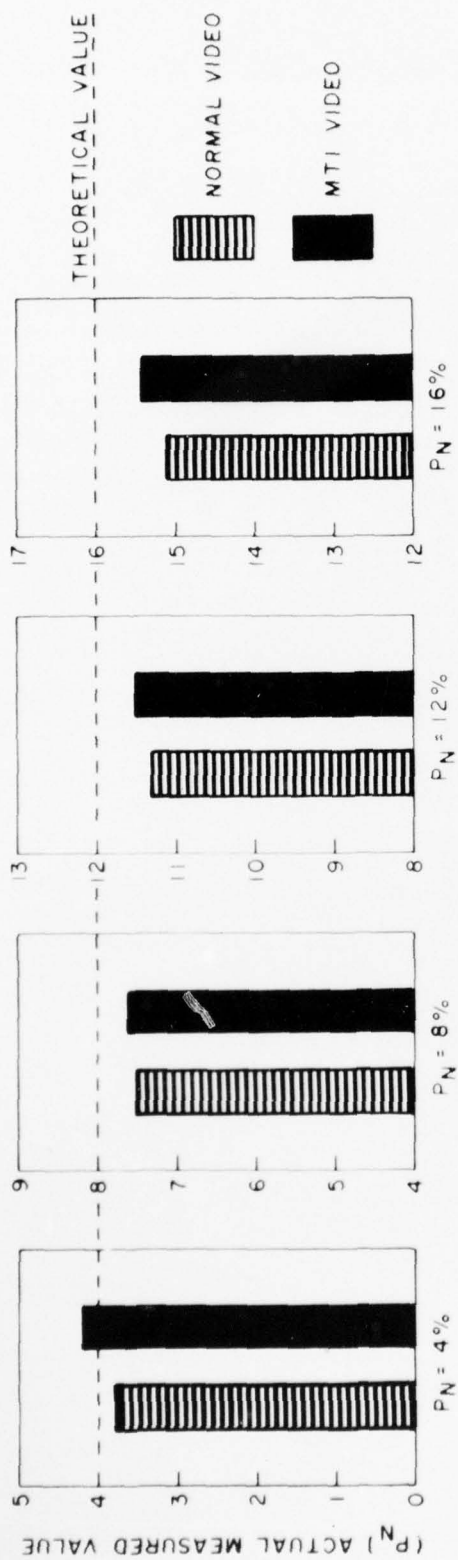


FIGURE C-8. CLUTTER P_N REGULATION SAMPLE ASR-7 4/15/75 PM

76-22-C8



76-22-09

FIGURE C-9. CLUTTER P_N REGULATION SAMPLE ASR-7 7/14/75

APPENDIX D

ISOLATED-HIT PERFORMANCE

APPENDIX D

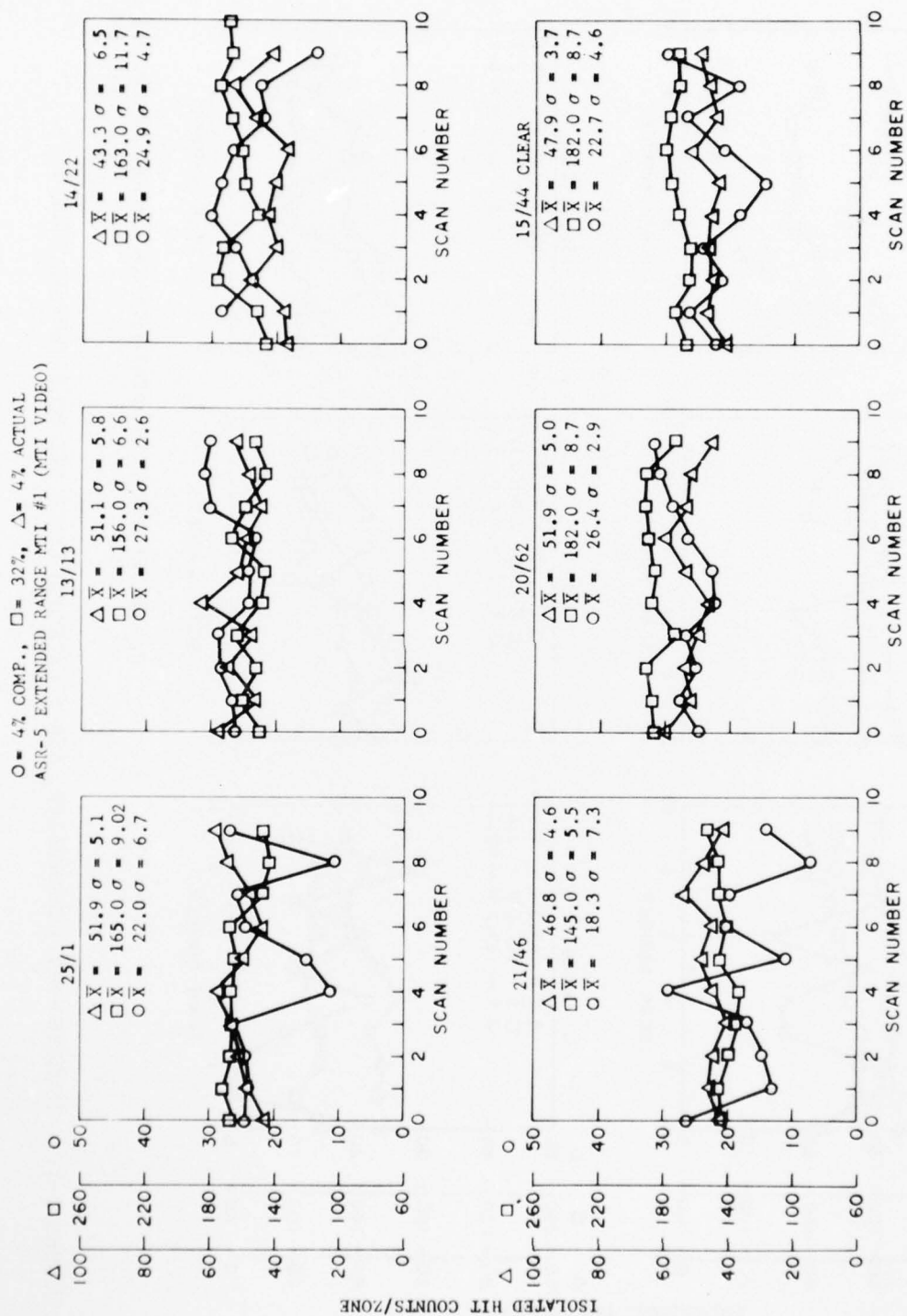
LIST OF ILLUSTRATIONS

Figure		Page
D-1	Isolated-Hit Performance, ASR-5 Extended Range MTI No. 1 (MTI Video)	D-1
D-2	Isolated-Hit Performance, ASR-5 Extended Range MTI No. 1 (Normal Video)	D-2
D-3	Isolated-Hit Performance, ASR-5 WW29 (MTI Video)	D-3
D-4	Isolated-Hit Performance, ASR-5 WW29 (Normal Video)	D-4
D-5	Isolated-Hit Performance, ASR-5 Angel Clutter No. 4 (MTI Video)	D-5
D-6	Isolated-Hit Performance, ASR-5 Angel Clutter No. 4 (Normal Video)	D-6
D-7	Isolated-Hit Performance, ASR-5 WW34 (MTI Video)	D-7
D-8	Isolated-Hit Performance, ASR-5 WW34 (Normal Video)	D-8
D-9	Isolated-Hit Performance, ASR-5 WW49 (MTI Video)	D-9
D-10	Isolated-Hit Performance, ASR-5 WW49 (Normal Video)	D-10
D-11	Isolated-Hit Processing, ASR-7, 3-12-75 (MTI Video, Map 1)	D-11
D-12	Isolated-Hit Processing, ASR-7, 3-12-75 (MTI Video, Map 1) Continued	D-12
D-13	Isolated-Hit Performance, ASR-7, 3-12-75, (Normal Video Map 1)	D-13
D-14	Isolated-Hit Processing, ASR-7, 3-12-75 (MTI Video) (Normal, Map 1)	D-14
D-15	Isolated-Hit Processing, ASR-7, 3-12-75 (MTI Video, Map 2)	D-15
D-16	Isolated-Hit Performance, ASR-7, 3-12-75, (MTI Video Map 2) Continued	D-16
D-17	Isolated-Hit Performance, ASR-7, 3-12-75 (Normal Video Map 2)	D-17

APPENDIX D

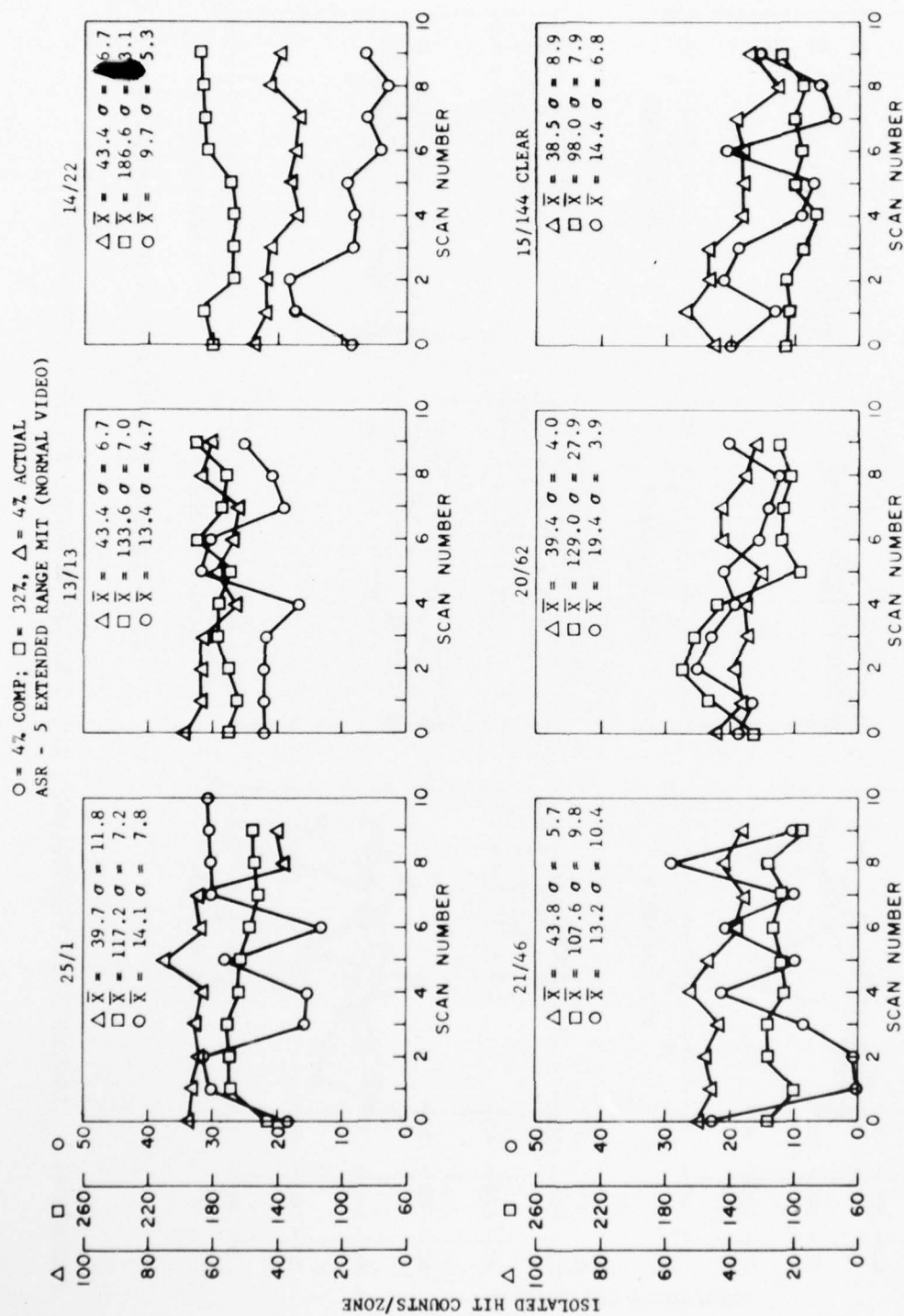
LIST OF ILLUSTRATIONS (Continued)

Figure		Page
D-18	Isolated-Hit Performance, ASR-7, 3-12-75 (Normal Video Map 2) Continued	D-18
D-19	Isolated-Hit Performance, ASR-7, 4-15-75 PM (MTI Video)	D-19
D-20	Isolated-Hit Performance, ASR-7, 4-15-75 PM (MTI Video) Continued	D-20
D-21	Isolated-Hit Performance, ASR-7, 4-15-75 PM (Normal Video)	D-21
D-22	Isolated-Hit Performance, ASR-7, 4-15-75 PM (Normal Video) Continued	D-22
D-23	Isolated-Hit Performance, ASR-7, 4-15-75 PM (MTI Video Map 2)	D-23
D-24	Isolated-Hit Performance, ASR-7, 4-15-75 PM (Normal Video Map 2)	D-24
D-25	Isolated-Hit Performance, ASR-7, 4-15-75 AM (MTI Video Map 1)	D-25
D-26	Isolated-Hit Performance, ASR-7, 4-15-75 AM (Normal Video Map 1)	D-26
D-27	Isolated-Hit Performance, ASR-7, 4-3-75 AM (MTI Video)	D-27
D-28	Isolated-Hit Performance, ASR-7, 4-3-75 (Normal Video)	D-28
D-29	Isolated-Hit Performance, ASR-7, 4-14-75 AM (MTI Video)	D-29
D-30	Isolated-Hit Performance, ASR-7, 4-14-75 AM (MTI Video) Continued	D-30
D-31	Isolated-Hit Performance, ASR-7, 4-14-75 AM (Normal Video)	D-31



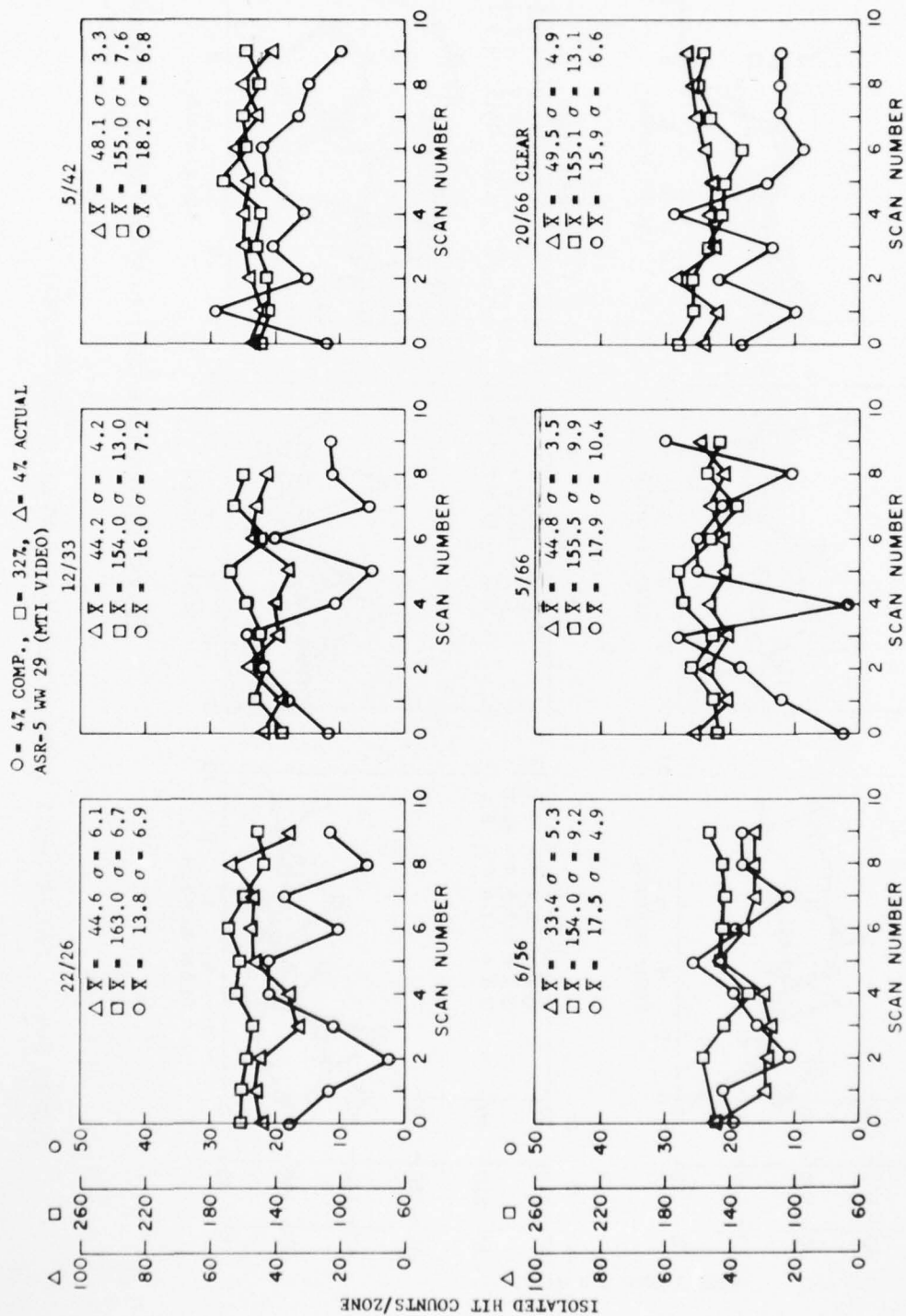
22/26 DENOTES ZONE IDENTIFICATION (RANGE / AZIMUTH)
76-22-D1

FIGURE D-1. ISOLATED-HIT PERFORMANCE, ASR-5 EXTENDED RANGE MTI NO.1 (NTI VIDEO)



22/26 DENOTES ZONE IDENTIFICATION (RANGE / AZIMUTH)
 76-22-D-2

FIGURE D-2. ISOLATED-HIT PERFORMANCE, ASR-5 EXTENDED RANGE MTI NO.1 (NORMAL VIDEO)



22 / 26 DENOTES ZONE IDENTIFICATION (RANGE / AZIMUTH)
76-22-D3

FIGURE D-3. ISOLATED-HIT PERFORMANCE ASR-5 WW29 (MTI VIDEO)

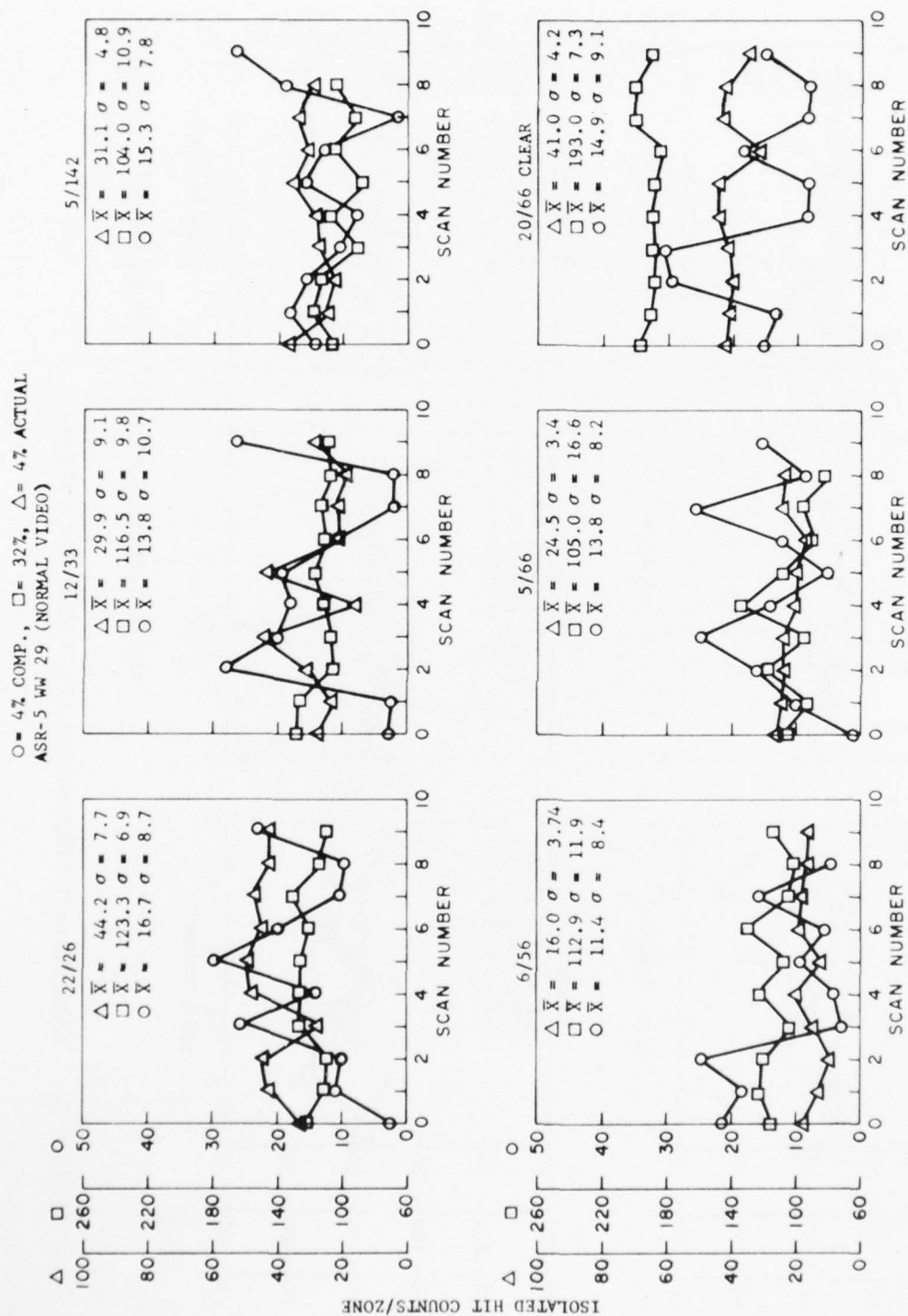


FIGURE D-4. ISOLATED-HIT PERFORMANCE, ASR-5 WW29 (NORMAL VIDEO)

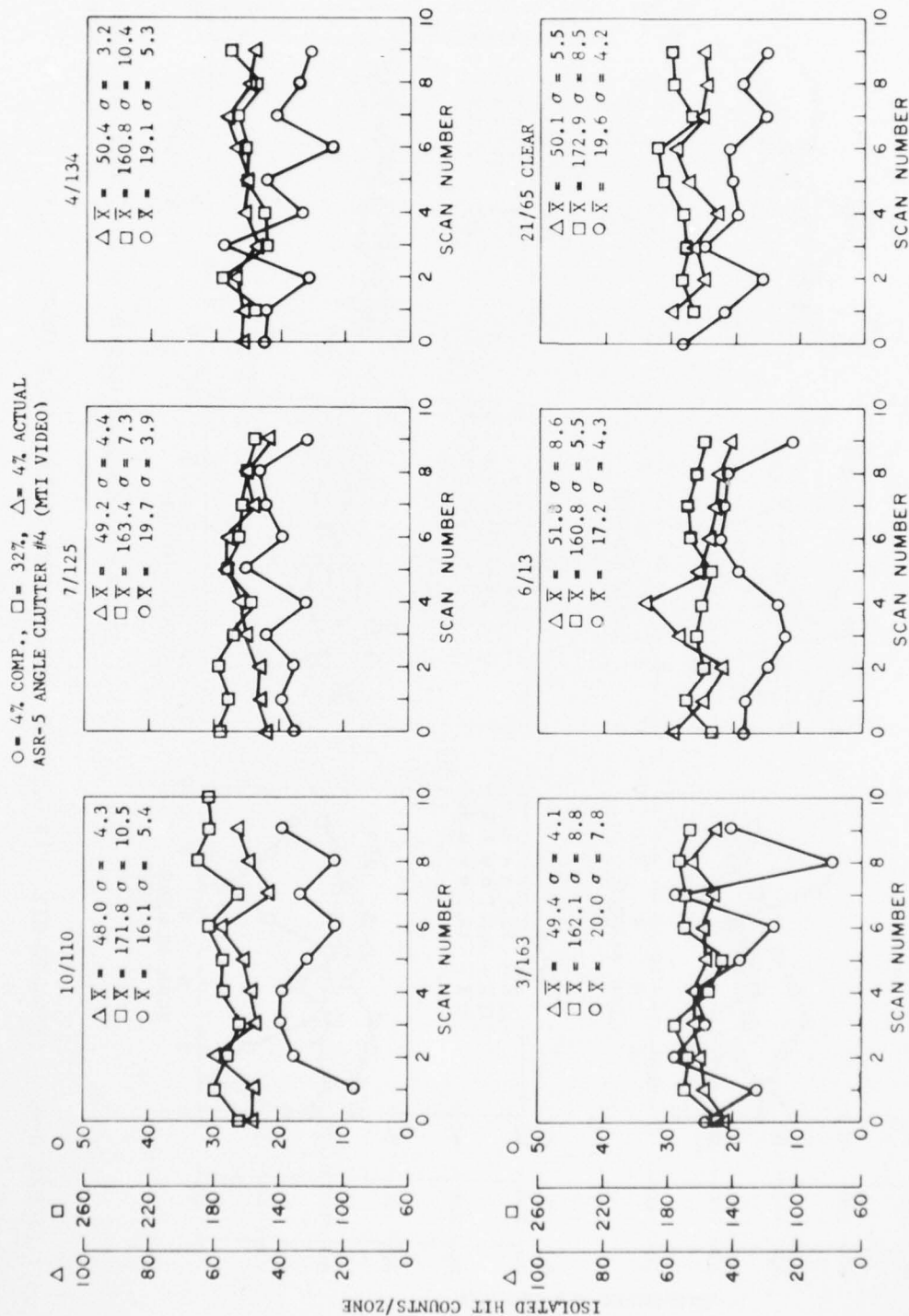
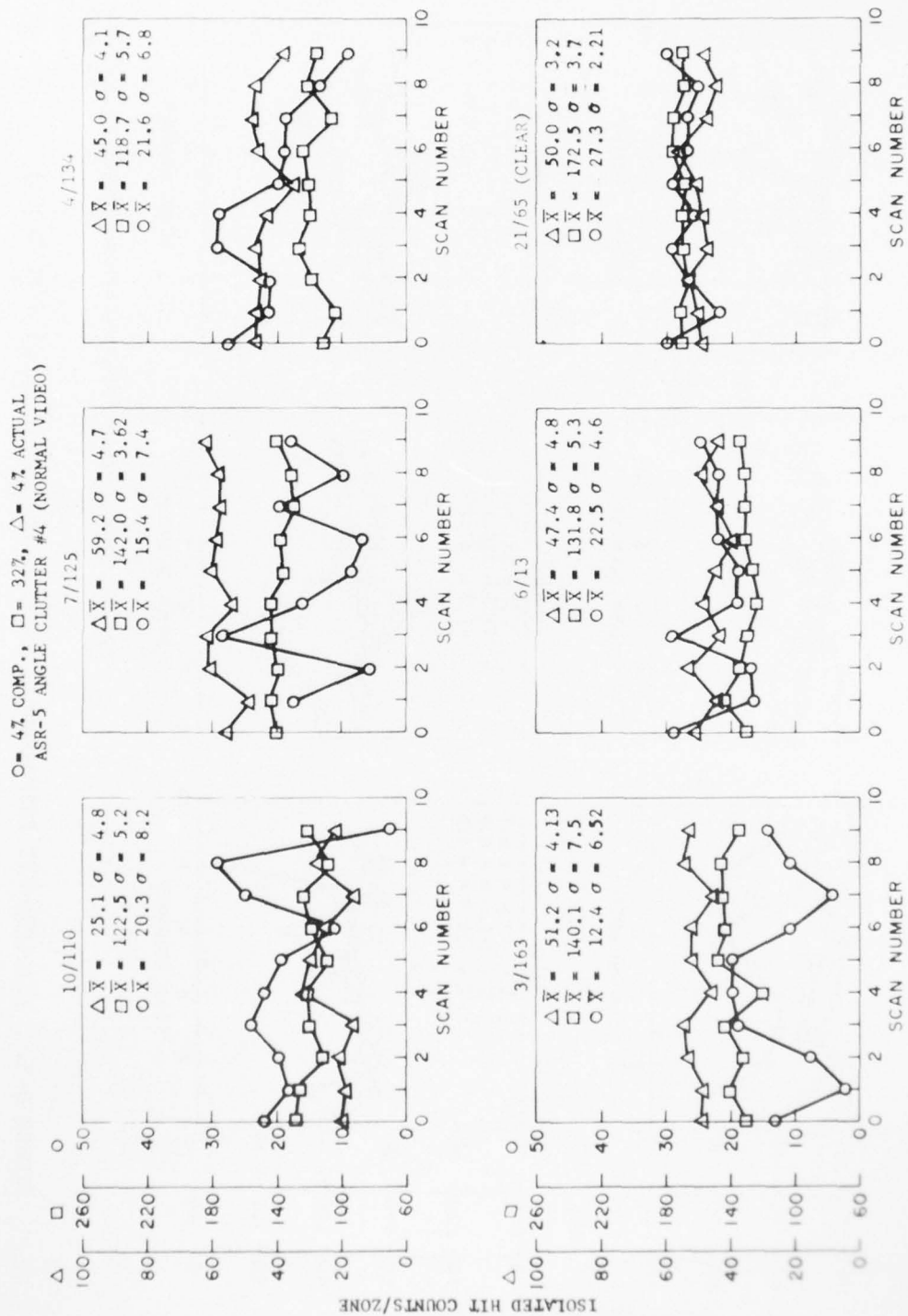


FIGURE D-5. ISOLATED-HIT PERFORMANCE, ASR-5 ANGEL CLUTTER NO.4 (MTI VIDEO)



22 / 26 DENOTES ZONE IDENTIFICATION (RANGE / AZIMUTH)
 76-22-D6

FIGURE D-6. ISOLATED-HIT PERFORMANCE, ASR-5 ANGEL CLUTTER NO.4 (NORMAL VIDEO)

AD-A038 624

NATIONAL AVIATION FACILITIES EXPERIMENTAL CENTER ATL--ETC F/G 17/9
TEST AND EVALUATION OF THE RADAR PROCESSING SUBSYSTEMS OF THE A--ETC(U)
MAR 77 M HOLTZ, L WAPELHORST

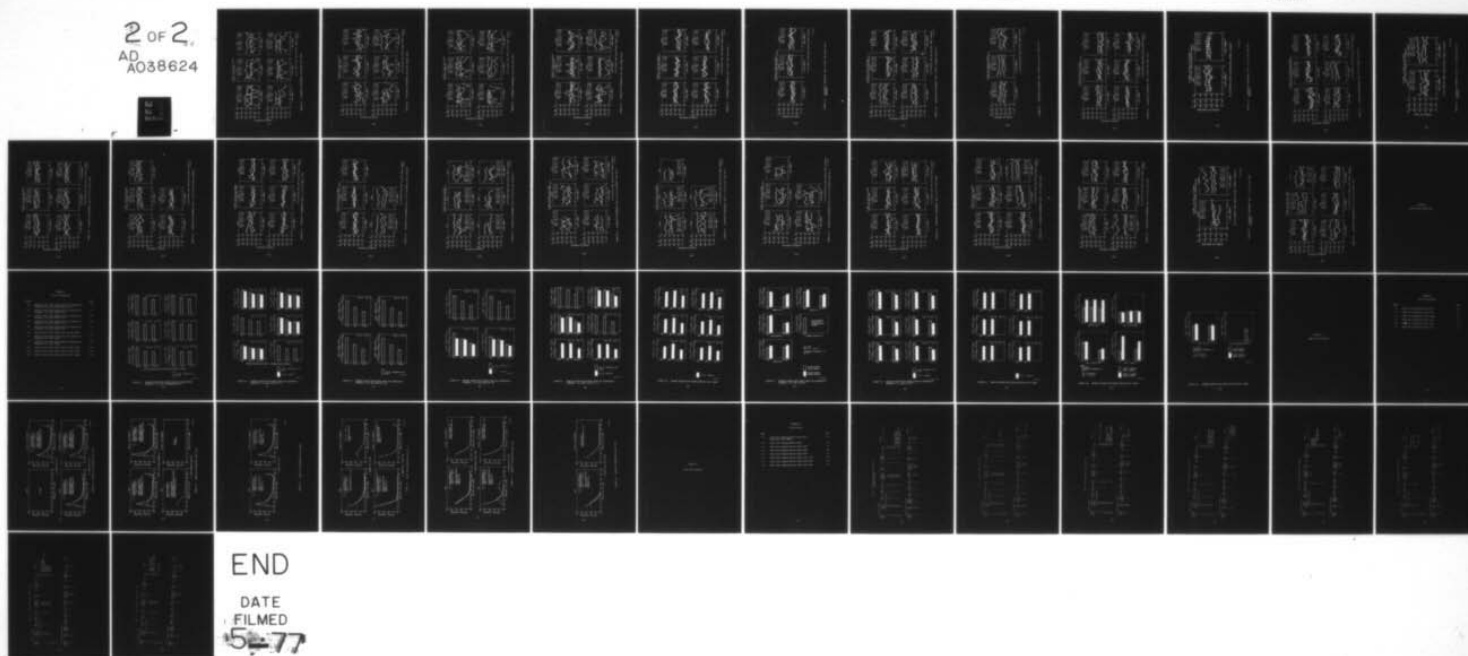
UNCLASSIFIED

FAA-NA-76-22

FAA-RD-76-197

NL

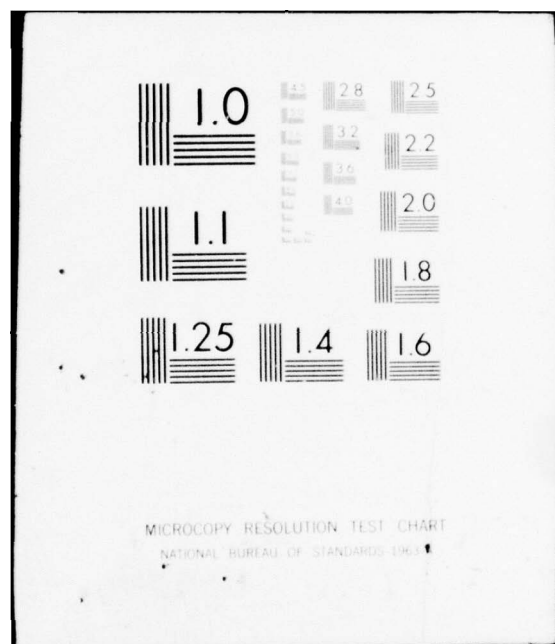
2 OF 2
AD
A038624

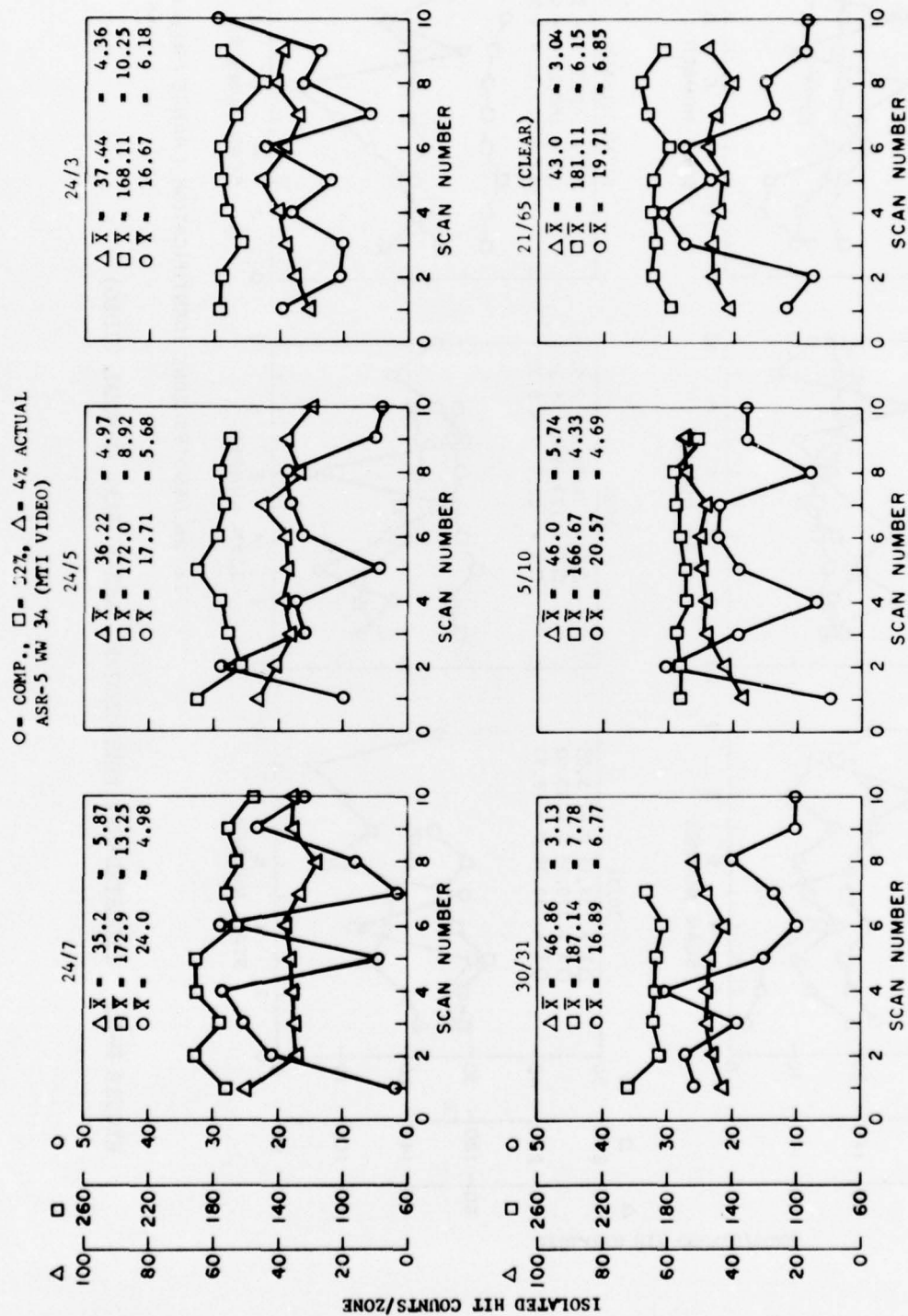


END

DATE
FILMED

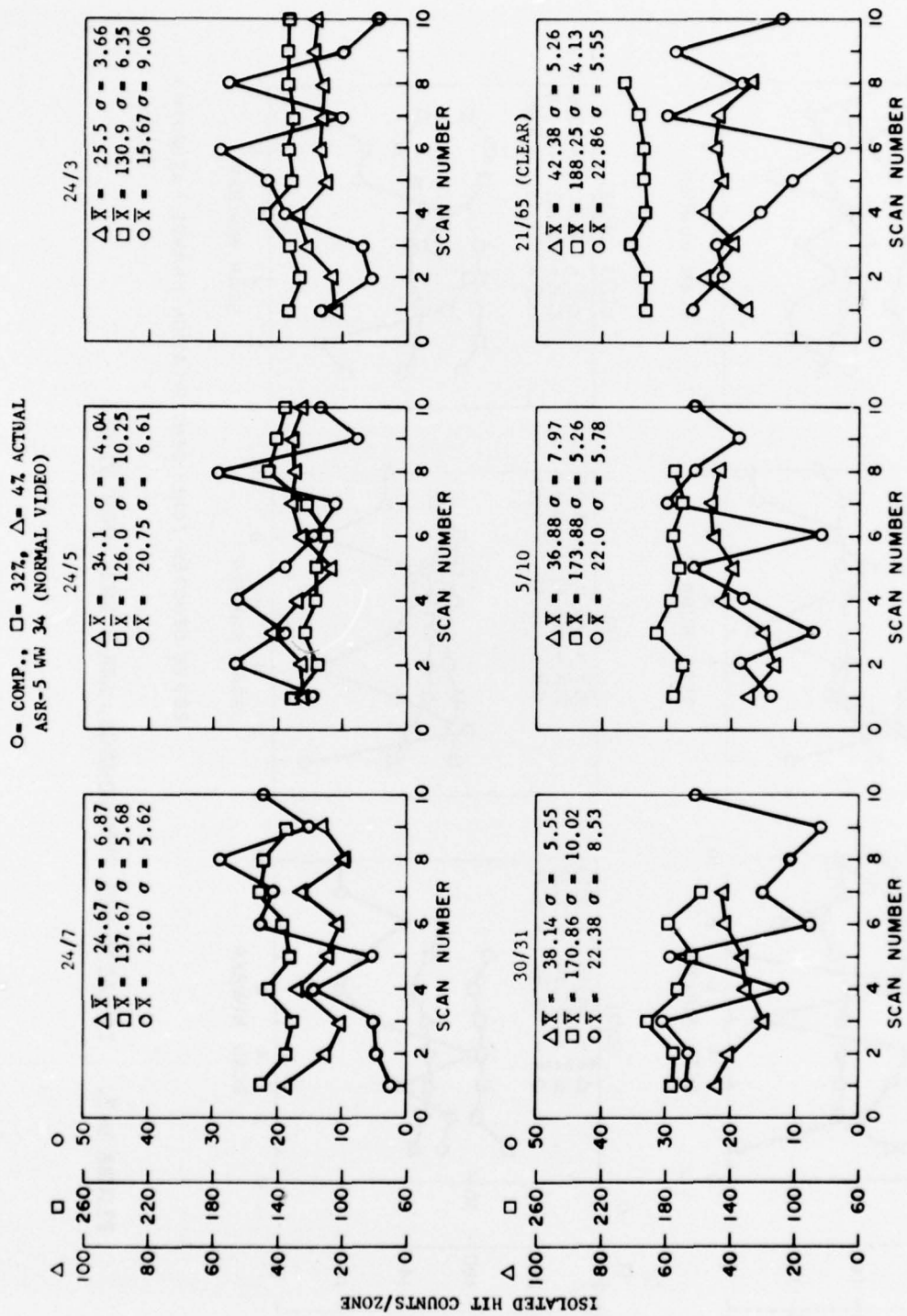
5-77





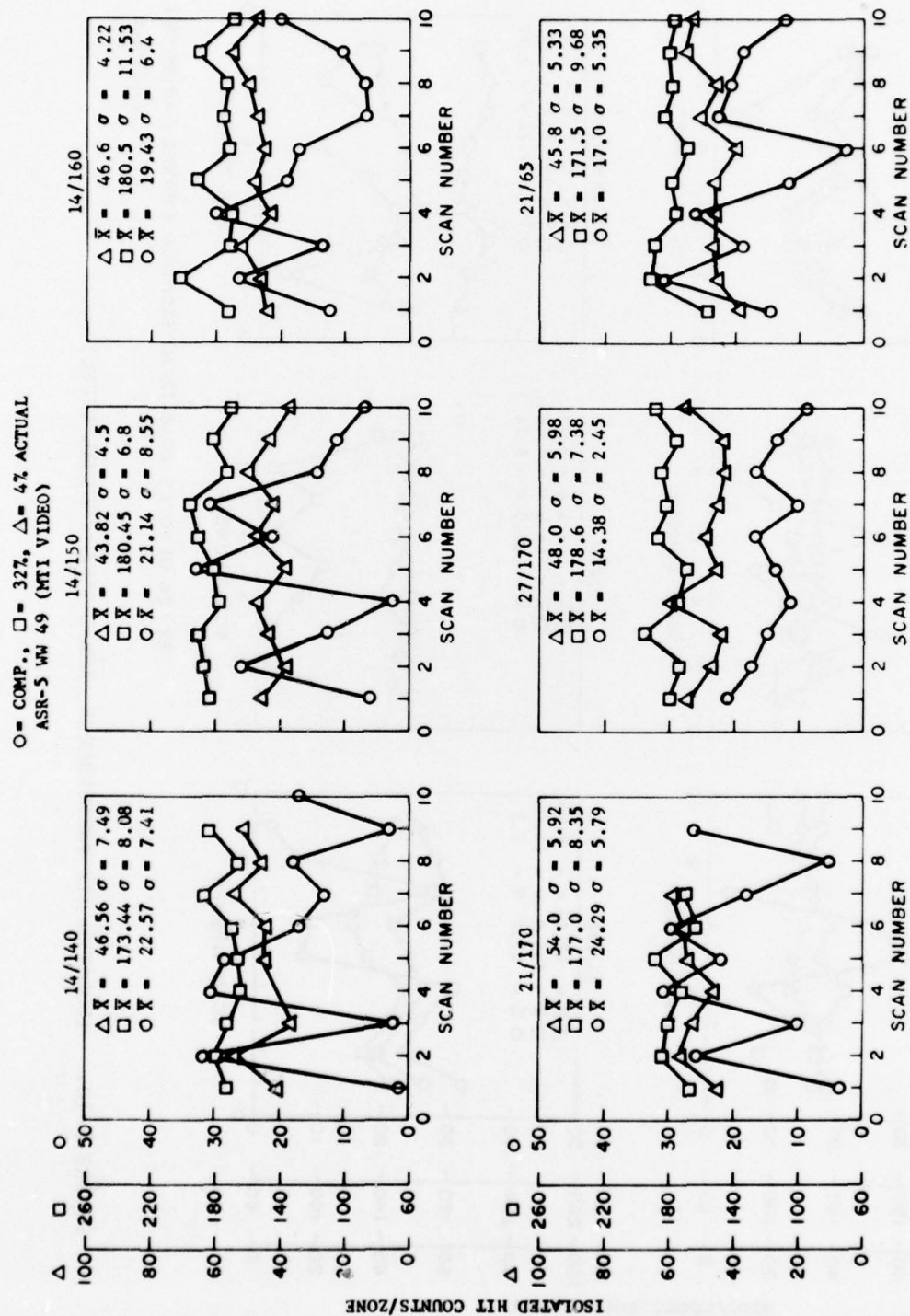
76-22-D7

FIGURE D-7. ISOLATED-HIT PERFORMANCE, ASR-5 WW34 (MTI VIDEO)



22 / 26 DENOTES ZONE IDENTIFICATION (RANGE / AZIMUTH)
76-22-D8

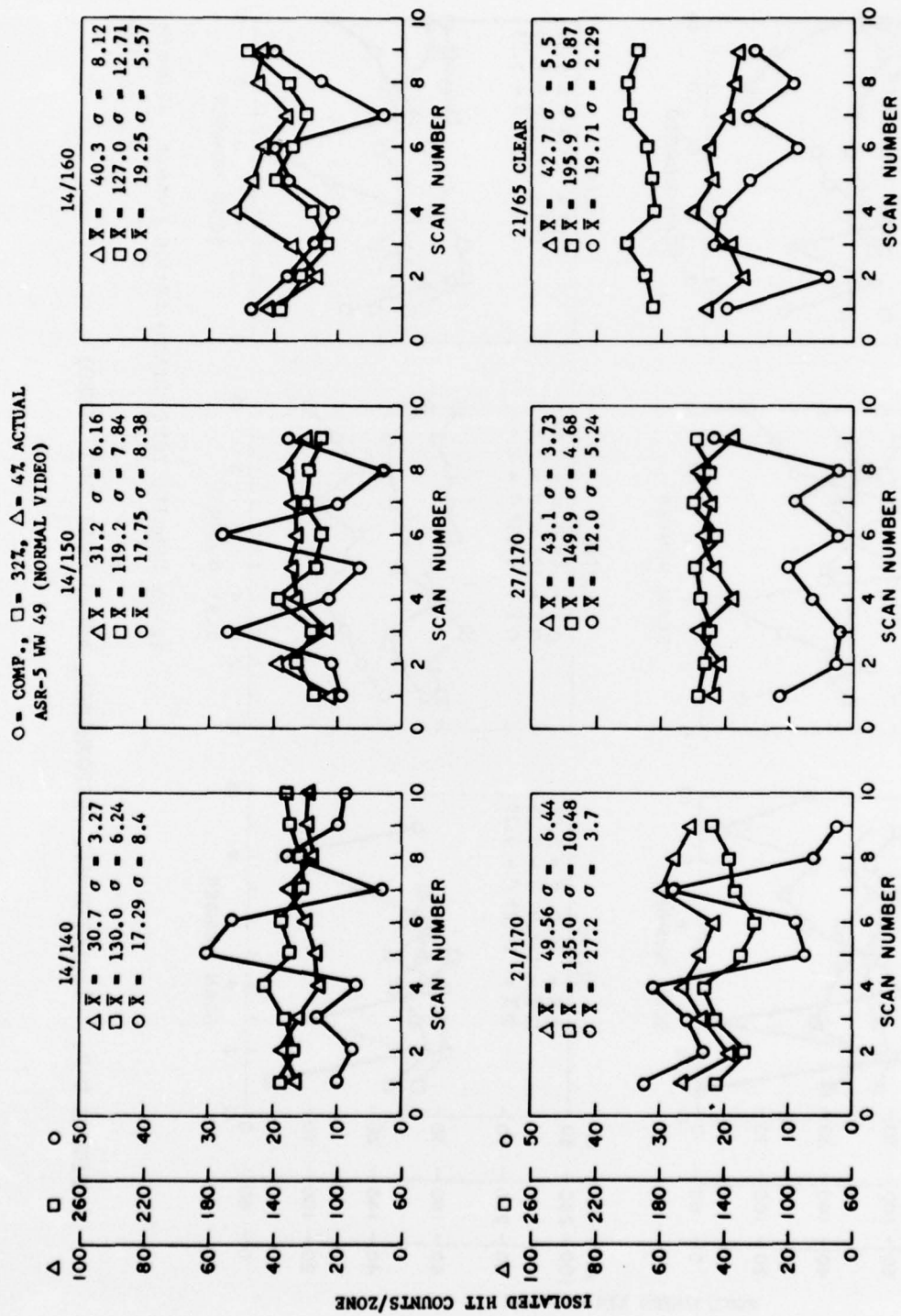
FIGURE D-8. ISOLATED-HIT PERFORMANCE, ASR-5 WW34 (NORMAL VIDEO)



22 / 26 DENOTES ZONE IDENTIFICATION (RANGE / AZIMUTH)

76-22-D9

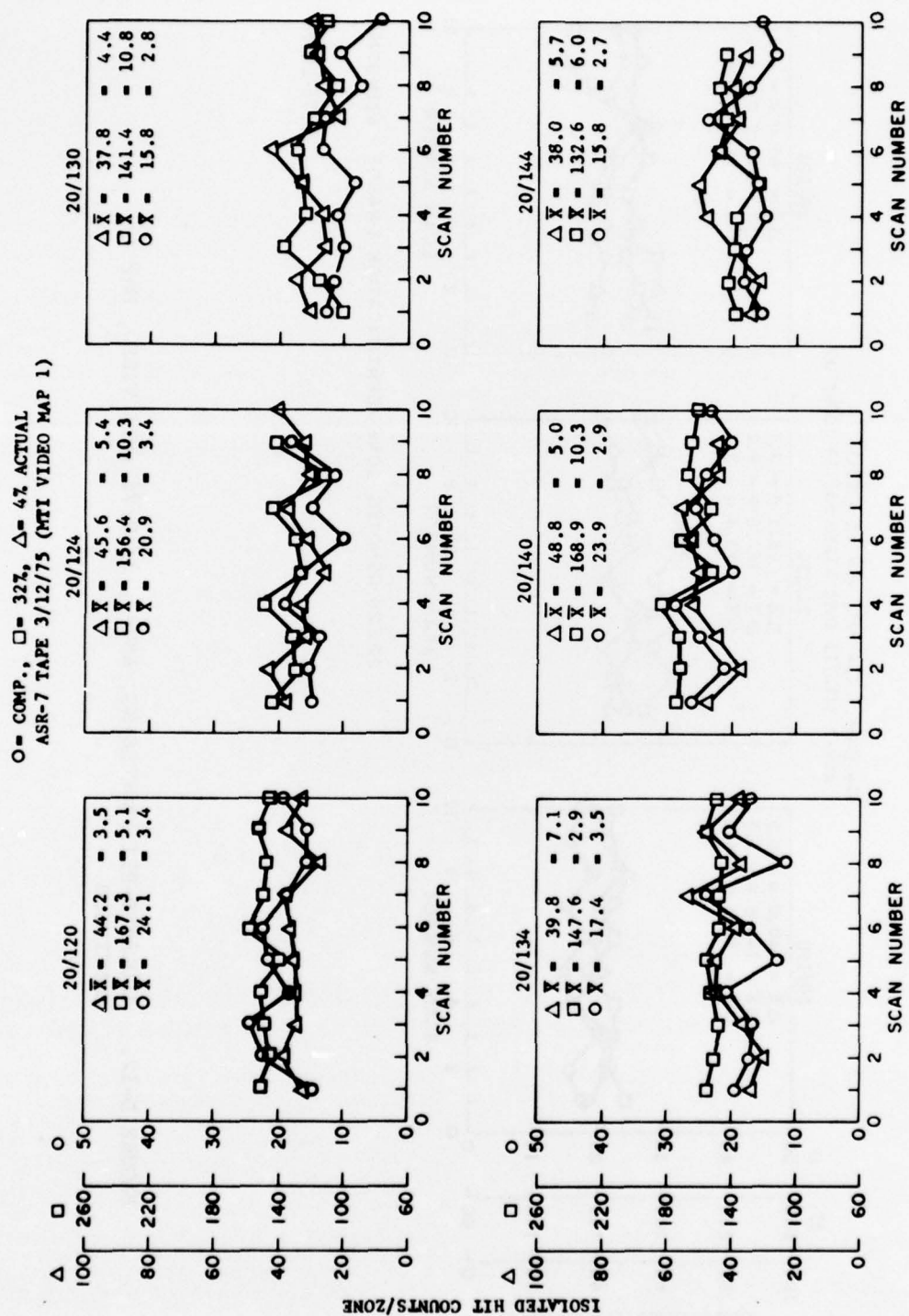
FIGURE D-9. ISOLATED-HIT PERFORMANCE, ASR-5 WW49 (MTI VIDEO)



22/26 DENOTES ZONE IDENTIFICATION (RANGE / AZIMUTH)

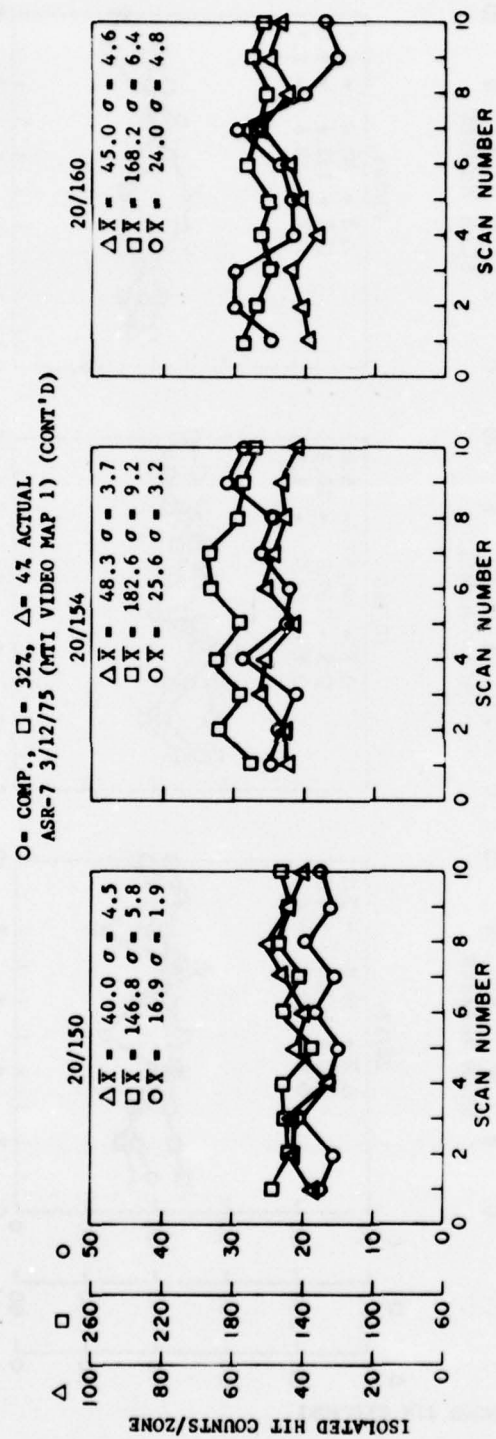
76-22-D10

FIGURE D-10. ISOLATED-HIT PERFORMANCE, ASR-5 WW49 (NORMAL VIDEO)



22 / 26 DENOTES ZONE IDENTIFICATION (RANGE / AZIMUTH)
76-22-D11

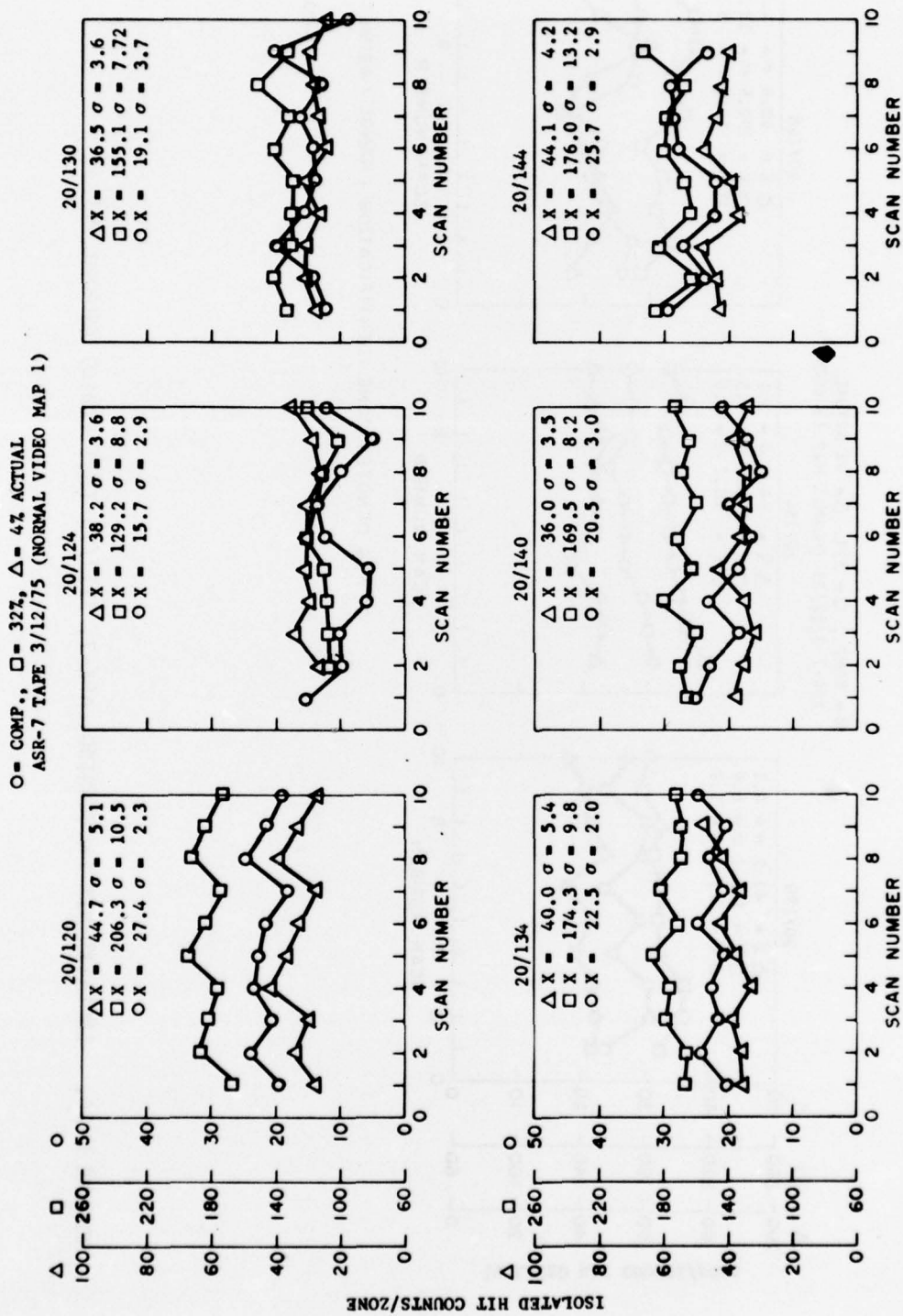
FIGURE D-11. ISOLATED-HIT PROCESSING, ASR-7, 3/12/75 (MTI VIDEO, MAP 1)



22/26 DENOTES ZONE IDENTIFICATION (RANGE / AZIMUTH)

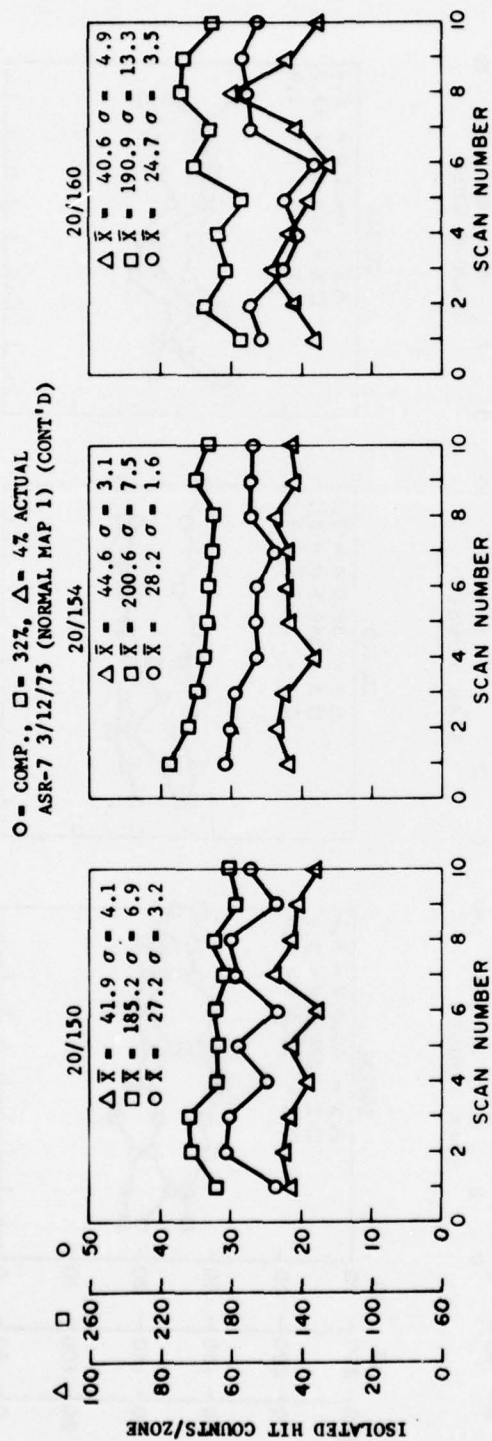
76-22-D12

FIGURE D-12. ISOLATED-HIT PROCESSING, ASR-7, 3/12/75 (MTI VIDEO, MAP 1)
CONTINUED



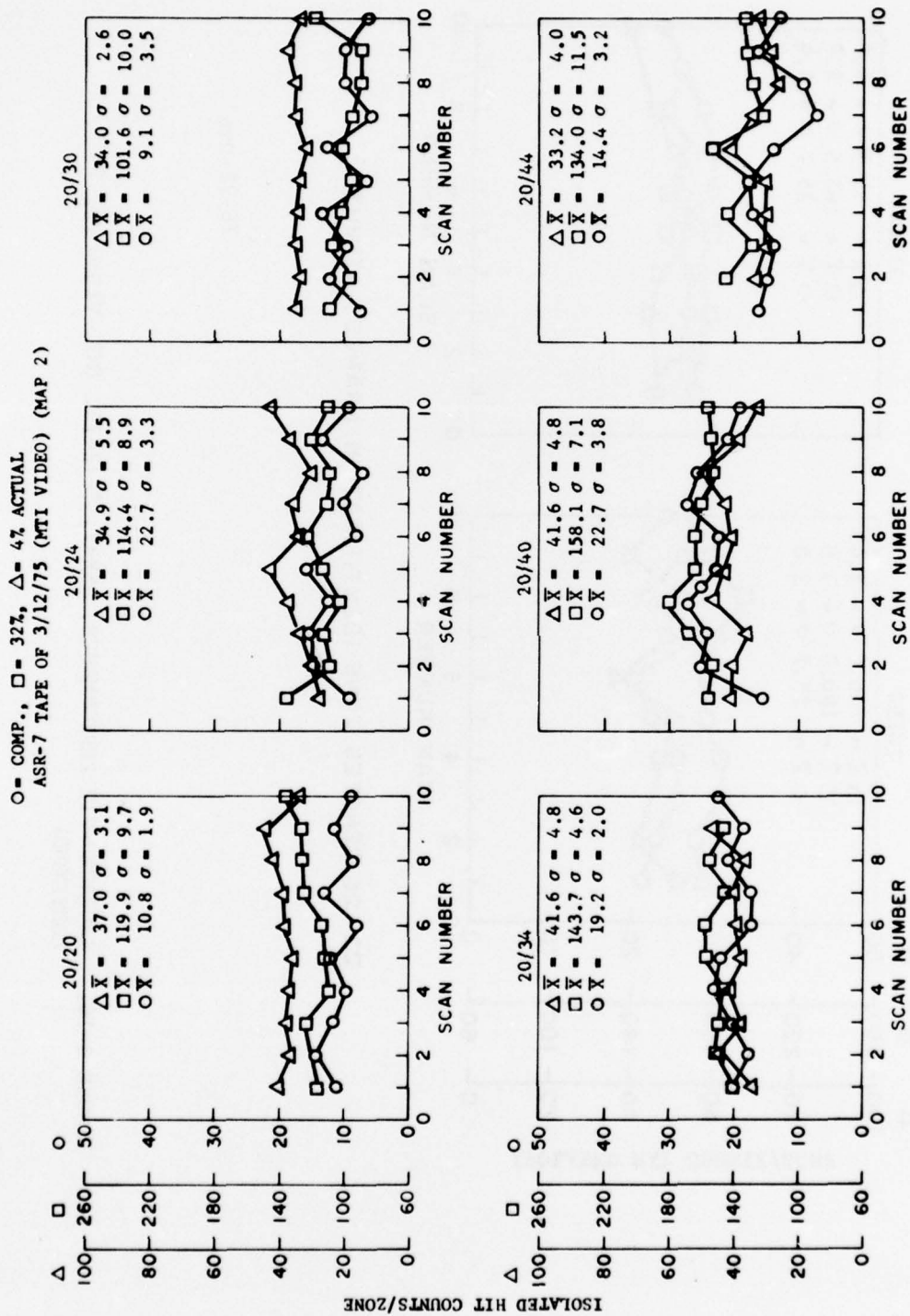
22/26 DENOTES ZONE IDENTIFICATION (RANGE / AZIMUTH)
 76-22-D13

FIGURE D-13. ISOLATED-HIT PERFORMANCE, ASR-7, 3/12/75, (NORMAL VIDEO MAP 1)



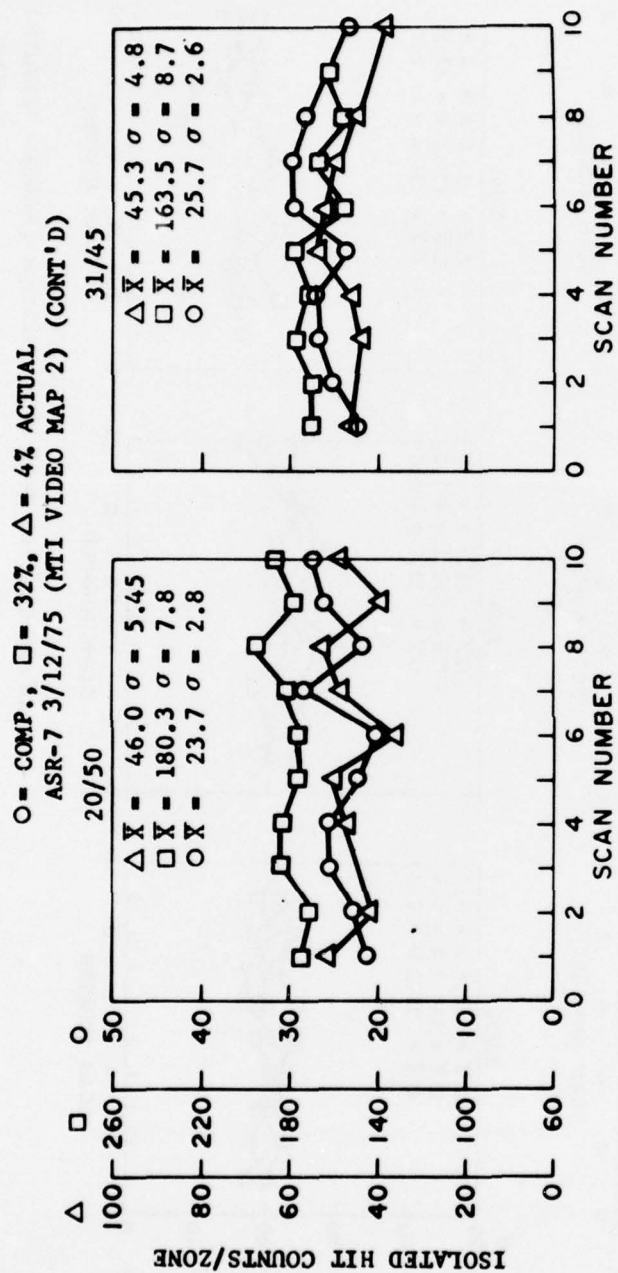
76-22-D14

FIGURE D-14. ISOLATED-HIT PROCESSING, ASR-7, 3/12/75 (MTI VIDEO) (NORMAL MAP 1)



22/26 DENOTES ZONE IDENTIFICATION (RANGE / AZIMUTH)
76-22-D15

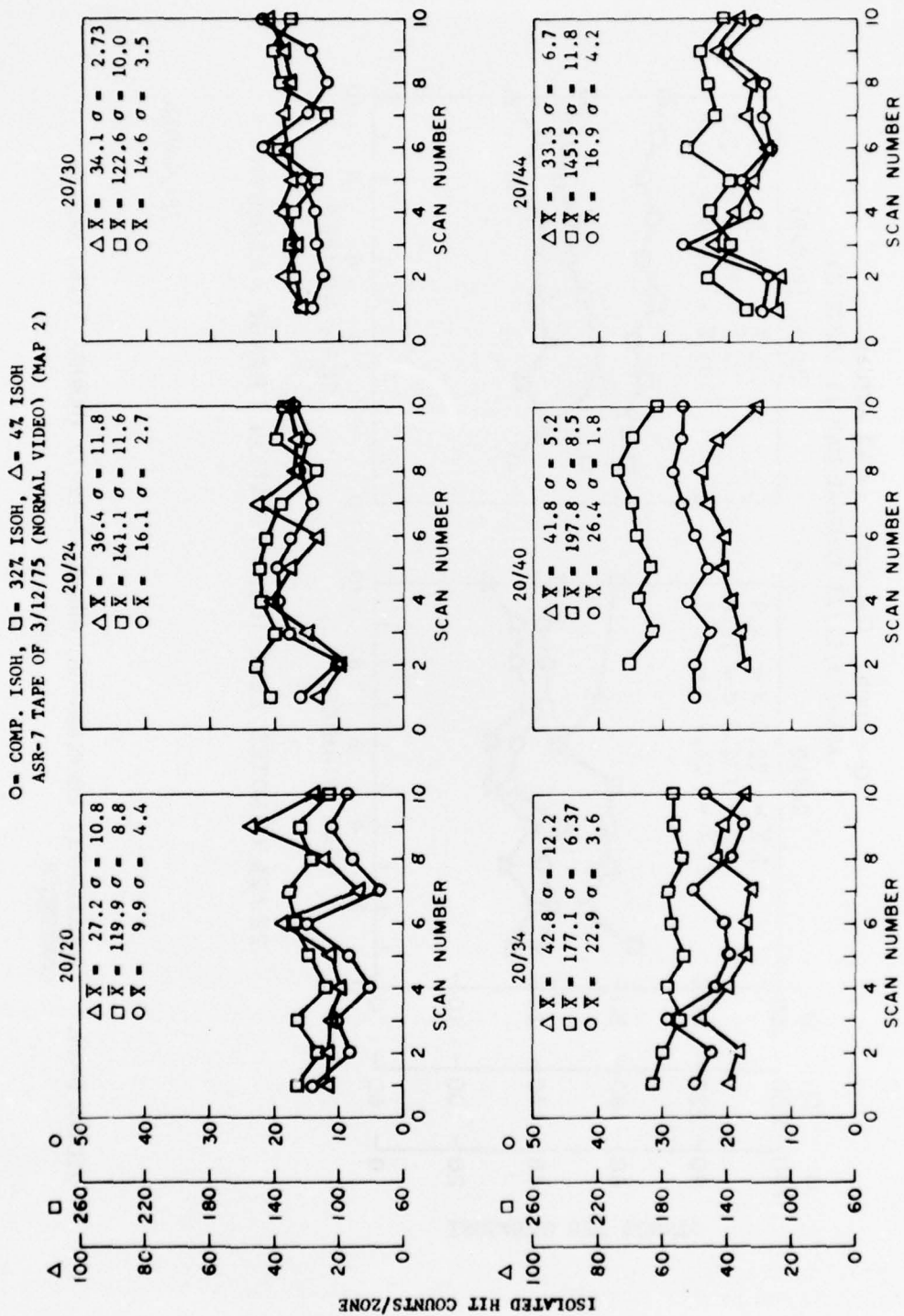
FIGURE D-15. ISOLATED-HIT PROCESSING, ASR-7, 3/12/75 (MTI VIDEO, MAP 2)



22/26 DENOTES ZONE IDENTIFICATION (RANGE / AZIMUTH)

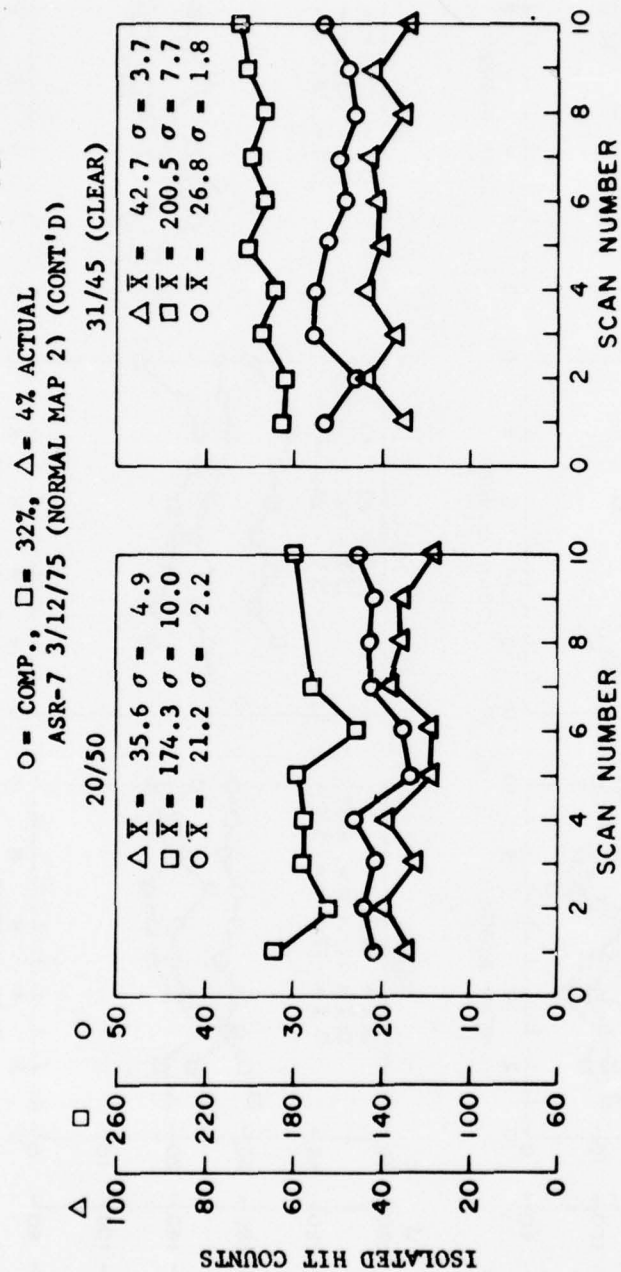
76-22-D16

FIGURE D-16. ISOLATED-HIT PERFORMANCE, ASR-7, 3-12-75, (MTI VIDEO MAP 2)
CONTINUED



22/26 DENOTES ZONE IDENTIFICATION (RANGE / AZIMUTH)
 76-22-D17

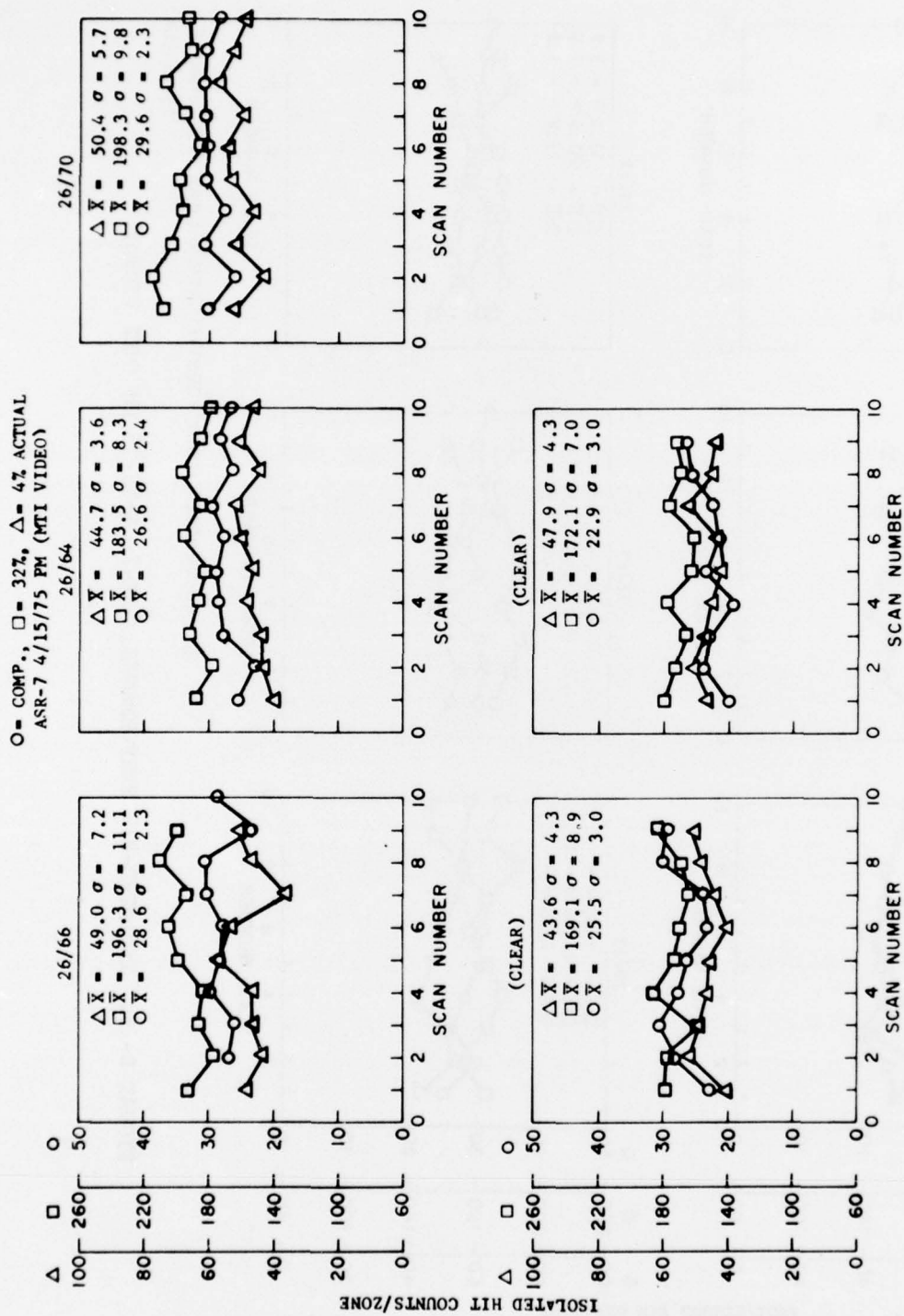
FIGURE D-17. ISOLATED-HIT PERFORMANCE, ASR-7, 3-12-75 (NORMAL VIDEO MAP 2)



22/26 DENOTES ZONE IDENTIFICATION (RANGE / AZIMUTH)

76-22-D18

FIGURE D-18. ISOLATED-HIT PERFORMANCE, ASR-7, 3-12-75 (NORMAL VIDEO MAP 2)
CONTINUED



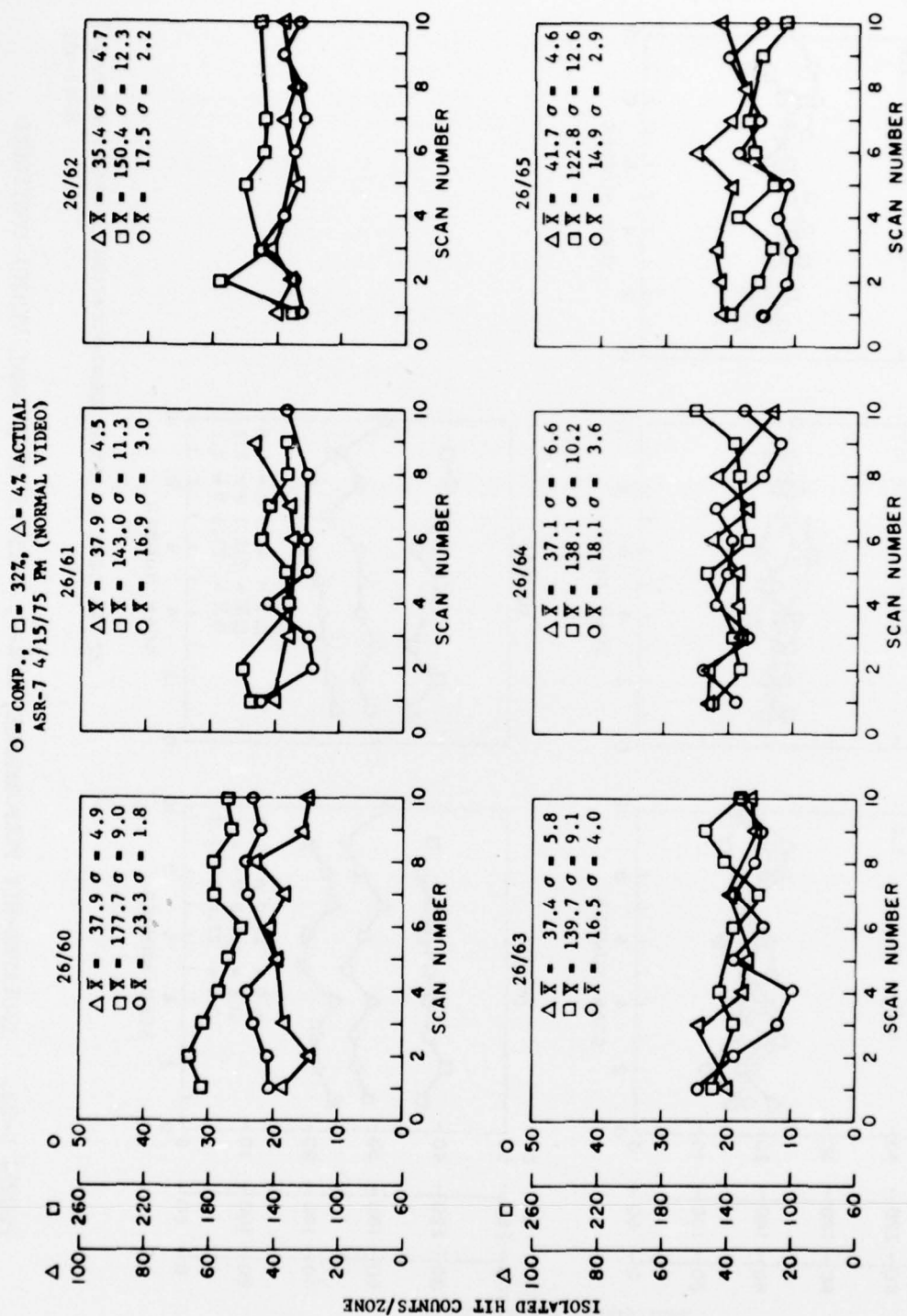
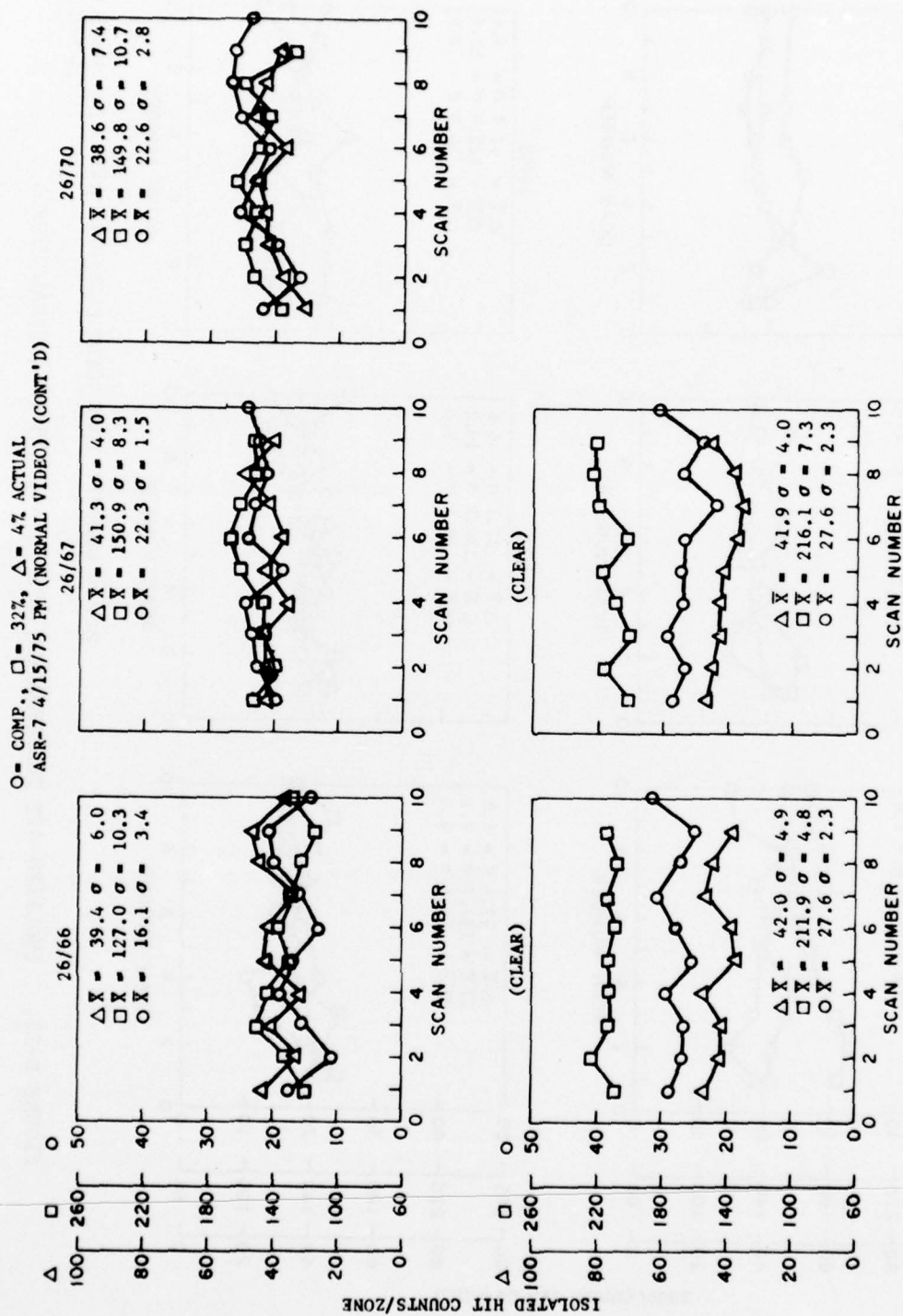


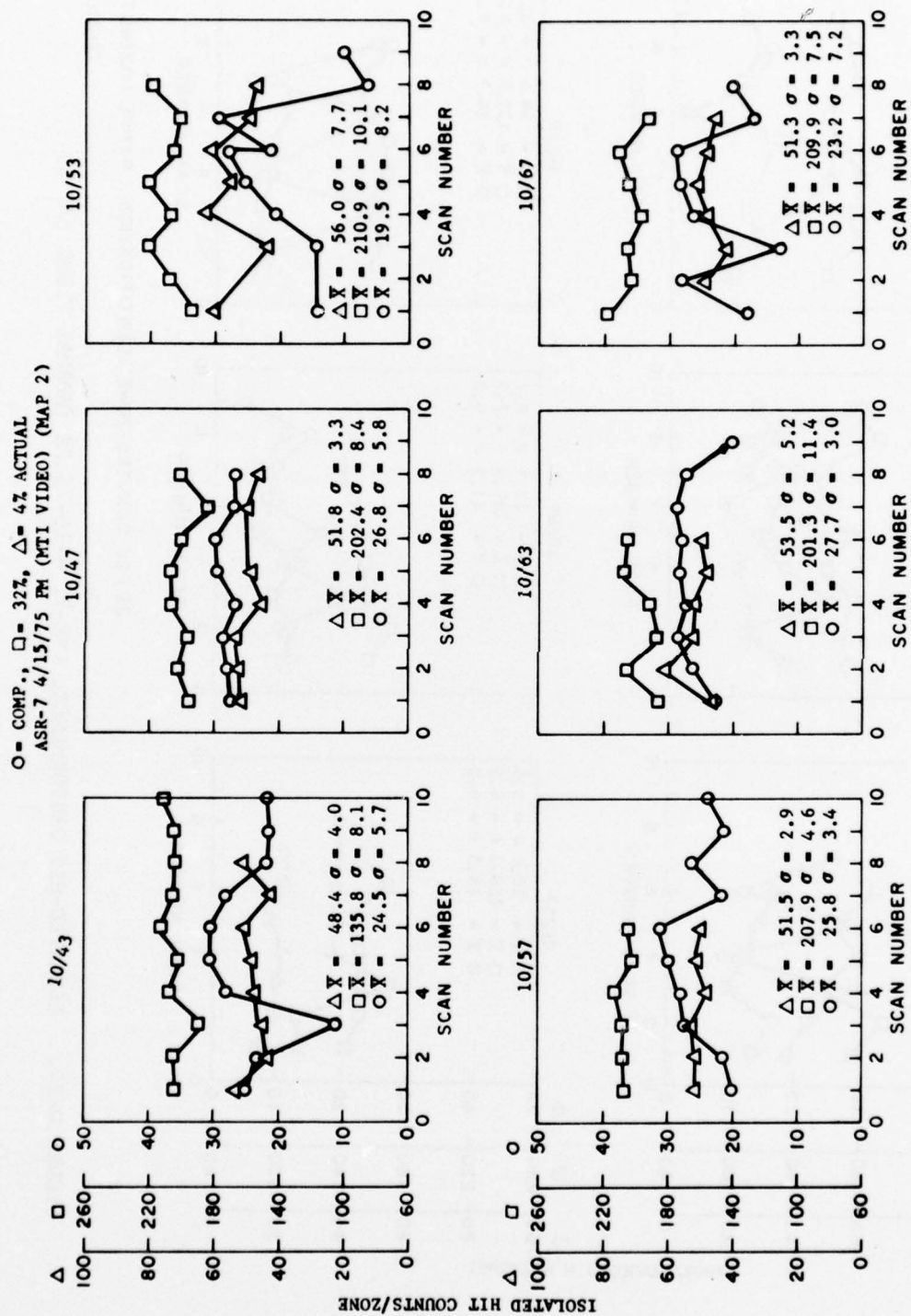
FIGURE D-21. ISOLATED-HIT PERFORMANCE, ASR-7, 4-15-75 PM (NORMAL VIDEO)

76-22-D21



22/26 DENOTES ZONE IDENTIFICATION (RANGE / AZIMUTH)
76-22-D22

FIGURE D-22. ISOLATED-HIT PERFORMANCE, ASR-7, 4-15-75 PM (NORMAL VIDEO) CONTINUED



22/26 DENOTES ZONE IDENTIFICATION (RANGE / AZIMUTH)
76-22-D23

FIGURE D-23. ISOLATED-HIT PERFORMANCE, ASR-7, 4-15-75 PM (MTI VIDEO MAP 2)

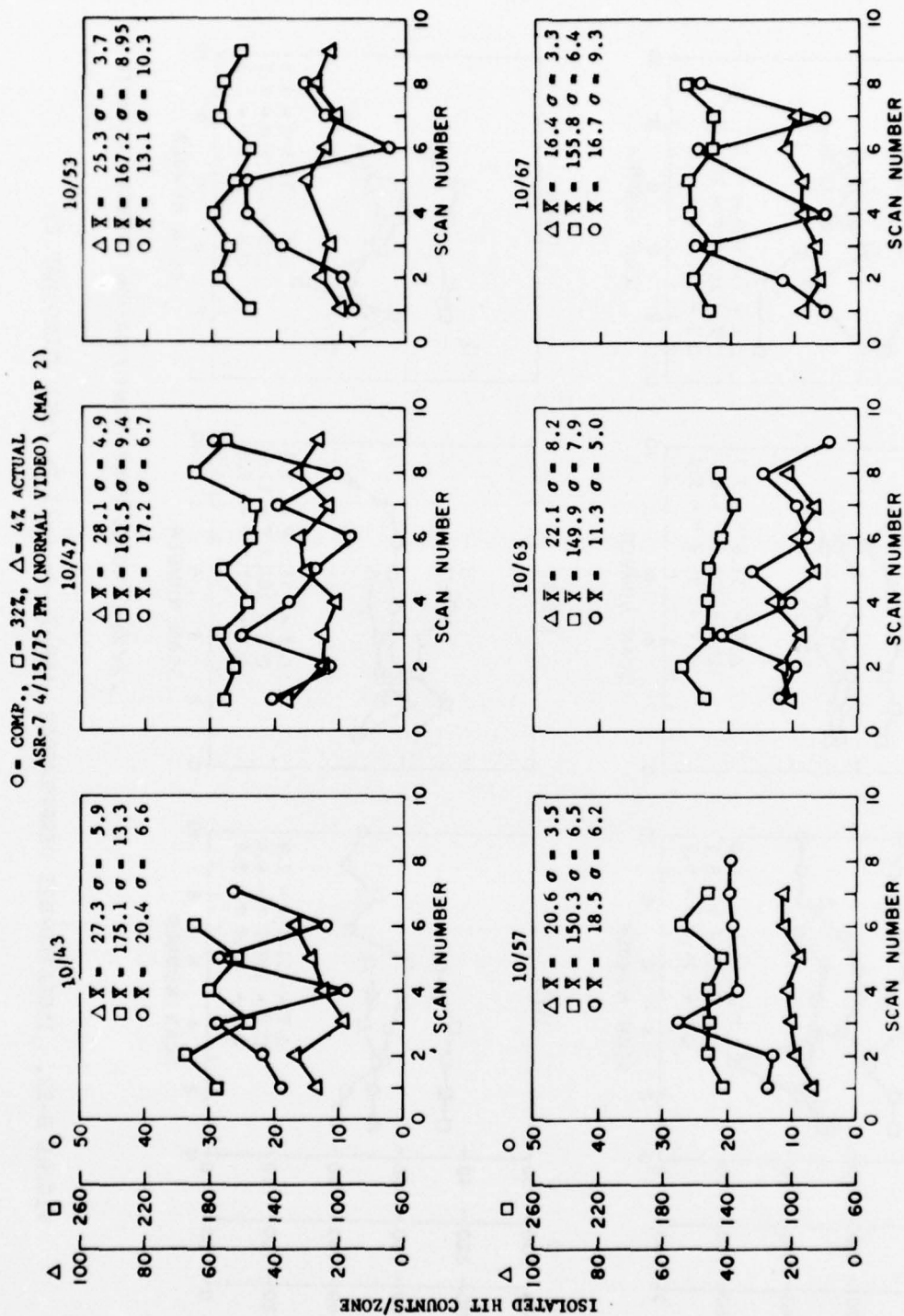
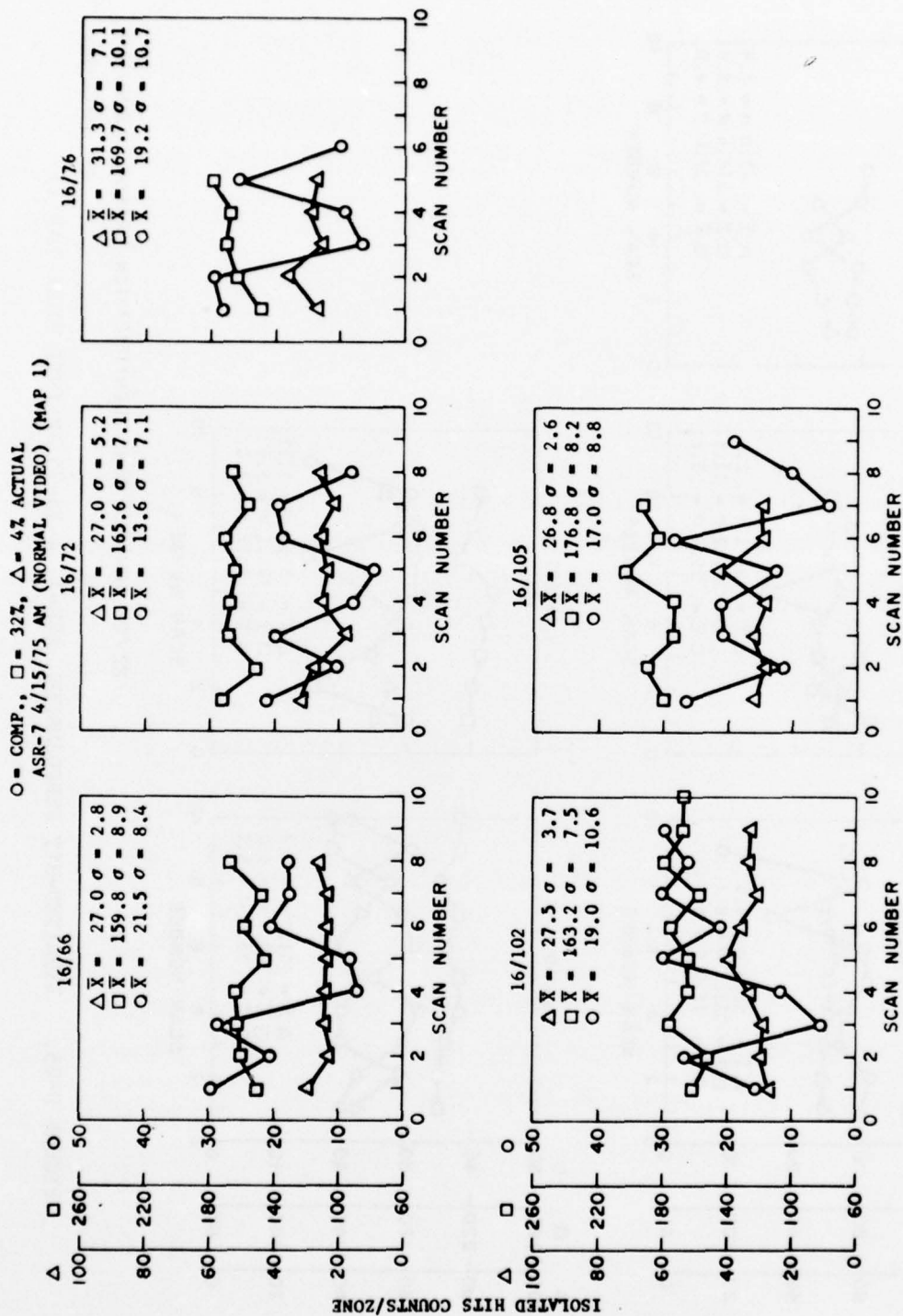
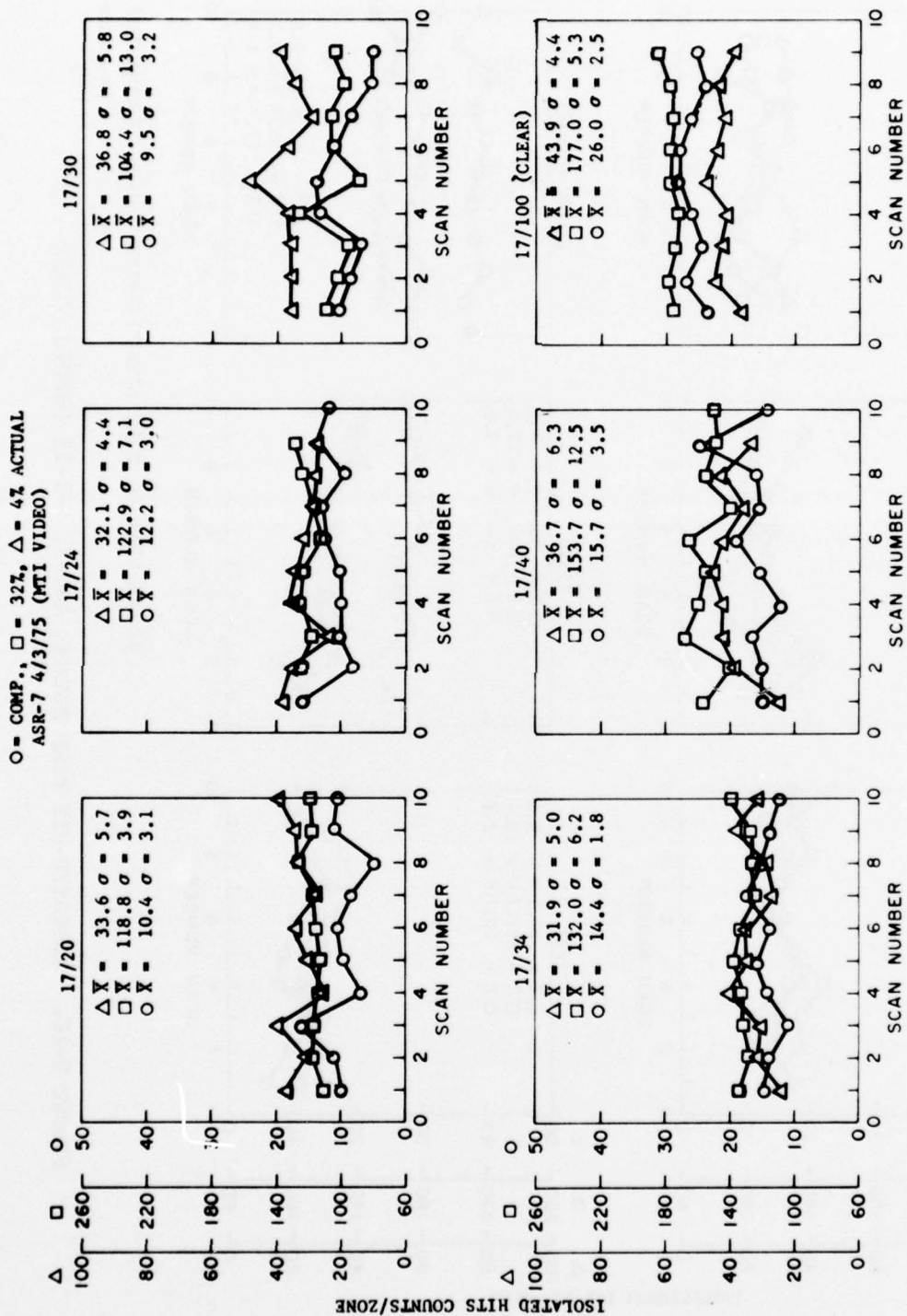


FIGURE D-24. ISOLATED-HIT PERFORMANCE, ASR-7, 4-15-75 PM (NORMAL VIDEO MAP 2)

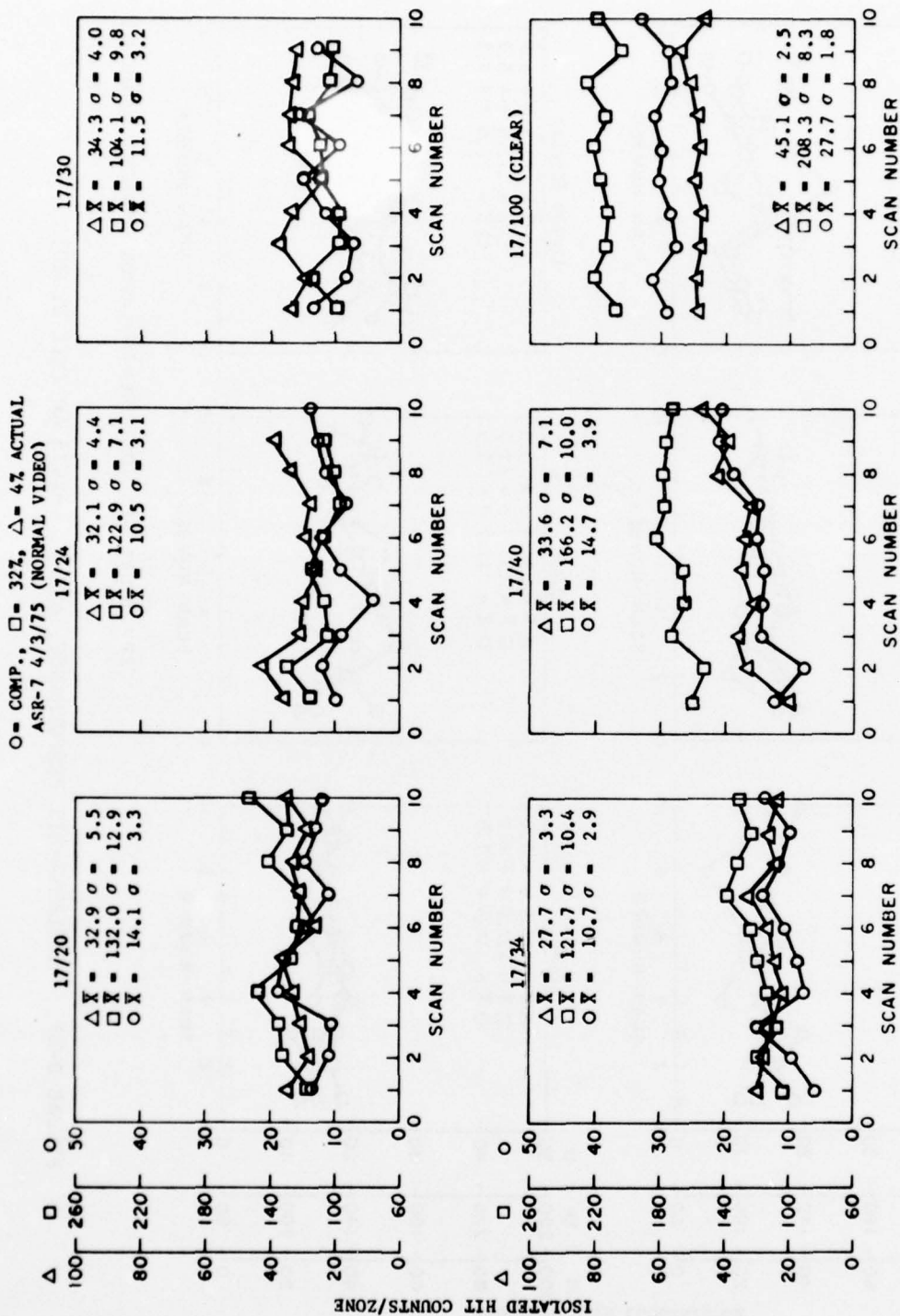
76-22-D24



22 / 26 DENOTES ZONE IDENTIFICATION (RANGE / AZIMUTH)
 76-22-D26
 FIGURE D-26. ISOLATED-HIT PERFORMANCE, ASR-7, 4-15-75 AM (NORMAL VIDEO MAP 1)



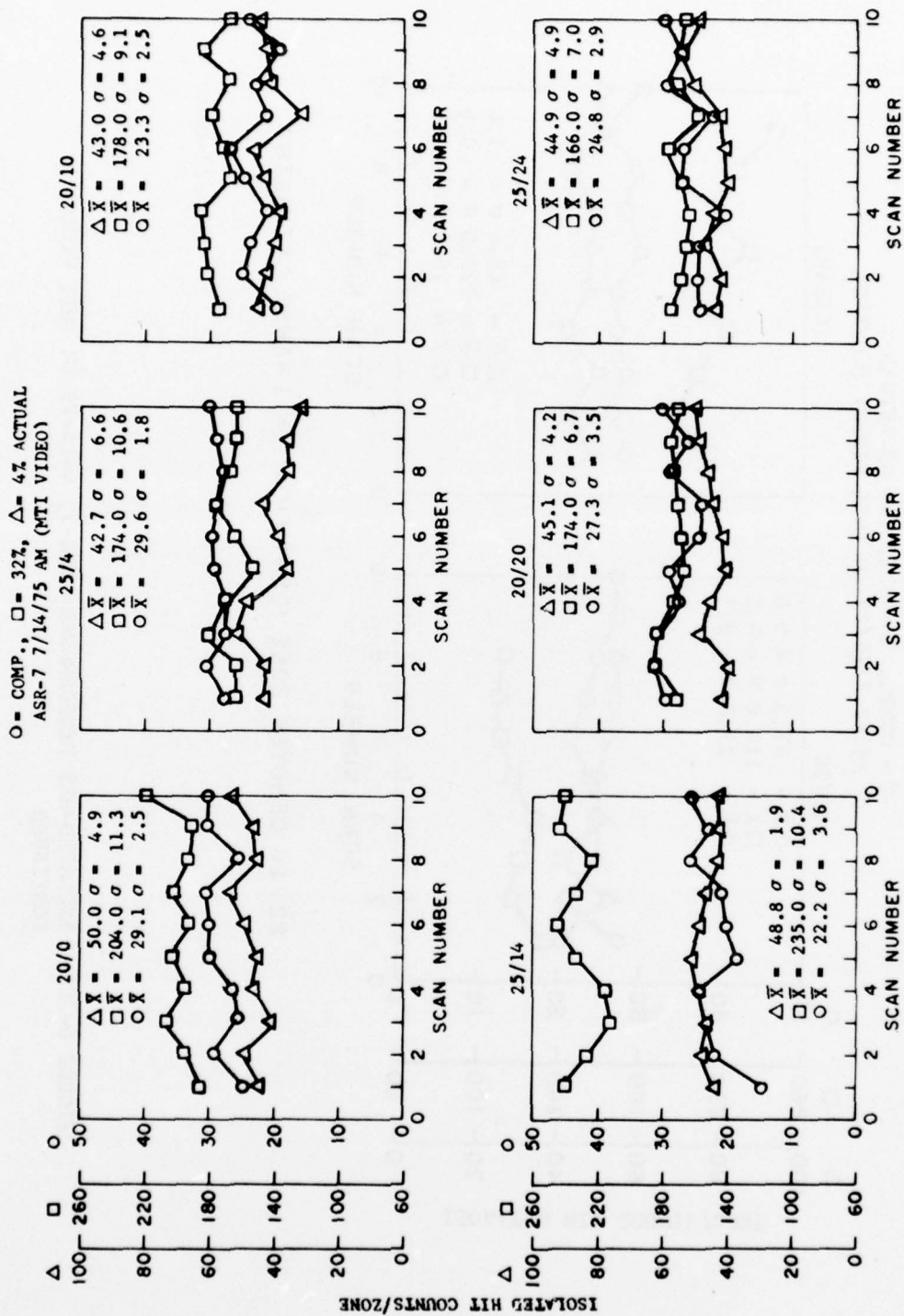
22 / 26 DENOTES ZONE IDENTIFICATION (RANGE / AZIMUTH)
 76-22-D27



22/26 DENOTES ZONE IDENTIFICATION (RANGE / AZIMUTH)

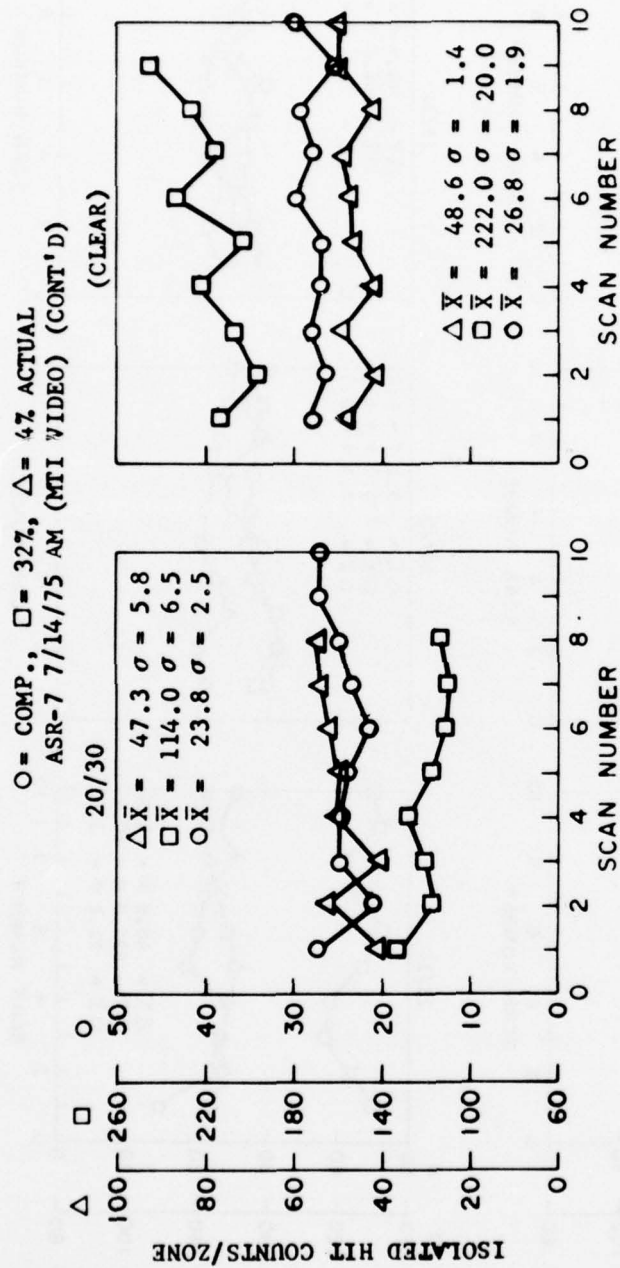
76-22-D28

FIGURE D-28. ISOLATED-HIT PERFORMANCE, ASR-7, 4-3-75 (NORMAL VIDEO)



22 / 26 DENOTES ZONE IDENTIFICATION (RANGE / AZIMUTH)
76-28-D29

FIGURE D-29. ISOLATED-HIT PERFORMANCE, ASR-7, 4-14-75 AM (MTI VIDEO)



76-22-D30

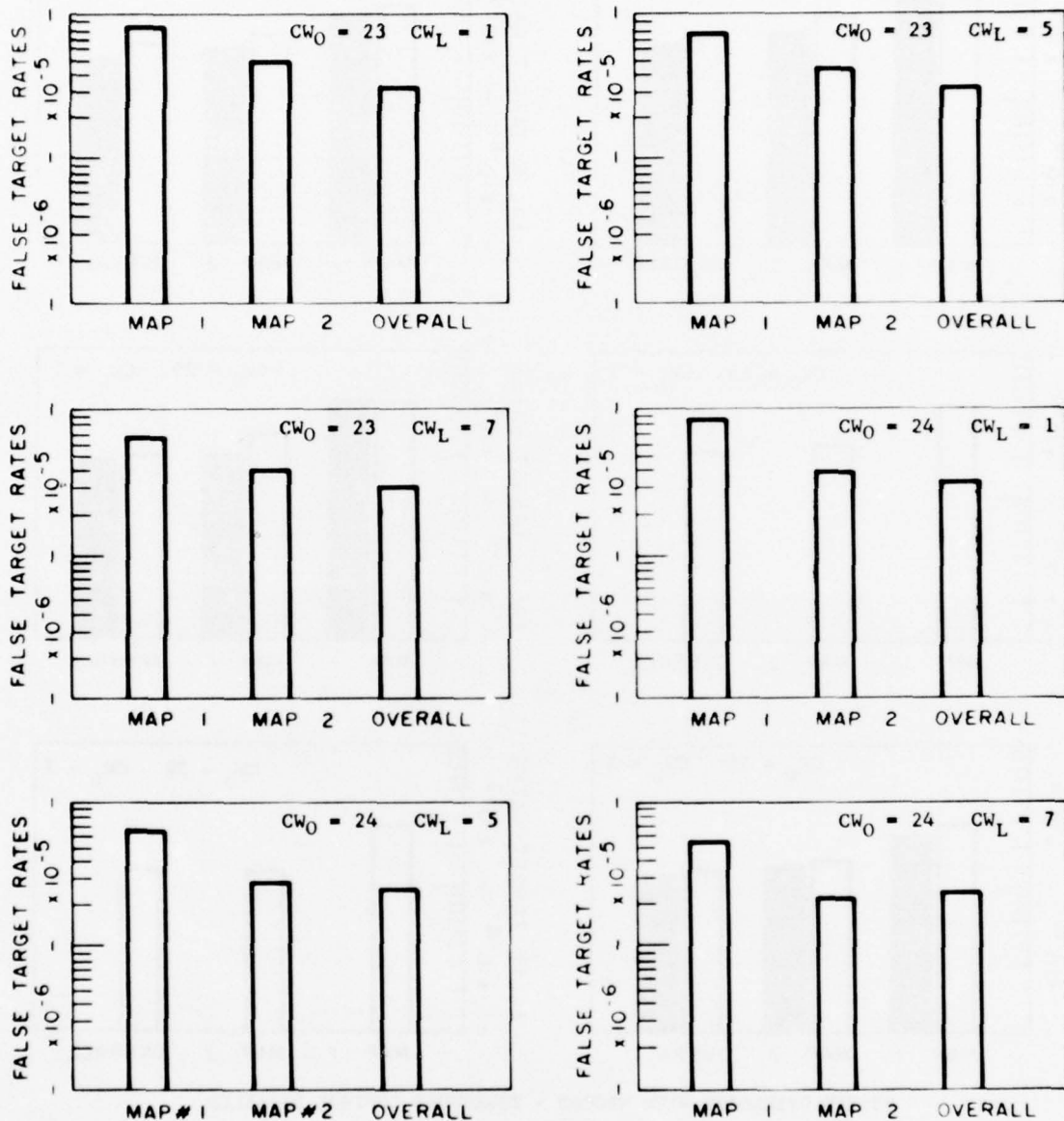
FIGURE D-30. ISOLATED-HIT PERFORMANCE, ASR-7, 4-14-75 AM (MTI VIDEO)
CONTINUED

APPENDIX E
WEATHER FALSE TARGET RATES

APPENDIX E

LIST OF ILLUSTRATIONS

Figure		Page
E-1	Weather Clutter False Target Rates for Predetection, Threshold = 10, ASR-5 Compressed MTI No. 2	E-1
E-2	Weather Clutter False Target Rates for Predetection Threshold = 10, ASR-5 WW48 MTI Log	E-2
E-3	Weather Clutter False Target Rates for Predetection Threshold = 10, ASR-5 WW48 MTI Log	E-3
E-4	Weather Clutter False Target Rates for Predetection Threshold = 10, ASR-5 WW48 MTI Log	F-4
E-5	Weather Clutter False Target Rates for Predetection Threshold = 10, ASR-5 WW48 LIN MTI	E-5
E-6	Weather Clutter False Target Rates for ASR-5 Radar	F-6
E-7	Weather Clutter False Target Rates for Predetection Threshold = 11, ASR-7 3/12/75	E-7
E-8	Weather Clutter False Target Rates for Predetection Threshold = 11, ASR-7 3/13/75	E-8
E-9	Weather Clutter False Target Rates for ASR-7 Radar	E-9
E-10	Weather Clutter False Target Rates for ASR-7 Radar	E-10
E-11	Weather Clutter False Target Rates for ASR-7 Radar	E-11

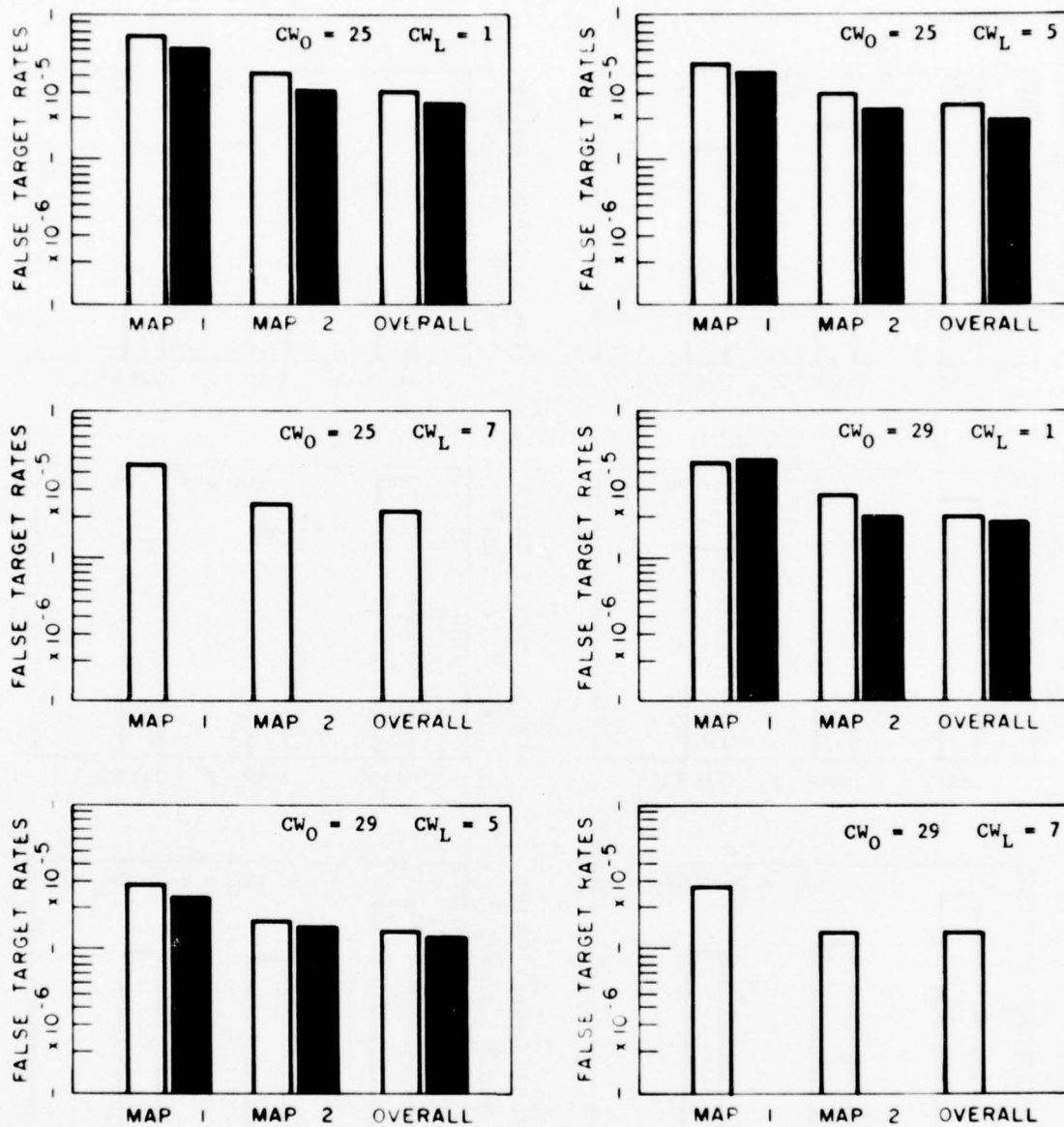


SYSTEM OVERLOADS WITH SECOND-THRESHOLD CONTROL DISABLED

1/64 nmi. MINIMUM PULSE WIDTH

76-22-E1

FIGURE E-1. WEATHER CLUTTER FALSE TARGET RATES FOR PREDETECTION, THRESHOLD = 10, ASR-5 COMPRESSED MTI NO.2



SYSTEM OVERLOADS WITH SECOND - THRESHOLD CONTROL DISABLED

76-22-E2

FIGURE E-2. WEATHER CLUTTER FALSE TARGET RATES FOR PREDETECTION THRESHOLD = 10, ASR-5 WW48 MTI LOG

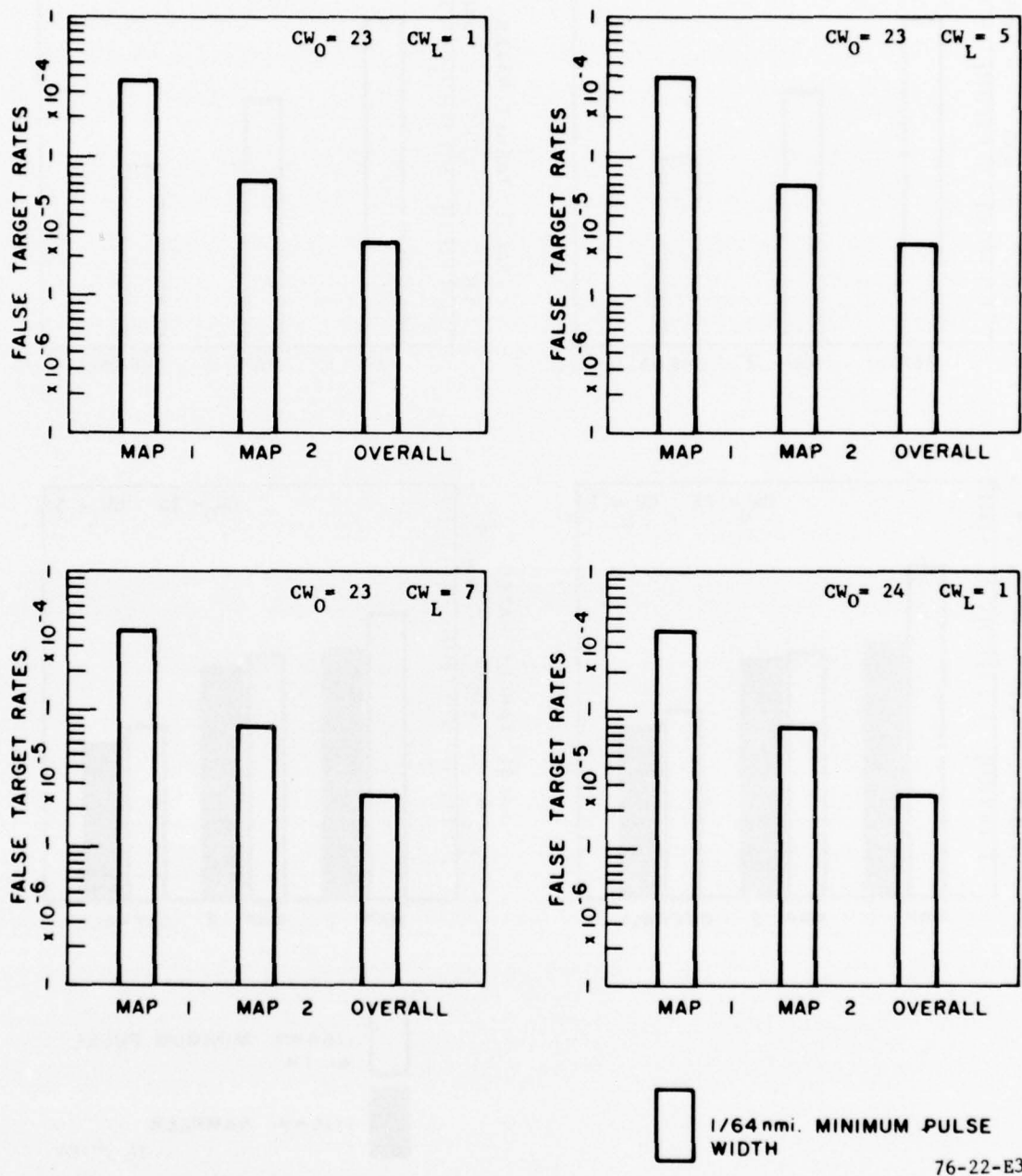


FIGURE E-3. WEATHER CLUTTER FALSE TARGET RATES FOR PREDETECTION THRESHOLD = 10, ASR-5 WW48 MTI LOG

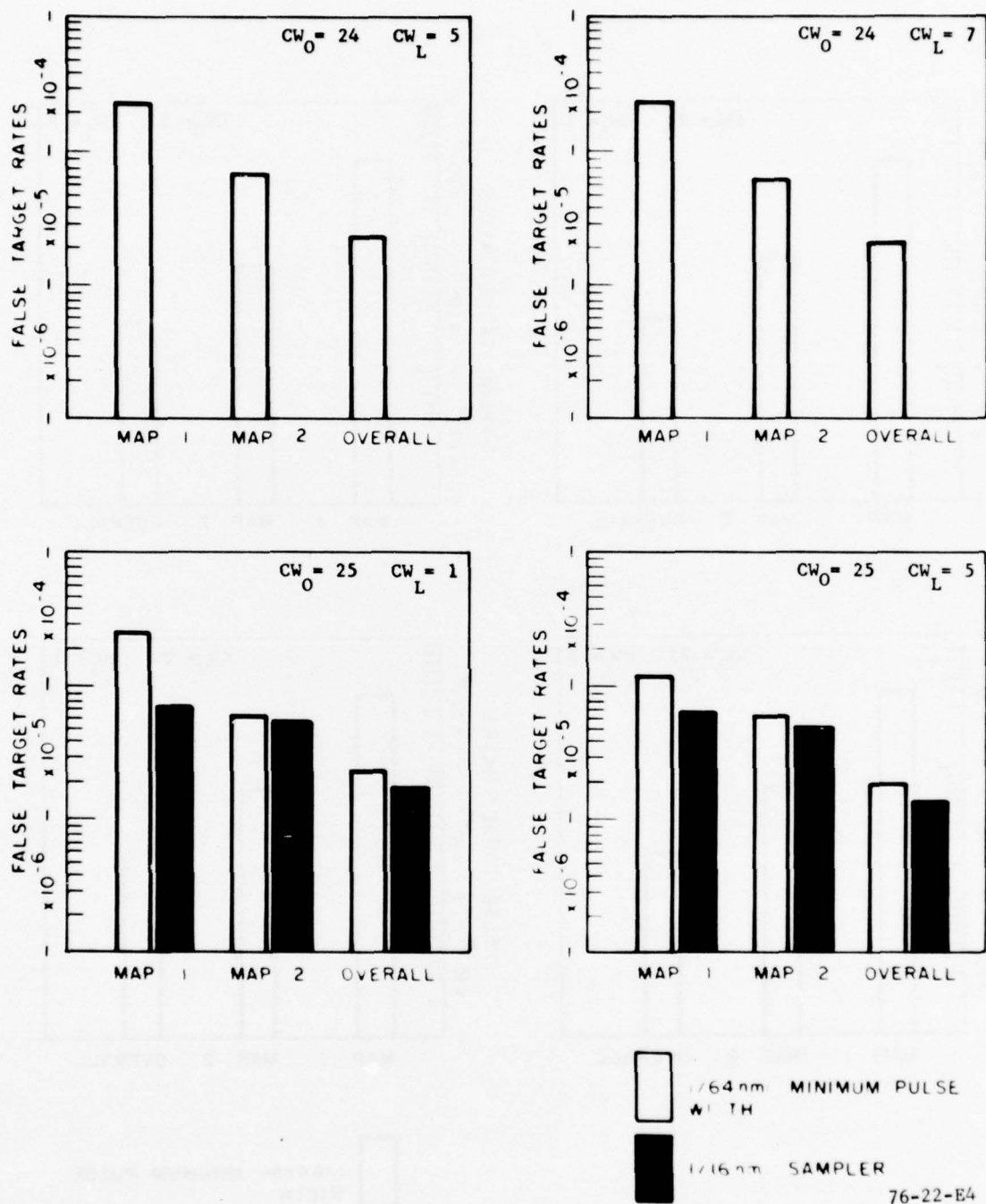
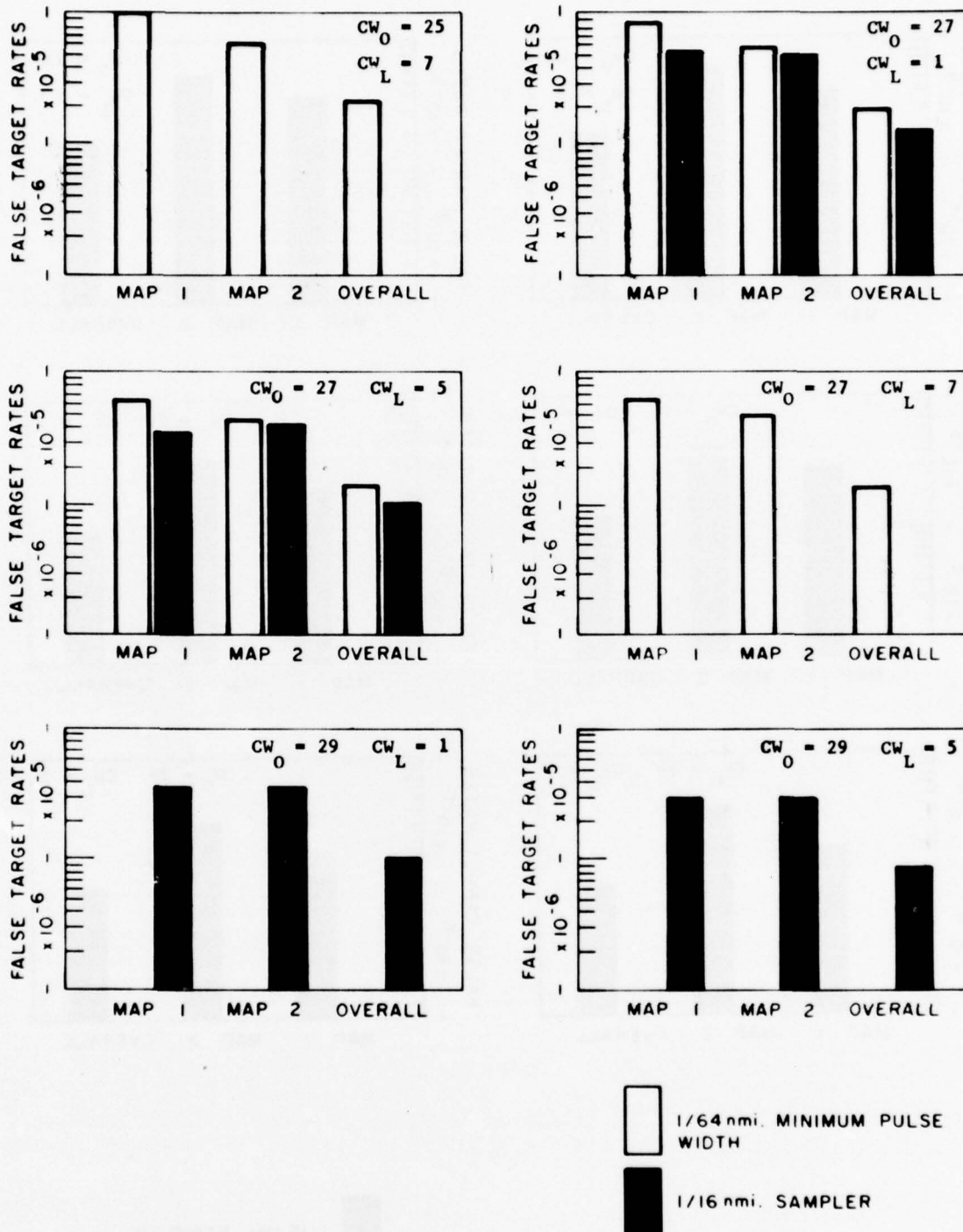
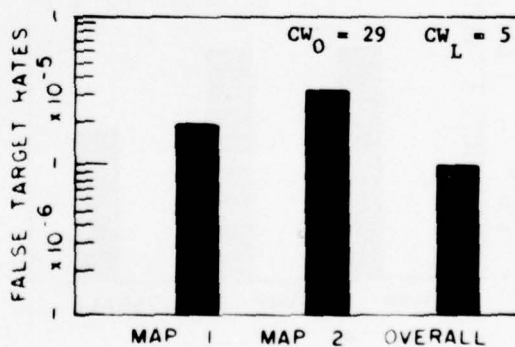
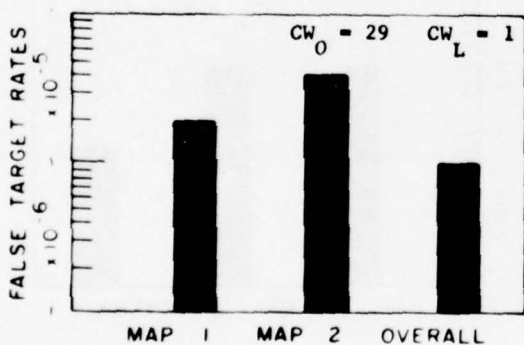
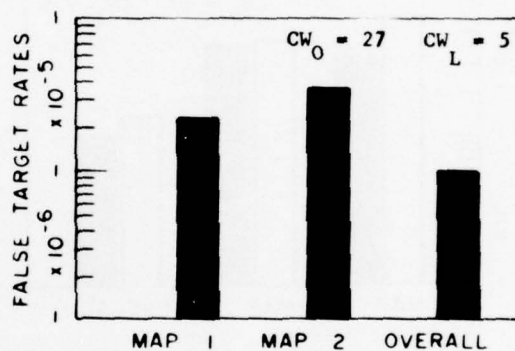
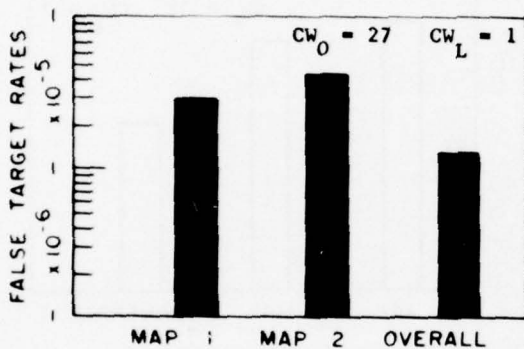
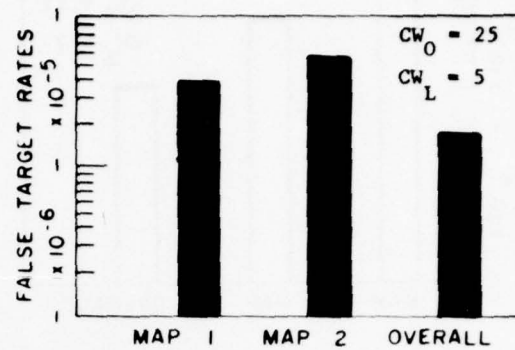
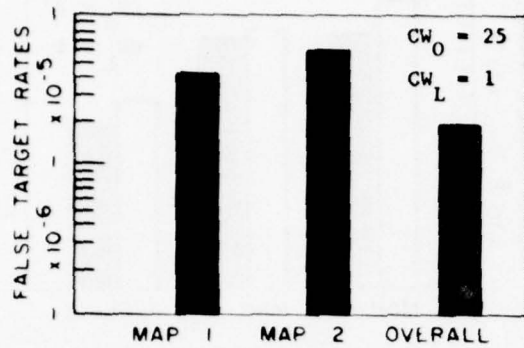


FIGURE E-4. WEATHER CLUTTER FALSE TARGET RATES FOR PREDETECTION THRESHOLD = 10, ASR-5 WW48 MTI LOG



76-22-E5

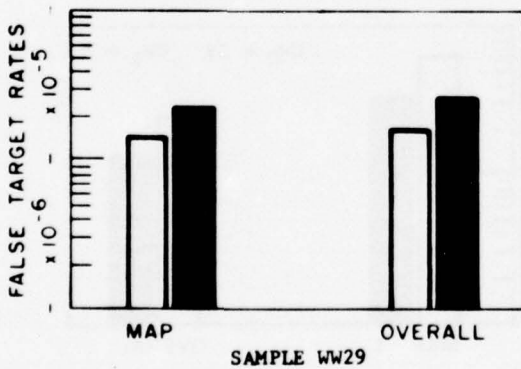
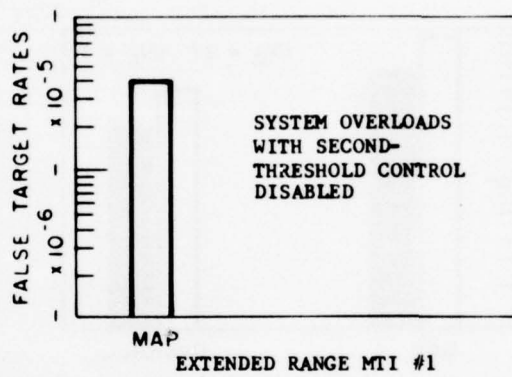
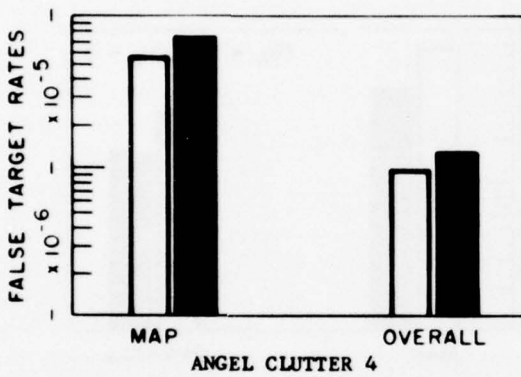
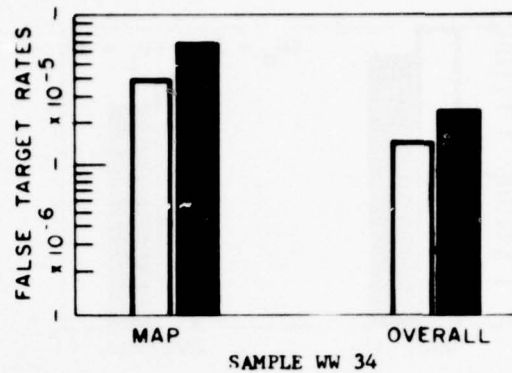
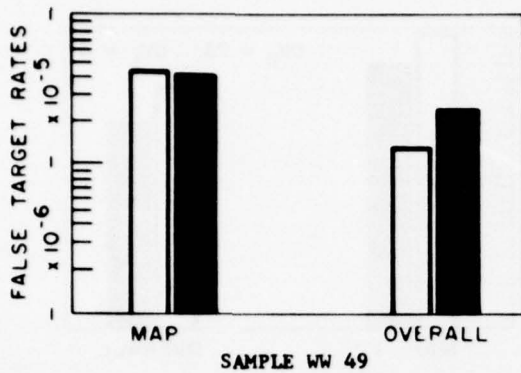
FIGURE E-5. WEATHER CLUTTER FALSE TARGET RATES FOR PREDETECTION THRESHOLD = 10, ASR-5 WW48 MTI LOG



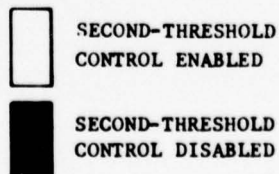
1/16 nmi. SAMPLER

76-22-E6

FIGURE E-6. WEATHER CLUTTER FALSE TARGET RATES FOR ASR-5 RADAR



MTI VIDEO
 $CW_0 = 27$, $CW_L = 5$
 PREDETECTION THRESHOLD = 10
 $P_N = 4\%$



76-22-E7

FIGURE E-7. WEATHER CLUTTER FALSE TARGET RATES FOR PREDETECTION THRESHOLD = 11, ASR-7 3/12/75

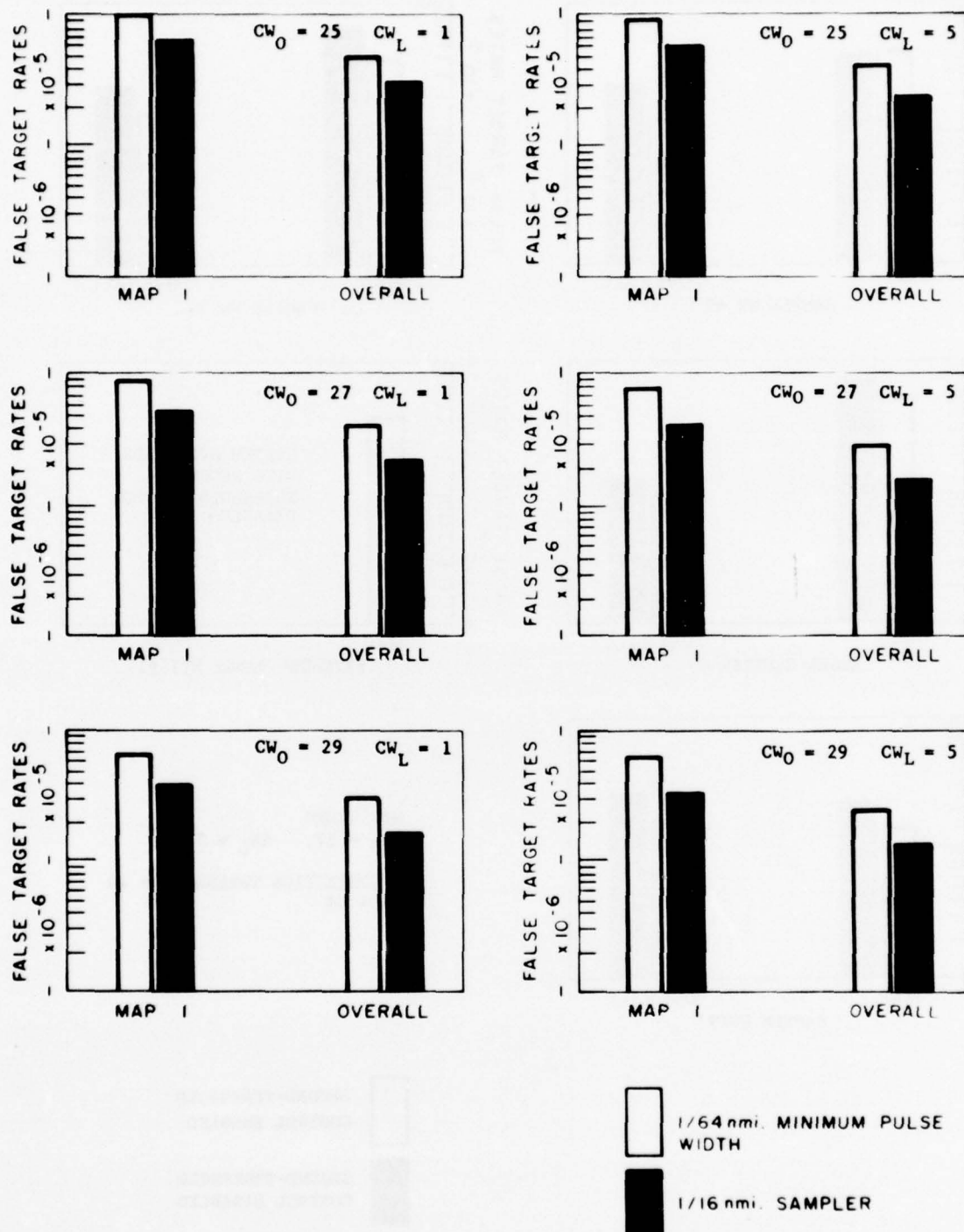
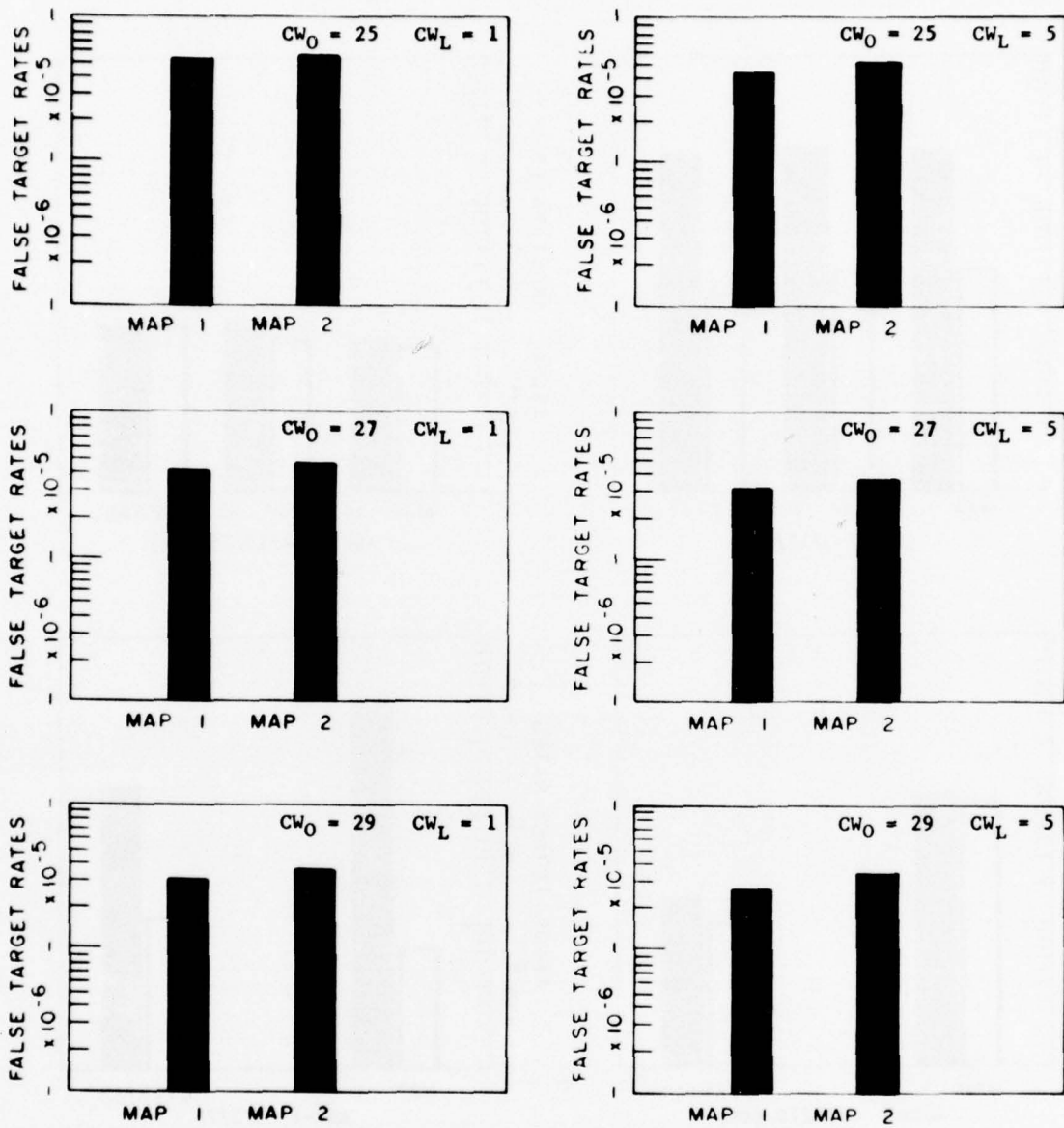


FIGURE E-8. WEATHER CLUTTER FALSE TARGET RATES FOR PREDETECTION THRESHOLD = 11, ASR-7 3/13/75

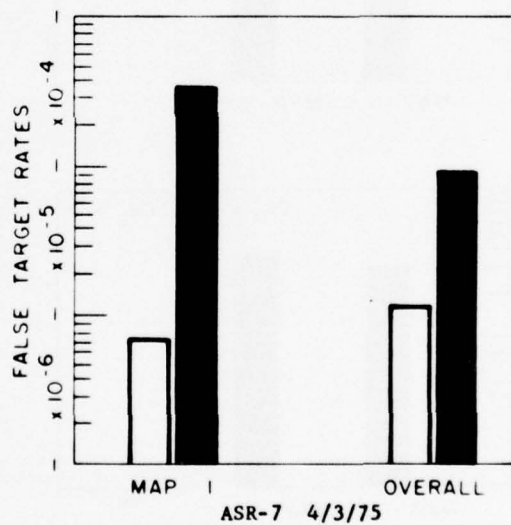
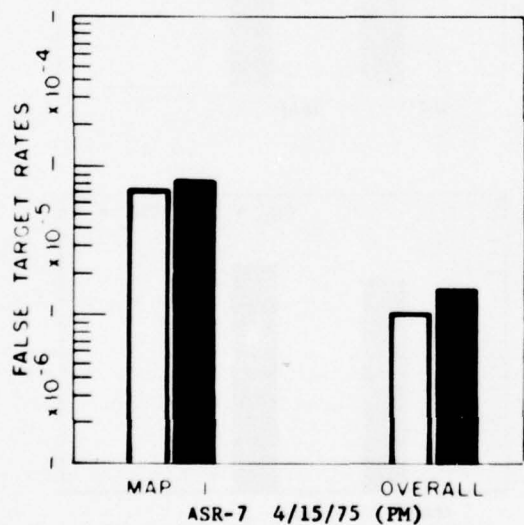
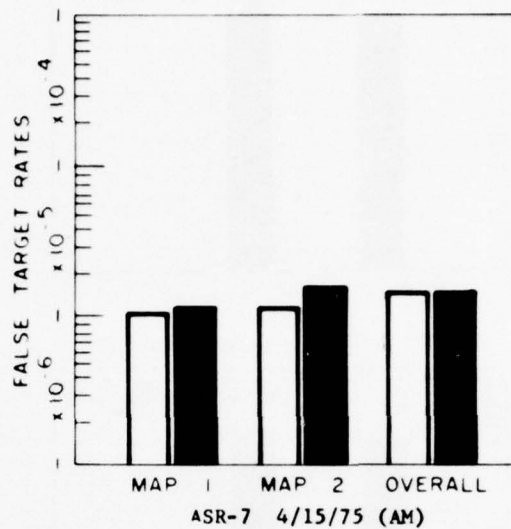
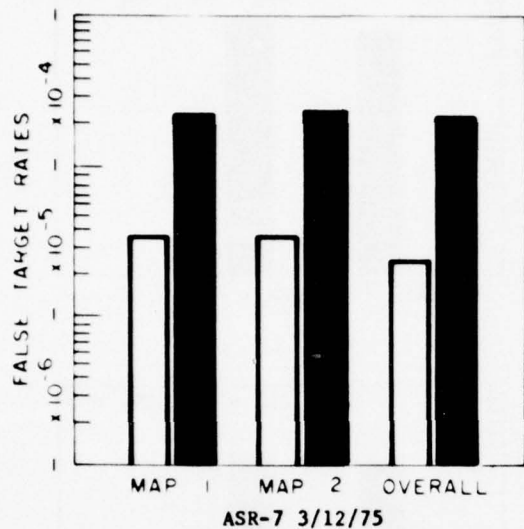
76-22-E8



1/16 nmi. SAMPLER

76-22-E9

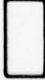

FIGURE E-9. WEATHER CLUTTER FALSE TARGET RATES FOR ASR-7 RADAR



NOTES:

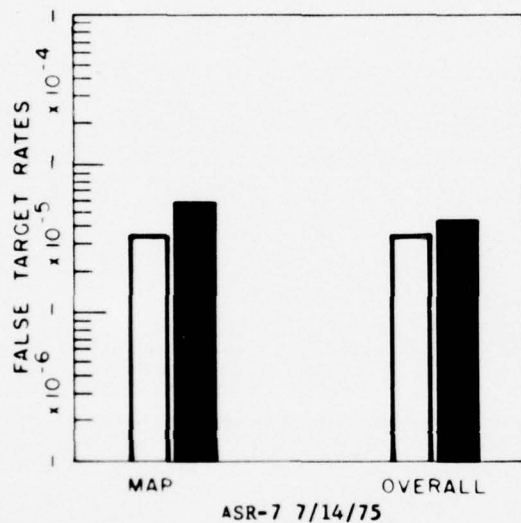
MTI VIDEO
 PREDETECTION THRESHOLD = 11
 $P_N = 4\%$

1/16 - NMI SAMPLER
 $CW_0 = 27$ $CW_L = 5$

 SECOND - THRESHOLD CONTROL ENABLED
 SECOND - THRESHOLD CONTROL DISABLED

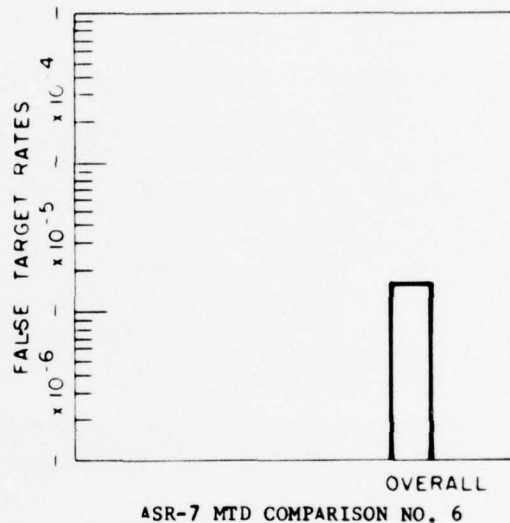
76-22-E10

FIGURE E-10. WEATHER CLUTTER FALSE TARGET RATES FOR ASR-7 RADAR



MTI VIDEO
 PREDETECTION THRESHOLD = 11
 $P_N = 4\%$

1/16-NMI SAMPLER
 $CW_0 = 27$ $CW_L = 5$



SECOND-THRESHOLD
 CONTROL ENABLED

SECOND-THRESHOLD
 CONTROL DISABLED

76-22-E11

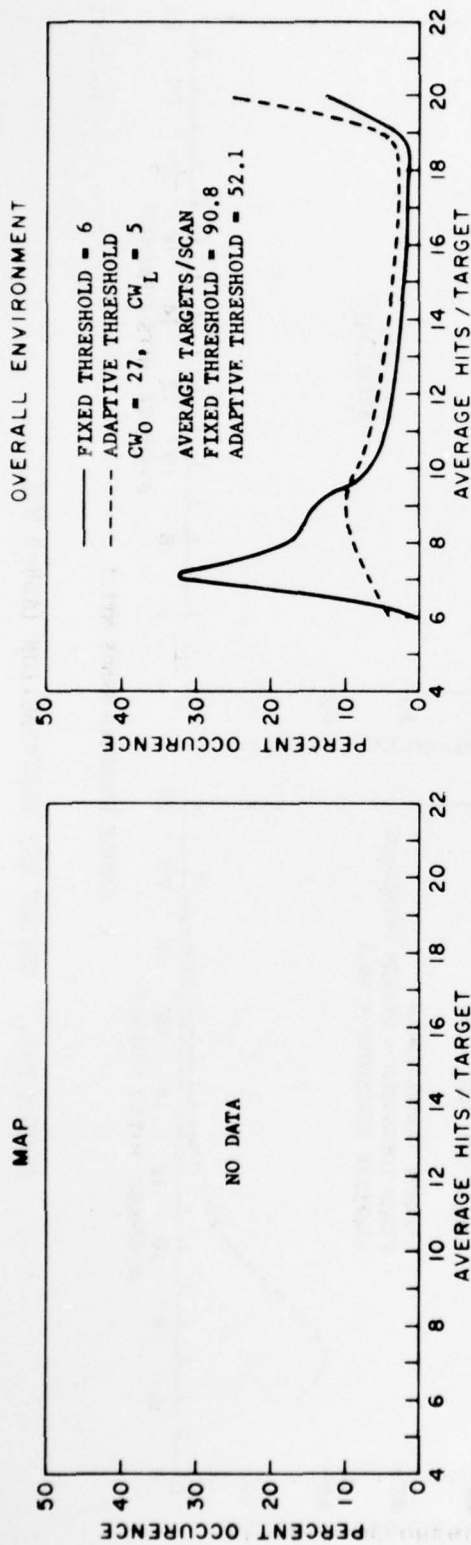
FIGURE E-11. WEATHER CLUTTER FALSE TARGET RATES FOR ASR-7 RADAR

APPENDIX F

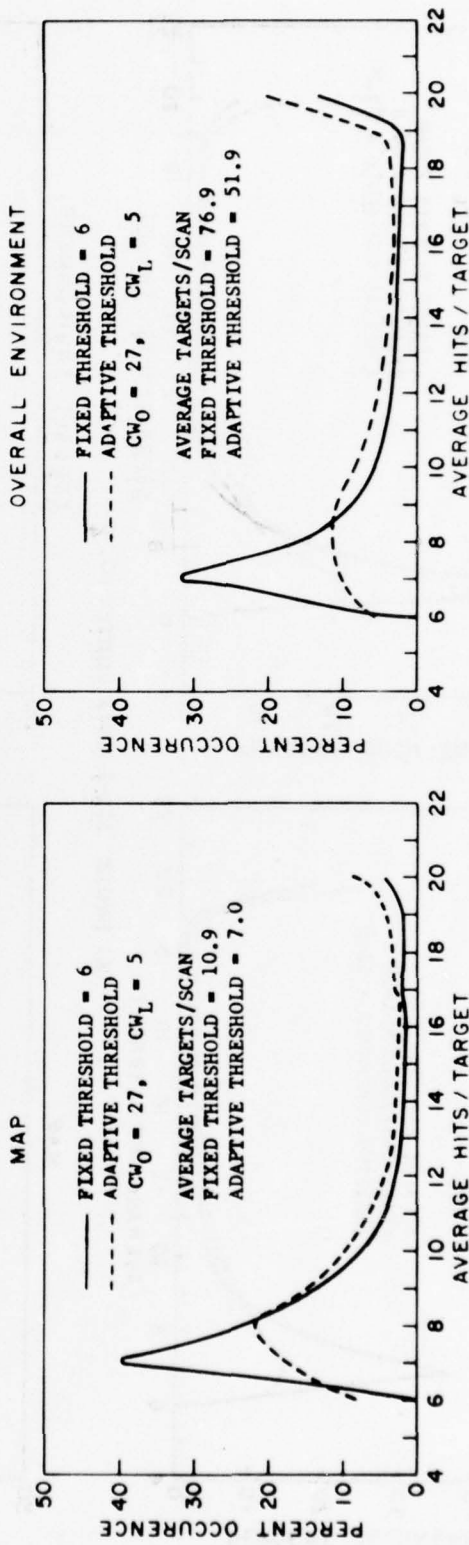
TARGET HIT DISTRIBUTION

APPENDIX F
LIST OF ILLUSTRATIONS

Figure		Page
F-1	Target Hit Distribution (ASR-5 MTI)	F-1
F-2	Target Hit Distribution (ASR-5 MTI)	F-2
F-3	Target Hit Distribution (ASR-5 Radar)	F-3
F-4	Target Hit Distribution (ASR-7 MTI)	F-4
F-5	Target Hit Distribution (ASR-7 MTI)	F-5
F-6	Target Hit Distribution (ASR-7 MTI)	F-6



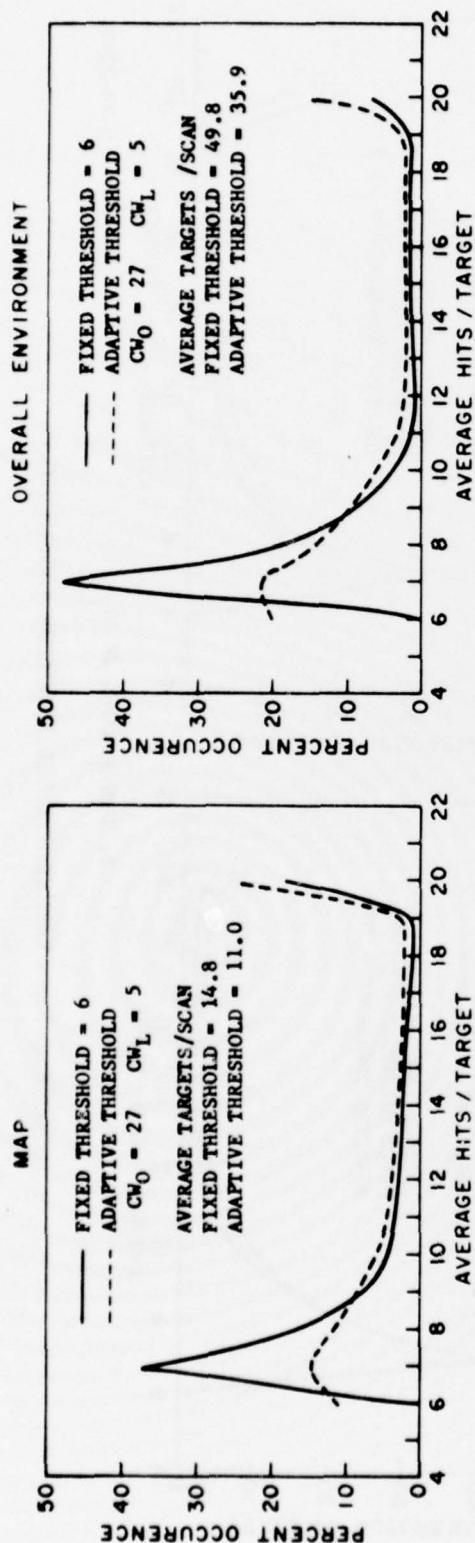
A. SAMPLE ASR-5 WW 49



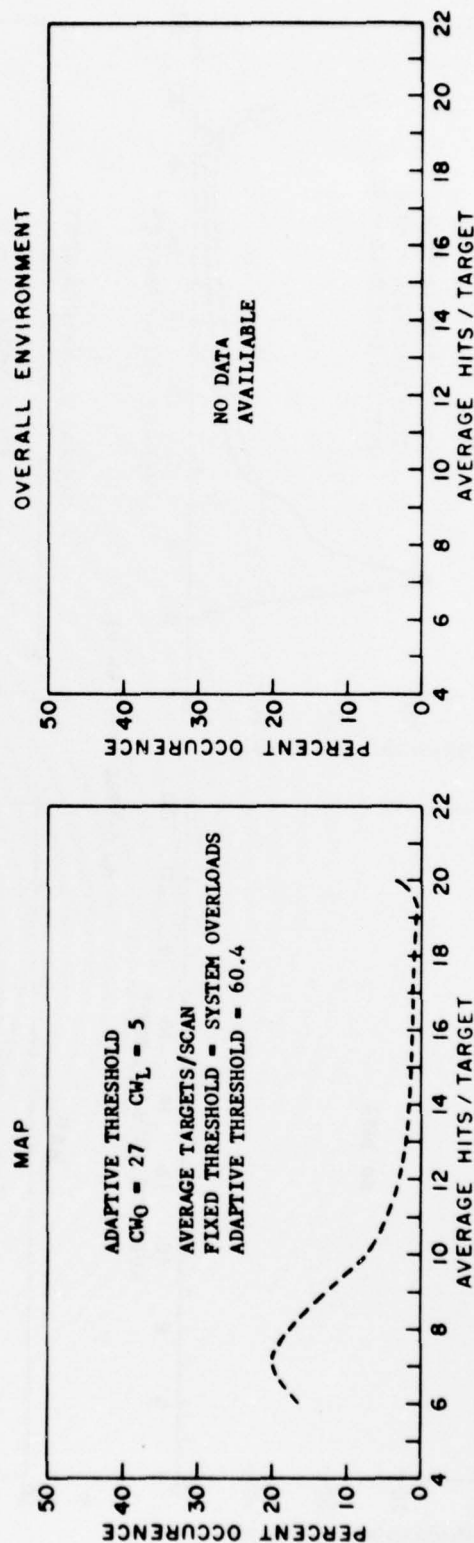
B. SAMPLE ASR-5 WW 34

76-22-F1

FIGURE F-1. TARGET HIT DISTRIBUTION (ASR-5 MTI)



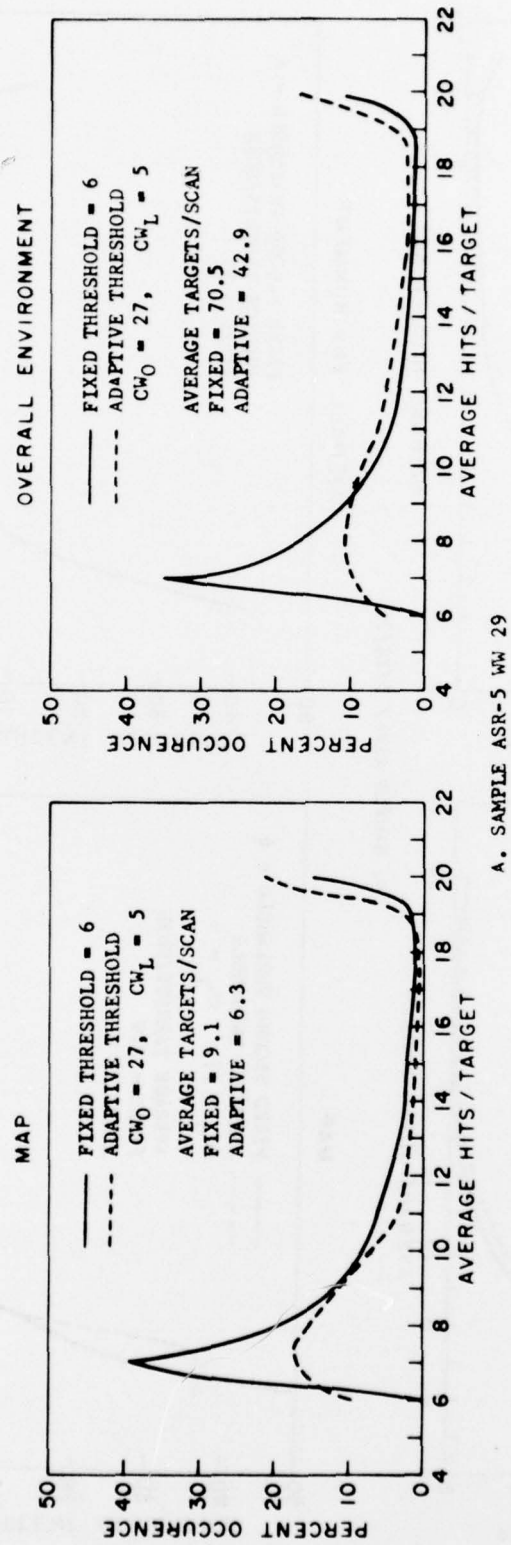
A. SAMPLE ASR-5 ANGLE CLUTTER NO. 4



B. SAMPLE EXTENDED RANGE MTI 1

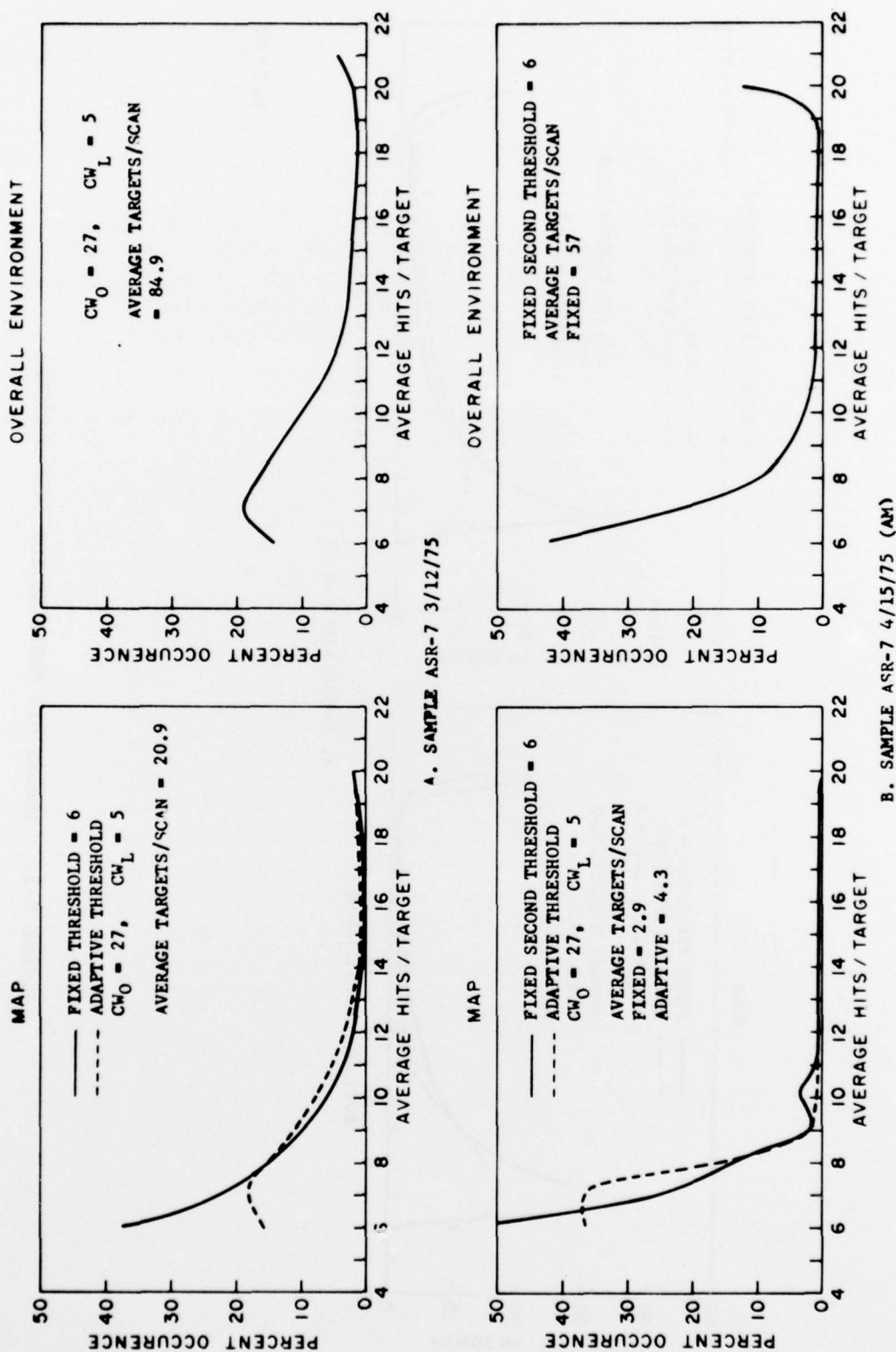
76-22-F2

FIGURE F-2. TARGET HIT DISTRIBUTION (ASR-5 MTI)



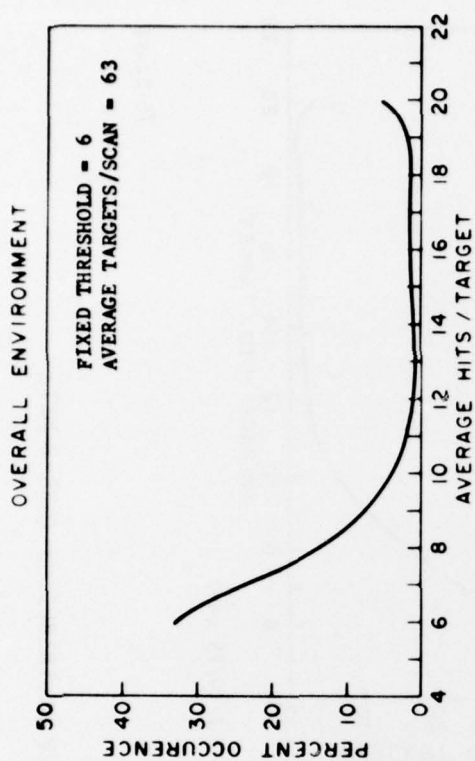
76-22-F3

FIGURE F-3. TARGET HIT DISTRIBUTION (ASR-5 RADAR)

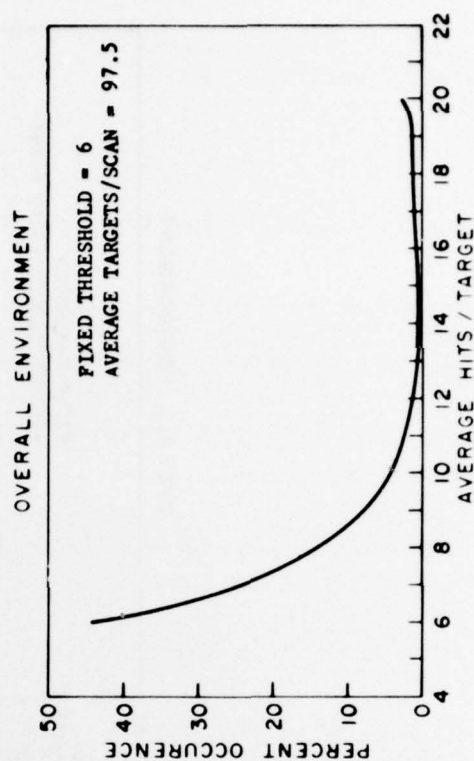


76-22-F4

FIGURE F-4. TARGET HIT DISTRIBUTION (ASR-7 MTI)



A. SAMPLE ASR-7 4/15/75 (PM)



B. SAMPLE ASR-7 4/3/75

FIGURE F-5. TARGET HIT DISTRIBUTION (ASR-7 MTI)

76-22-F5

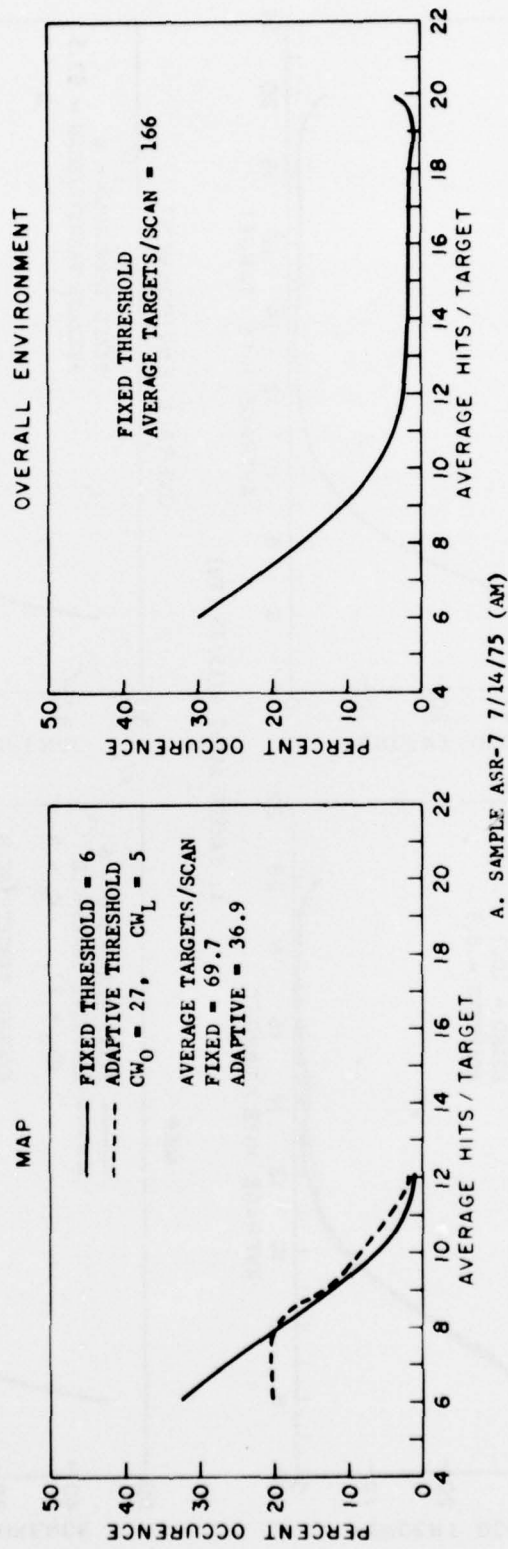


FIGURE F-6. TARGET HIT DISTRIBUTION (ASR-7 MTI)

APPENDIX G

VIDEO SELECT MAPPING

APPENDIX G
LIST OF TABLES

Table		Page
G-1	Video Select Mapping Results Sample MTD 6 Comparison (ASR-7 Radar)	G-1
G-2	Video Select Mapping Results Sample	G-2
G-3	Video Select Mapping Results Sample ASR-7	G-3
G-4	Video Select Mapping Results Sample ASR-7	G-4
G-5	Video Select Mapping Results Sample ASR-7	G-5
G-6	Video Select Mapping Results Sample ASR-5 WW49	G-6
G-7	Video Select Mapping Results Sample ASR-5 WW34	G-7
G-8	Video Select Mapping Results Sample ASR-5 WW29	G-8

TABLE G-1. VIDEO SELECT MAPPING RESULTS SAMPLE MTD 6
COMPARISON (ASR-7 RADAR)

A. Isolated - Hit Map

Parameter Set No.	Isolated-Hit Threshold	Scan Increment	Scan Decrement	Scan Threshold	Predetection Threshold Normal MTI	Sweeps Per Zone	Range	Soaking Added Range	Azimuth	Pfa X10-5	Comments
1	Q3	Forced with MTI Video									
2	29	2	1	15	9/11	31	1	2	1	1.9	
3	30	2	1	15	9/11		1	2		4.5	
4	29	2	1	15	10/11		1	2	1	3.86	
5	29	2	1	7	9/11		1	2	1	3.92	
6	30	2	1	10	9/11		1	2	1	3.57	
7	30	2	1	7	9/11		1	2	1	3.47	
8	31	2	1	7	9/11		1	2	1	3.32	
9	31	2	1	5	9/11		1	2	1	2.99	Maps Several Targets
10	30	2	1	5	9/11		1	2	1	3.01	Maps Several Targets
11	31	2	1	10	9/11		1	2	1	3.32	Maps Several Targets
12	29	2	1	5	9/11		1	2	1	3.26	Maps only a couple Targets
										3.58	Maps a Few Targets

B. Clutter Monitor Technique

Parameter Set No.	Slow Loop P _N	Range Density Threshold	Scan Increment	Scan Decrement	Scan Threshold	Azimuth Threshold	Predetection Threshold Normal MTI	Sweeps Per Zone	Range	Soaking Added Range	Azimuth	Pfa X10-5	Comments
1	3%	2	2	1	7	12	9/11	27	1	2	1	2.79	
2	3%	2	2	1	7	12	10/11	27	1	2	1	2.46	
3	3%	2	2	1	7	12	10/11	27	1	2	0	2.8	
4	3%	2	2	1	5	12	9/11	27	1	2	1	2.75	

TABLE G-2. VIDEO SELECT MAPPING RESULTS SAMPLE

A. Isolated - Hit Map

Parameter Set No.	Isolated-Hit Threshold	Scan Increment	Scan Decrement	Scan Threshold	Predetection Threshold Normal/MTI	Sweeps Per Zone	Range	Soaking Added Range	Azimuth	Pfa X10-5	Comments
1	Q3	Forced with MTI Video									
2	29	2	1	15	9/11	31	1	2	1	4.19	
3	30	2	1	15	9/11		1	2	1	5.83	
4	29	2	1	10	9/11		1	2	1	5.42	
5	29	2	1	7	9/11		1	2	1	5.18	
6	30	2	1	10	9/11		1	2	1	4.9	
7	30	2	1	7	9/11		1	2	1	4.83	
8	31	2	1	7	9/11		1	2	1	4.71	
9	31	2	1	5	9/11		1	2	1	4.59	
10	30	2	1	5	9/11		1	2	1	4.47	
11	29	2	1	5	9/11		1	2	1	4.66	
12	31	2	1	10	9/11		1	2	1	4.84	
13											
14											

Seems to Map Targets

B. Clutter Monitor Technique

Parameter Set No.	Slow Loop Pn	Range Density Threshold	Scan Increment	Scan Decrement	Scan Threshold	Azimuth Threshold	Predetection Threshold Normal MTI	Sweeps Per Zone	Range	Soaking Added Range	Azimuth	Pfa X10-5	Comments
1	3%	2	2	1	7	12	9/11	27	1	2	1	4.24	
2	3%	2	2	1	5	12	9/11	27	1	2	1	4.22	
3	3%	2	2	1	7	12	10/11	27	1	2	1	4.14	
4	3%	2	2	1	7	12	10/11	27	1	2	0	Over-load	Bombs Program

TABLE G-3. VIDEO SELECT MAPPING RESULTS SAMPLE ASR-7

A. Isolated - Hit Map

Parameter Set No.	Isolated-Hit Threshold	Scan Increment	Scan Decrement	Scan Threshold	Predetection Threshold Normal MTI	Sweeps Per Zone	Range	Soaking Added Range	Azimuth	Pfa X10-5	Comments
1	Q3	Forced with MTI Video									
2	29	2	1	15	9/11	31	1	2	1	1.8	
3	29			15						5.27	
4	30			15						4.01	
5	29			10						3.92	
6	29			7						3.53	
7	30			10						3.0	
8	30			7						2.88	
9	31			7						2.55	
10	31			5						2.41	
11	30			5						2.77	
12	29			5						3.28	
13	31			10						2.67	

Fringes of Clutter not Mapping

Mapped a Couple Targets

Maps Targets

Maps Targets

Mapped a Couple Targets

Mapped a Couple Targets

B. Clutter Monitor Technique

Parameter Set No.	Slow Loop FN	Range Density Threshold	Scan Increment	Scan Decrement	Scan Threshold	Azimuth Threshold	Predetection Threshold Normal MTI	Sweeps Per Zone	Range	Soaking Added Range	Azimuth	Pfa X10-5	Comments
1	32	2	2	1	7	12	9/11	27	1	2	1	2.39	
2	32	2			7	12	10/11	27	1	2	1	2.14	
3	32	2			7	12	10/11	27	1	2	0	Bombs Program	
4	32	2			5	12	9/11	27	1	2	1	2.16	

TABLE G-4. VIDEO SELECT MAPPING RESULTS SAMPLE ASR-7

A. Isolated - Hit Map

Parameter Set No.	Isolated-Hit Threshold	Scan Increment	Scan Decrement	Scan Threshold	Predetection Threshold Normal MTI	Sweeps Per Zone	Range	Soaking Added Range	Azimuth	Pfa X10-5	Comments
1	Q3	Forced with MTI Video									
2	29	2	1	15	9/11	31	1	2	1	1.97	
3	30	2		15						6.12	
4	29	2		10						4.95	
5	29	2		7						4.01	
6	30	2		10						3.95	
7	30	2		7						3.22	
8	31	2		7						3.09	Maps a Couple Targets
9	31	2		5						2.52	Maps a Couple Targets
10	30	2		5						2.47	Maps Targets
11	29	2		5						2.85	Maps a Couple Targets
12	29	2		5						3.48	Maps a Couple Targets
13	31	2		10						2.57	Maps a Couple Targets
14											

B. Clutter Monitor Technique

Parameter Set No.	Slow Loop Pn	Range Density Threshold	Scan Increment	Scan Decrement	Scan Threshold	Azimuth Threshold	Predetection Threshold Normal MTI	Sweeps Per Zone	Range	Soaking Added Range	Azimuth	Pfa X10-5	Comments
1	3%	2	2	1	7	12	9/11	27	1	2	1	2.44	Map Takes too long to develop
2	3%	2	2	1	7	12	10/11	27				2.34	Map Takes too long to develop
3	3%	2	2	1	5	12	9/11	27				2.02	Good Map
4	3%	2				12		27					

TABLE G-5. VIDEO SELECT MAPPING RESULTS SAMPLE ASR-7

A. Isolated - Hit Map

Parameter Set No.	Isolated-Hit Threshold	Scan Increment	Scan Decrement	Scan Threshold	Predetection Threshold Normal MTI	Sweeps Per Zone	Range	Soaking Added Range	Azimuth Range	Pfa X10 ⁻⁵	Comments
1	Q3	Forced with MTI Video									
2	29	2	1	15	9/11	31	1	2	1	3.0	Program Bombs
3	30			15							Program Bombs
4	29			15							Program Bombs
5	29			10							Program Bombs
6	29			7						6.77	High Computer Load
7	30			10						5.17	High Computer Load
8	30			7						4.67	
9	31			7						3.81	
10	31			5						3.57	
11	30			5						4.27	
12	29			5						5.36	
13	31			10						4.06	
14											

B. Clutter Monitor Technique

Parameter Set No.	Slow Loop PN	Range Density Threshold	Scan Increment	Scan Decrement	Scan Threshold	Azimuth Threshold	Predetection Threshold Normal MTI	Sweeps Per Zone	Range	Soaking Added Range	Azimuth Range	Pfa X10-5	Comments
1	3%	2	2	1	7	12	9/11	27	1	2	1	Program Bombs	
2	3%	2	2	1	7	12	10/11	27				3.0	
3	3%	2	2	1	5	12	9/11	27				2.98	

TABLE G-6. VIDEO SELECT MAPPING RESULTS SAMPLE ASR-5 W49

A. Isolated - Hit Map

Parameter Set No.	Isolated-Hit Threshold	Scan Increment	Scan Decrement	Scan Threshold	Predetection Threshold Normal MTI	Sweeps Per Zone	Range	Soaking Added Range	Azimuth	Pfa X10 ⁻⁵	Comments
1	Q3	Forced with MTI Video									
2	29	2	1	15	8/10	31	1	2	1	1.27	
3	30	2		15						2.39	
4	29	2		15						1.41	Maps in Clear
5	29	2		10						1.9	
6	29	1		15						2.85	Maps in Clear
7	29	1		10						2.39	
8	29	1		7						2.38	
9	29	1		5							Maps in Clear
10											
11											
12											
13											
14											

B. Clutter Monitor Technique

Parameter Set No.	Slow Loop PN	Range Density Threshold	Scan Increment	Scan Decrement	Scan Threshold	Azimuth Threshold	Predetection Threshold Normal MTI	Sweeps Per Zone	Range	Soaking Added Range	Azimuth	Pfa X10 ⁻⁵	Comments
1	3%	2	2	1	7	12	8/10	27	1	2	1	2.65	
2	3%	2	2	1	7	12	9/10	27	1	2	1	2.09	
3	3%	2	2	1	7	12	9/10	27	1	2	0	2.73	
4	3%	2	2	1	5	12	8/10	27	1	2	1	2.6	Maps in Clear

TABLE G-7. VIDEO SELECT MAPPING RESULTS SAMPLE ASR-5 WW34

A. Isolated - Hit Map

Parameter Set No.	Isolated-Hit Threshold	Scan Increment	Scan Decrement	Scan	Predetection Threshold Normal MTI	Sweeps Per Zone	Soaking Range	Added Azimuth	Pfa X10-5	Comments
1	Q3	Forced with MTI	Video	1	15	31	1	2	1.5	Maps 1 or 2 Targets
2	29	2	2	15	8/10				3.25	Maps 95% of Targets
3	30	2	2	15	9/10				2.2	Occasional Mapping of Targets
4	29	2	2	10	8/10				2.73	Maps Clear
5	29	2	2	15	8/10				3.4	Good Map
6	29	1	1	10	8/10				3.35	Best Map
7	29	1	1	7	8/10				3.1	Fair Map
8	29	1	1	5	8/10				3.1	Poor Map
9	29	1	1							
10										
11										
12										
13										
14										

B. Clutter Monitor Technique

Parameter Set No.	Slow Loop Pn	Range Density Threshold	Scan Increment	Scan Decrement	Scan	Scan Threshold	Azimuth Threshold	Predetection Threshold Normal MTI	Sweeps Per Zone	Soaking Range	Added Azimuth	Pfa X10-5	Comments
1	3%	2	2	1	7	12	8/10	27	1	2	1	3.4	
2	3%	2	2	7	9/10	12	9/10	27	1	2	1	2.9	
3	3%	2	7	5	12	8/10	27	1	2	2	0	3.8	
4	3%	2	5	12	8/10	27	8/10	27	1	2	1	3.5	

TABLE G-8. VIDEO SELECT MAPPING RESULTS SAMPLE ASR-5 W29

A. Isolated - Hit Map

Parameter Set No.	Isolated-Hit Threshold	Scan Increment	Scan Decrement	Scan Threshold	Predetection Threshold Normal MTI	Sweeps Per Zone	Soaking Range	Soaking Added Azimuth	Pfa X10-5	Comments
1	Q3	Forced with MTI Video								
2	29	2	1	15	8/10	31	1	2	2.12	
3	30	2	1	15	8/10				6.1	Maps a Couple Targets
4	29	2	1	15	9/10				3.4	Maps 90% of Clear
5	29	2	1	10	8/10				4.59	Maps a Couple of Targets
6	29	1	1	15	8/10				4.91	Maps a Couple of Targets
7	29	1	1	10	8/10				6.47	
8	29	1	1	10	9/10				5.78	
9	29	1	1	7	8/10				4.76	
10									5.54	Maps Targets
11										
12										
13										
14										

B. Clutter Monitor Technique

Parameter Set No.	Slow Loop Pn	Range Density Threshold	Scan Increment	Scan Decrement	Scan Threshold	Azimuth Threshold	Predetection Threshold Normal MTI	Sweeps Per Zone	Soaking Range	Soaking Added Azimuth	Pfa X10-5	Comments
1	3%	2	2	1	7	12	8/10	27	1	2	1	7.1
2	3%	2	2	1	7	12	9/10	27	1	2	1	5.99
3	3%	2	2	1	7	12	9/10	27	1	2	0	6.99
4	3%	2	2	1	5	12	8/10	27	1	2	1	6.76